From the: *Institut für Schlaganfall- und Demenzforschung*

Klinikum der Universität München, Großhadern

Ludwig-Maximilians-Universität zu München

Dissertation

zum Erwerb des Doctor of Philosophy (Ph.D.) an der

Medizinischen Fakultät der

Ludwig-Maximilians-Universität zu München

Unraveling proteomic changes of heterogeneous SARS-CoV-2 infection identified by panoptic imaging

vorgelegt von:

Zhouyi Rong

aus:

Macheng, Hubei, China

Jahr:

2023

Mit Genehmigung der Medizinischen Fakultät der

Ludwig-Maximilians-Universität zu München

First supervisor: *Prof. Dr. Nikolaus Plesnila*

Second supervisor: *Prof. Dr. Ali Ertürk*

Third supervisor: *Prof. Dr. Dominik Paquet*

Dean: **Prof. Dr. med. Thomas Gudermann**

Datum der Verteidigung:

10.5.2023

Table of content

Abstract (English):

The severe acute respiratory syndrome coronavirus type 2 (SARS-CoV-2) caused an infectious disease that began in Wuhan, China in 2019 and resulted in a worldwide pandemic that did not end until second half of 2022, namely the coronavirus disease 2019 (COVID-19) (1). Most COVID-19 patients show mild to moderate symptoms, but the SARS-CoV-2 infection can occasionally cause severe symptoms and even death. The persistent symptoms after recovery from the acute phase also raises more and more concerns about the long term effects. To explain the various severities of infection and disease, we hypothesized that: 1) SARS-CoV-2 infection is heterogenous in different organs of the body and there are potential unknown infected regions to be explored, 2) the skull-meninges connections might contribute to the COVID-19 related brain disorders. Therefore, we aim to map all the infection sites of SARS-CoV-2, examine the lung, kidney, and brain samples from postmortem COVID-19 patients, and also investigate the role of skull-meninges in COVID-19.

In this thesis: 1) first, we studied the heterogenous tissue tropism of SARS-CoV-2 using a mouse model and various human organs, taking advantage of the optical clearing technology, which enables imaging of large tissue volumes at the cell level, 2) then, to unravel the proteome changes due to SARS-CoV-2 infection in lung, kidney, and brain tissues of COVID-19 patients, we compared the Spike protein-positive region with the Spike protein-negative region by proteomics combined with laser capture dissection microscopy (2). We identified differentially expressed proteins consistent with previous publications and several novel dysregulated proteins whose role in COVID-19 remains to be clarified. A closer examination of the mouse head and human skull revealed SARS-CoV-2 accumulation in the skull bone marrow. Using COVID-19 patients' tissue samples collected postmortem, viral spike protein accumulation was also observed in the skull, meninges, and brain, whereas viral RNA and nucleocapsid protein were only found outside the brain. Proteomics and imaging data showed neutrophil activation, inflammation, and vascular changes in the skull, meninges, and brain.

Overall, our experimental results suggest that SARS-CoV-2 Spike protein accumulates at the central nervous system (CNS) borders, where it might use the skull-meninges connections to reach the brain parenchyma and trigger long-term changes.

List of figures

List of tables

List of abbreviations

COVID-19	Coronavirus disease 2019
SARS-CoV-2	Severe acute respiratory syndrome-coronavirus-2
ACE2	Angiotensin-converting enzyme 2
CNS	Central nervous system
CT	Computed tomography
ARDS	Acute respiratory distress syndrome
3D	Three-dimensional
mRNA	Messenger ribonucleic acid
SMC	Skull-meninges connection
CSF	Cerebrospinal fluid
CRP	C-reactive protein
IFN	Interferon
TNF	Tumor necrosis factor
IL	Interleukin
SHANEL	Small-micelle-mediated Human orgAN Efficient clearing and Labeling
3DISCO	Three-dimensional imaging of solvent-cleared organs
MS	Mass spectrometry
LC	Liquid chromatography
DIA	Data independent acquisition
RT-PCR	Reverse transcription polymerase chain reaction
LCM	Laser capture microdissection
NET	Neutrophil extracellular trap
PMPI	P-maleimidophenyl isocyanate
DTT	Dithiothreitol
TRITC	Tetramethylrhodamine isothiocyanate
THF	Tetrahydrofuran
DCM	Dichloromethane
BABB	Benzyl alcohol, benzyl benzoate

Iba1	Ionized calcium-binding adaptor molecule 1
IHC	Immunohistochemistry
NETs	Neutrophil extracellular traps
PCA	Principle components analysis
diH_2O	Deionized water
PI	Propidium iodide
NMDEA	N-methyldiethanolamine
DMSO	Dimethyl sulfoxide
DAB	3,3’-diaminobenzidine
HRP	Horseradish peroxidase
min	minute
RT	Room temperature

1. Introduction

The severe acute respiratory syndrome coronavirus 2 (SARS-CoV-2) is responsible for the coronavirus disease 2019 (COVID-19) (1). Numerous studies, including proteomics and single-cell RNA sequencing, have been conducted since then to understand the mechanisms of COVID-19 pathology (3–12), focusing on specific organs or specific cell types. Considering that multiple organs are affected in COVID-19 patients, further research is required to understand to what extent SARS-CoV-2 infects human tissues, and whether these molecular changes resulted from the systematic response to the cytokine storm or direct tissue response to viral infection.

1.1 Epidemiology, virology, and pathology of COVID-19

1.1.1 Epidemiology and clinical manifestations of COVID-19

The first reported case of COVID-19 developed symptoms on December 1, 2019, in Wuhan, China (13). Rapid human-to-human transmission led to intercontinental spread, and COVID-19 was declared as a pandemic by the World Health Organization (WHO) in March 2020. The mean incubation time from exposure to infection source to symptom onset is about five to six days (14,15), and the reproduction number (R_0) is estimated to be 3.32 (95% CI, 2.81 to 3.82) (16), meaning that every infected patients spreads the infection to three to four susceptible persons on average. The asymptomatic rate is estimated to be 17.9% to 30.8% (17,18). Globally, the WHO reported 587,396,589 confirmed cases as of 15 August 2022, 4:42 pm CEST, including 6,428,661 deaths (Fig. 1).

Typical symptoms of acute COVID-19 patients are fever, cough, anosmia, hyposmia, myalgia, breathing difficulties, and fatigue. Headache, sore throat, and rhinorrhea were also reported as less prevalent symptoms. Ground-glass opacity on chest computed tomography (CT) was very common in hospitalized patients (13,19–21). More than 75% of COVID-19 patients admitted to hospital needed supplemental oxygen. Age appears to be the most important risk factor predicting the progression of critical illness, acute respiratory distress syndrome (ARDS). Males, those over the age of 60, and those who have concomitant medical conditions are more prone to a severe respiratory illness that necessitates hospitalization. In contrast, the majority of adolescents and children mainly have minor

symptoms or do not have any symptoms (22). The key risk factors for worse outcomes and higher mortality are underlying comorbidities such as hypertension, cardiovascular disease, and diabetes (20,22). Acute renal, hepatic or cardiac injury and increased levels of blood biomarkers (CRP and D-dimer) are associated with adverse outcomes and death (23).

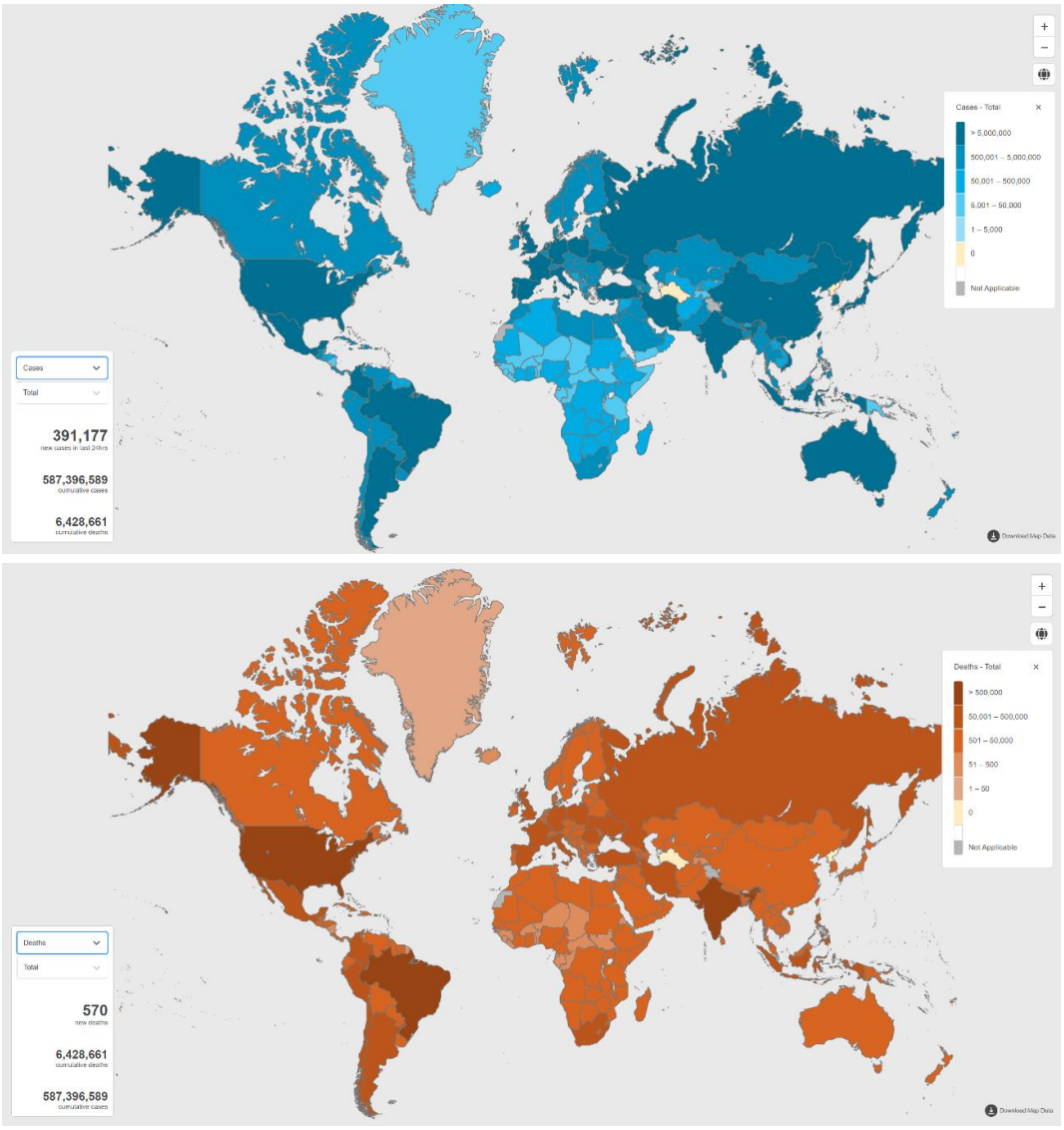

Figure 1. WHO COVID-19 Dashboard. Geneva: World Health Organization, 2020. Available online: https://covid19.who.int/ (last cited: [August 15, 2022]).

1.1.2 Virology of COVID-19

SARS-CoV-2 is a single-stranded RNA virus that has a genome of about 30 kb and encodes at least 29 proteins, including four structural proteins: nucleocapsid protein, envelope protein, membrane protein, and spike protein (24). Although

SARS-CoV-2 encodes a RNA polymerase with proofreading function, many mutations have been detected. The variant with amino acid substitution D614G on the Spike protein became the most common form in the global pandemic as of March 2020 (25). Subsequently, several variants with a recurrent mutation have been reported in addition to the principle D614G, and causing several waves of infection in some countries and regions. There are five variants of concern according to the WHO: The Alpha variant, the Beta variant, the Gamma variant, the Delta variant, and the Omicron variant (26).

Mutations in the Spike protein lead to different transmissibility of these variants, for example, the Omicron variants are more transmissible than the previous lineages, and the convalescent plasma in a person infected with early variants exhibited decreased neutralizing ability against it (26,27). In addition, compared to the SARS-CoV-2 Delta variants, the Omicron variants infection showed a significantly reduced probability of severe consequences (28).

Furthermore, when we look at the different sublineages of the Omicron variants, we will notice that the transmissibility of newly developed sublineages is increasing, as is the evasion of neutralizing antibodies against plasma from vaccination or infection with previous sublineages. BA.2 is more pathogenic and has higher replication efficacy than BA.1 (29). BA.4 and BA.5 have higher transmissibility than the BA.2 lineage (30).

1.1.3 Pathophysiology and cytokine storm

SARS-CoV-2 infection is mediated by the binding of its Spike protein and the angiotensin-converting enzyme 2 (ACE2) receptor on host cell surface. ACE2 is extensively expressed throughout the body (31,32). The type 2 transmembrane serine protease (TMPRSS2) promotes the cell entry via the cleavage and activation of the SARS-CoV-2 Spike protein (33). Early in infection, SARS-CoV-2 attacks the ciliated cells of the respiratory epithelium and sustentacular cells in the olfactory mucosa (34). As virus replication increases over time, the epithelial-endothelial barrier is impaired, leading to infection in endothelial cells, the amplification of inflammation causes infiltration of immune cells. According to postmortem studies, the alveolar wall has diffusely thickened, and the air gaps have been invaded by mononuclear cells and macrophages (35).

The virus particles induce the pathogen-associated molecular patterns of the immune response and cause an increase in proinflammatory cytokines, chemokines, and type I interferons (36). Severe COVID-19 patients showed elevated levels of proinflammatory macrophages in the bronchoalveolar lavage fluid (7).

The upregulated genes for innate immune and inflammatory pathways were enriched in lung alveoli, including neutrophil degranulation, IFNγ signaling, and interleukin signaling (37). Proinflammatory cytokines including IFNγ, IL-1β, IL-6, CXCL10, and CCL2 were found to be increased in the serum of COVID-19 patients (13). Overproduction of proinflammatory cytokines early in the disease leads to a cytokine storm (38), if the elevated cytokine concentrations continue dysregulated, the risk of multiple organ failure and eventual death will be higher. Markedly increased concentrations of cytokines (IFN, MCSF, IL-2) and chemokines (CCL1, CCL2, CLL2) were detected in non-survivors of COVID-19 (39). Additionally, T lymphocytes were seen in much lower numbers and frequencies in COVID-19 patients (39,40). Lymphopenia was reported to predict mortality and correlate with the severity of COVID-19 (41).

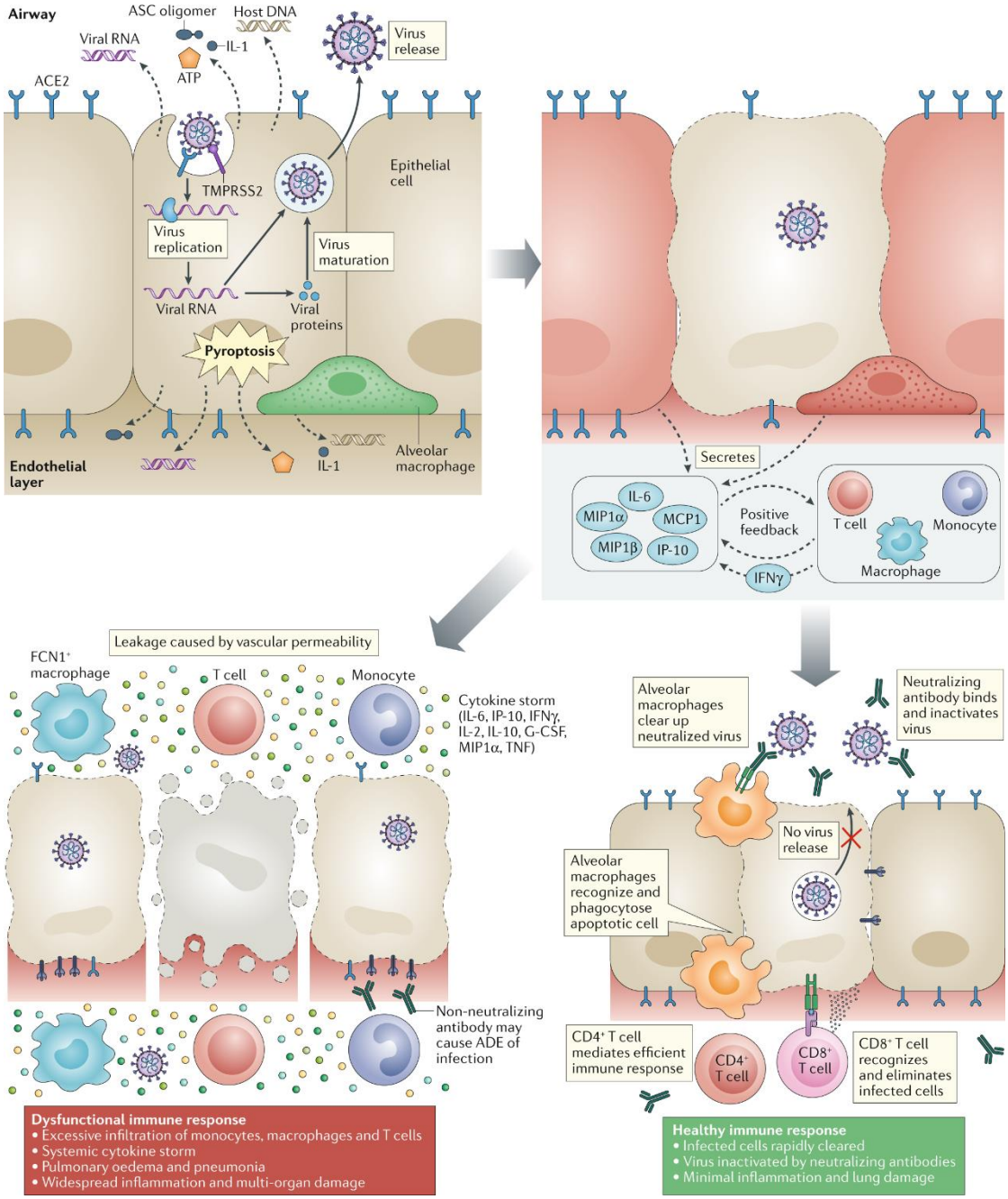

Figure 2. Schematic of immune response during SARS-CoV-2 infection. SARS-CoV-2 infects bronchoalveolar epithelial cells through binding with ACE2, virus replication causes host cell pyroptosis and release of damage-associated molecular patterns, leading to generation of proinflammatory cytokines and chemokines. The elevated cytokines and chemokines recruit T cell, monocyte, and macrophage to the infection site, promoting inflammation and eliminating the infected cells. Overproduction of proinflammatory cytokines cause local damage, the cytokine storm causes multiorgan damage (42).

SARS-CoV-2 infection also activates the complement cascade (42). The level of C-reactive protein (CRP) is significantly increased in COVID-19 patients (43). Complement activation is associated with advanced severity of COVID-19, e.g., C4 and factor B levels increase in hospitalized patients requiring oxygen support, and C3 overactivation and consumption may predict mortality (44). Patients with severe illness or died of COVID-19 had lower serum C3 and C4 levels than those with moderate cases (45).

SARS-CoV-2 infection also results in endothelial damage and thrombosis (46–48). Consumption of ACE2 by the virus could lead to increased angiotensin II concentration (49), contributing to microvascular thrombosis (50). Diffuse alveolar damage and capillary microthrombi were observed in most COVID-19 cases (51). D-dimer levels, indicating activation of the coagulation and fibrinolysis systems, are also increased in COIVD-19 patients (52).

1.1.4 Damage to other tissues

Despite that COVID-19 is mainly a respiratory disorder, the virus antigen or RNA can be detected in many organs, including the pharynx, kidney, heart, liver, intestine, and brain (53), which is consistent with the broad expression of ACE2 in various organs (31,32).

Significant increases in interferon responses are reported in SARS-CoV-2 infected liver, and infectious pathogen can be isolated in postmortem liver sample (12,54). SARS-CoV-2 also infects gastrointestinal organs because ACE2 is abundantly expressed, and antigen persistence is reported in gastrointestinal tissues seven months after infection (55,56). Direct viral infection of the kidney was reported in biopsy, and associated with acute kidney injury, glomerular and tubular damage (53,57). Proteomic research shows that COVID-19 patients have dysregulated clotting, angiogenesis, and fibrosis-related pathways, for instance, the coagulation factors are unbalanced in heart, thyroid, and kidney cortical tissues (58).

Neurological and neuropsychiatric complications such as loss of smell or taste, fatigue, myalgia, depression, and headache are common in COVID-19 patients, SARS-CoV-2 infection is also associated with encephalopathy and meningitis (59–65). There are also reports that observed some ocular manifestations similar to conjunctivitis in COVID-19 patients (66).

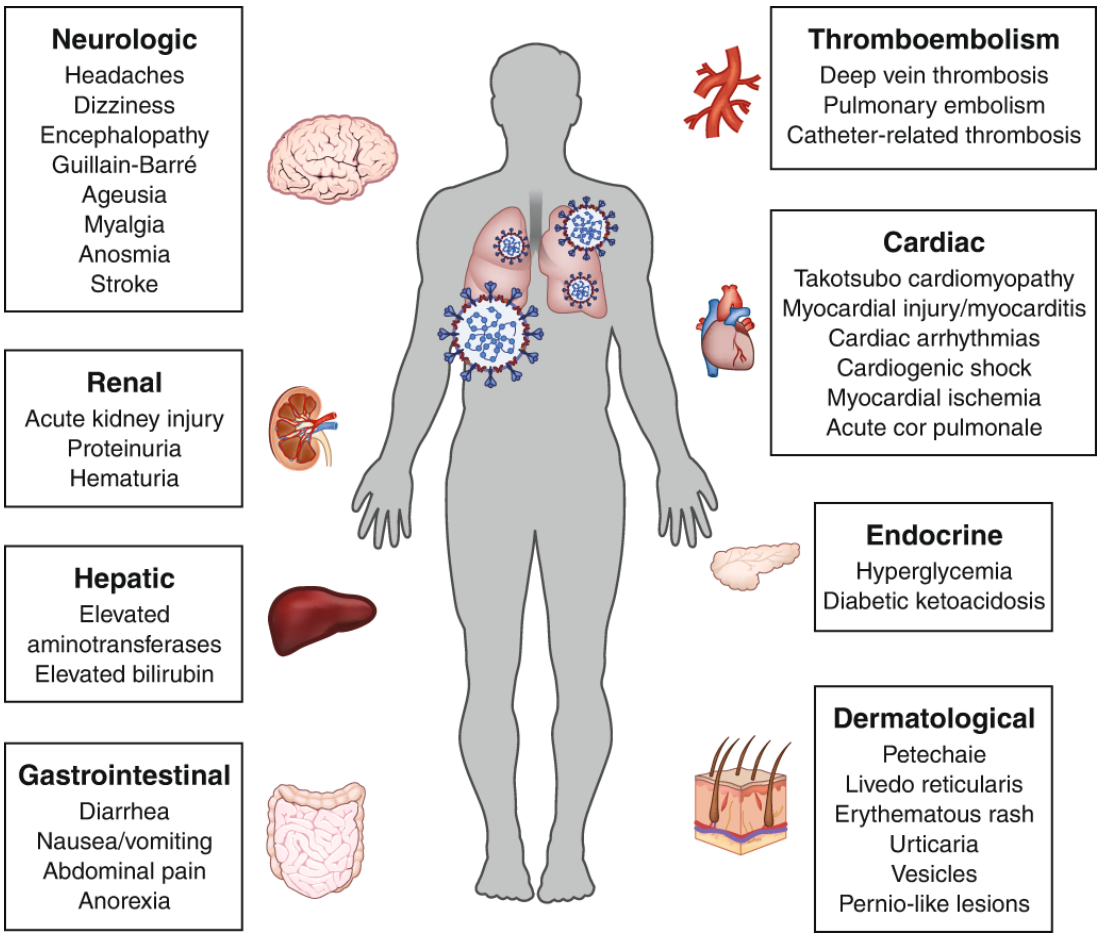

Figure 3. Extrapulmonary manifestations of COVID-19. Besides pneumonia and ARDS, abnormal manifestations in many organ systems are associated with COVID-19 (68).

1.2 Treatments and vaccination

There is no standardized treatment for COVID-19 patients; instead, the optimal course of action should be determined entirely by the patient's individual condition. The treatments of COVID-19 mainly include antiviral therapy, immunotherapy, anticoagulant therapy, antifibrotic therapy, respiratory support for critically ill patients, and treatment of acute renal injury. There are multiple medications to pre-

vent the disease progression, for example, remdesivir, favipiravir, and convalescent plasma can be used as antiviral treatments (67). Dexamethasone, tocilizumab, and ruxolitinib can be used to relieve infalmmation (68).

Vaccination is the most effective method of preventing infectious diseases. Vaccine development has continued from the earliest trials to the present day and is based on the same principles. Typically, a vaccine comprises a substance that mimics the pathogen. There are various methods to formulate a vaccine, for example, live-attenuated vaccine, inactivated vaccine, subunit vaccine, toxoid, conjugate vaccine, and genetic vaccine (69).

The development of vaccines against COVID-19 employed a variety of vaccine formulation strategies, including the use of purified inactivated virus, viral subunit particles, recombinant viral proteins, and nucleic acid-based vaccines. Sinovac Biotech's vaccine (CoronaVac), for example, is inactivated virus. Pfizer/BioNTech (BNT162b2) and Moderna (mRNA-1273) vaccines formulate mRNA in lipid nanoparticles, enabling an antibody response against the viral Spike protein (70,71). The AstraZeneca-Oxford (ChAdOx1 nCov-19), Johnson & Johnson (Ad26.CoV2-S), and Gamaleya (Sputnik V) vaccines use adenovirus vectors to encode the Spike protein of SARS-CoV–2. The above vaccines showed 95% (BNT162b2), 94% (mRNA-1273), 67% (ChAdOx1 nCov-19), 67% (Ad26.CoV2-S), and 91% (Sputnik V) efficacy in preventing COVID-19 infection (72). COVID-19 vaccination does not completely prevent against infection, whereas immunity acquired after vaccination helps to reduce susceptibility to severe disease (73).

The adverse effect develops following vaccination is the typical pain at the injection site which lasts around one to two days, ~1% of recipients experienced severe adverse effects (70,71,74).

1.3 Prognosis

1.3.1 Acute and convalescent-phase

The recovery rate after infection with COVID-19 varies according to severity. People with mild disease often recover in two weeks, but in case of severe illness, recovery can take up to six weeks. Time from the symptom onset to death was observed to be two to eight weeks. Various complications and health problems associated with COVID-19 have been reported, including pneumonia, ARDS, abnormal blood clotting, sepsis, and multiple organ failure (75–77). Readmission

rates for acute COVID-19 patients account for approximately one-third, and significantly increased rates of cardiovascular disease and diabetes were reported in hospitalized patients (78).

Following recovery from COVID-19, around 80% of patients experienced chronic symptoms, namely post-COVID-19 syndrome (79). Up to 44.9% of patients suffer from pulmonary fibrosis, and Patients with fibrosis more frequently experience lasting symptoms like breathlessness, cough, chest discomfort, tiredness, and muscle pain (80). Studies suggest that renin-angiotensin-aldosterone system imbalance worsens the prognosis of COVID-19 with increased pulmonary artery pressure and coagulation (81). People with COVID-19 also have dysfunction of extrapulmonary organ systems, including cardiovascular disease, acute coronary syndrome, myocarditis, acute kidney injury, and chronic kidney disease (82–84).

Immune memory of SARS-CoV-2 persists eight months or more after infection, and the number of memory B cells increases between one and eight months after infection. The number of memory T cells decreased with an initial half-life of three to five months, and the antibodies against SARS-CoV-2 decreased moderately over eight months (85). According to a different study, the antibodies were detectable for at least 11 months after infection (86).

1.3.2 Potential long-term effect

Fatigue, headaches, attention deficit, and shortness of breath were most frequently experienced in long COVID. Memory loss, depression, and sleep disturbances were also reported as persistent sequelae, suggesting long-term effects on the central nervous system (87–89). Indeed, many patients suffer from prevalent brain fog (90–93). Surprisingly, even patients with mild COVID-19 disease suffer from the long-term effects on the brain, including fogging and decreased grey matter thickness and overall brain size (63,93,94). The consequences of brain damage could be due to systemic inflammation or, in severe cases, viral infection of the brain (95,11,96). In some cases, invasion of the brain has been demonstrated, for example, Spike protein immunostaining was positive in brain tissue from COVID-19 human autopsies (97,98), and viral RNA can also be detected in multiple organs, including the brain (53). It has been suggested that the virus infects the brain through an impaired blood-brain barrier (99,100) and via the olfactory nerve (101–103), although there are controversial reports that SARS-CoV-2 infection was not observed in olfactory sensory neurons or olfactory bulb parenchyma (34,104,105), the route of viral infection to the brain remains

elusive. Tissue clearing methods would be beneficial to understand the extent and route of infection at the body level.

1.4 Tissue clearing technology

1.4.1 Overview of tissue clearing technology

Tissue clearing technologies are state-of-the-art methods to obtain information with subcellular resolution for intact organs and even for some whole organisms. Transparency is achieved by removing pigments to reduce light absorption and changing the tissue's refractive index (RI) to minimize light scattering (106). Depending on the chemical reagents used, tissue clearing methods can be classified as: Hydrophilic methods such as Sca*l*e (107) and CUBIC (108) can expand tissue to increase effective resolution. Hydrophobic methods such as 3DISCO (109) generally shrink the tissue, allowing imaging of larger samples. Hydrogel-based tissue clearing methods such as CLARITY (110) transform the tissue into a tissue-hydrogel hybrid by crosslinking it with hydrogel monomers. Combined with light-sheet fluorescence microscopy (111), these methods reveal the 3D structural cellular structural information of large biological samples for unbiased analysis.

1.4.2 Tissue clearing for intact human organs

For the purpose of labeling and imaging human organ pieces, numerous techniques have been developed, including methods focusing on human brain tissue (112–118), myocardial tissue (119), and lung tissue (120). However, these techniques are only applicable to human organ sections and not to whole human organs. To overcome the limited size of human sample tissue clearing and enable imaging and 3D rendering of whole human organs, we developed the SHANEL pipeline (121,122). The human lung, spleen, pancreas, kidney, heart, and brain, as well as rigid tissues like the skull, have all been successfully cleared.

1.5 Mass spectrometry-based proteomics

Proteomics based on mass spectrometry is now a common technique for identifying, characterizing, and quantifying proteins, as well as verifying and validating biological functional analyses (123). A mass spectrometer is based on an ion

source, a mass analyzer, and an ion detector. Sample molecules are ionized with the ion source in vaccum condition. The excess energy acquired causes the ionized molecule to further fragment into different ions and neutral particles of smaller mass. They enter the mass analyzer with the impact of the accelerating electric field. A mass analyzer is a device that separates ions of different masses according to the mass-to-charge ratio (m/z). The separated ions enter the ion detector and the amplified ion signals are collected, processed by the computer, and drawn into a mass spectrum (124).

Tandem mass spectrometry (MS/MS) is the use of two mass spectrometers linked together to improve the analysis. The first mass spectrometer analyzes the ionized samples, then a specific range of abundant ions are selected for fragmentation and proceeded to the second mass spectrometer for further analysis; this is also called data-dependent acquisition MS (DDA-MS). The development of data-independent acquisition MS (DIA-MS) allows fragmentation of all detected ions in the MS1 spectra range, achieving better reproducibility and sensitivity (125). The most popular separation technique for the examination of biological specimens is high performance liquid chromatography (HPLC). Generally, the application of liquid chromatography and mass spectrometry involves separating proteins from biological samples into peptide fragments using enzymes; the amount of proteins contained in the biological samples is then determined using LC/MS. Sequencing time and sensitivity benefits from trapped ion mobility spectrometry (TIMS) and parallel accumulation–serial fragmentation (PASEF) are especially remarkable (126).

1.6 Objectives of this project

Considering the diversity of each patient, including gender, age, diet, and habits, we aim to find the pathophysiological changes by comparing the virus infection site with internal controls, i.e., regions without infection from the same patient. In this way, we can understand the direct virus-related response rather than the systemic changes resulting from a cytokine storm.

On the other hand, the extent to which tissues in the body are affected by SARS-CoV-2 is still unclear, although multiorgan infection has been demonstrated (53,127,12). Therefore, we aim to investigate the pattern of infection in different organs and inspect the potential sites of infection throughout the body using an

experimental mouse model. We are also interested in understanding how the brain is affected by SARS-CoV-2.

2. Material and Methods

2.1 Material

2.1.1 Human organ sources and experimental mouse

Origin of human tissue and related work

PFA-fixed human brains and human skull blocks were obtained from donors and autopsies from COVID-19 diagnosed patients during their lifetime or positive SARS-CoV-2 PCR test post-mortem following the European Control for Infectious Diseases. The post-mortem interval was, on average five days. All donors or their next-of-kin provided informed, written consent for donation for educational and research purposes. Human brain tissue was obtained from the Anatomical Institute of the University of Leipzig, Germany, and the Institute of Pathology Technical University of Munich, Germany. Human lung, kidney and skull samples were collected during autopsies at the Institute of Legal Medicine of the University Medical Center Hamburg-Eppendorf. The 1994 Saxon Death and Burial Act and the independent ethics committee of the Hamburg Chamber of Physicians (protocol 2020-10353-BO-ff) were followed to acquire institutional approval. Patient information are listed in the following table (Table. 1).

Table 1. Clinical background of human samples.

Group	Sex	Age range	PMI	Comorbidities	Brain weight[g]	Days of disease	Macroscopic findings	Brain CT findings
COVID-19	f	80~100	5	Uterus myomatosus, Diverticulosis, Gall bladder stones	1230	n/a		Edema. Cerebral vasosclerosis.
COVID-19	f	60~80	3	Liver zirrhosis with esophageal varices	1050	n/a		
COVID-19	f	40~60	8	Ethanol dependency, Gastritis, Hypothyreosis	1140	6		
COVID-19	m	40~60	7	Arterial Hypertension, Arterial disease, Adipositas	1570	14		
COVID-19	m	80~100	3	Arteriosclerosis, coronary artery disease (3VD), COPD	950	12		
COVID-19	m	40~60	3	CI, IHD, DM	1535	9		
COVID-19	f	80~100	5	Emphysema, IHD, CI, CKD	1030	n/a		
COVID-19	m	60~80	6	Metastased rectal CA, mitral valve sclerosis	1390	n/a	Brain and Dura without gross pathologic changes. Mild unspecific inflammatory changes DD COVID-19.	
COVID-19	m	40~60	6	liver cirrhosis, esophagus vericosis, CKD, emphysema	1500	1		
COVID-19	m	80~100	4	asbestosis, IHD, bronchial CA,	1385	n/a		
COVID-19	f	80~100	3	Colon-CA, Apoplex, dementia, IHD	1290	n/a		
Ctrl	m	80~100	1	intestinal infections; Atherosclerosis; Heart failure	1268	none		
Ctrl	m	60~80	2	chronic ischemic heart disease; Essential hypertension	1270	none		
Ctrl	m	80~100	2	nutrition/metabolic; mental/behavioral disorders; Renal failure; heart disease	1183	none		
Ctrl	m	80~100	2	Malignant neoplasm of prostate	1204	none		
Ctrl	f	80~100	3	Mental/behavioral disorders; Essential hypertension	1190	none		
Ctrl	f	80~100	n/a	n/a	1150	none		
COVID-19	n/a	n/a	2	Essential hypertension; chronic lower respiratory diseases; Alzheimer's disease	1045	n/a		
COVID-19	n/a	n/a	n/a	n/a	n/a	n/a		
COVID-19	n/a	n/a	n/a	n/a	n/a	n/a		
COVID-19	n/a	n/a	n/a	n/a	n/a	n/a		
COVID-19	n/a	n/a	n/a	n/a	n/a	n/a		
COVID-19	n/a	n/a	n/a	n/a	n/a	n/a		
COVID-19	n/a	n/a	n/a	n/a	n/a	n/a		
n/a: not available								
PMI: postmortem interval (days)								
co-morbidities: CI: cardiac insufficiency, COPD: chronic obstructive pulmonary disease, DM: diabetes mellitus, IHD: ischemic heart disease, RI: renal insufficiency, Tx: Transplantation								

Animals involved in the study

We used the following animals for the Spike protein trafficking study: 2-month-old wildtype C57Bl6/J mixed-sex mice purchased from Charles River Laboratories (Germany). Based on previous experience with similar models, the sample size was selected. Animals were housed in conditions that included free access to food and water, a 12-hour light/dark cycle, a temperature range of 18 to 23°C, and a humidity range of 40 to 60 percent. The animal experiments were performed according to institutional guidelines of the Helmholtz Center Munich and the Ludwig Maximilian University of Munich after approval by the Ethical Review Board of the Government of Upper Bavaria (Regierung von Oberbayern, Munich, Germany) (Vet 15-236, 19-036, 03-21-2, and 51-15) and according to the European Directive 2010/63/EU for animal experiments. All data are reported according to the criteria of ARRIVE.

2.1.2 Equipment and consumables

- UltraMicroscope II light-sheet microscope (Miltenyi Biotec)
- UltraMicroscope Blaze light-sheet microscope (Miltenyi Biotec)
- Zeiss inverted laser-scanning confocal microscope (LSM 880)
- Laser Microdissection Microscopes (Leica LMD7000)
- EASY-nLC 1200 (Thermo Fischer)
- Orbitrap Exploris 480 Mass Spectrometer (Thermo Fischer)
- timsTOF SCP (Bruker)
- Cryostat (Thermo Fischer)
- Peristaltic pump (ISMATEC, REGLO Digital MS-4/8 ISM 834)
- Glass chamber (Omnilab, cat. No. 5163279)
- Shaker (IKA, model KS 260 basic)
- pH meter (WTW, model pH7110)
- Incubator (Memmert, model UN160)
- Falcon tubes (Thermo Fisher)
- Polyethylene Naphthalate (PEN) Membrane Slides (Carl Zeiss, cat. No. 15350731)

2.1.3 Chemicals and antibodies

- 4% paraformaldehyde (PFA) (Morphisto, cat. No. 11762.01000)
- Heparin (Ratiopharm, cat. No. N68542.03)
- Ethylenediaminetetraacetic acid (EDTA) (Carl Roth, cat. No. 1410.4)
- Guanidine hydrochloride (Carl Roth, cat. No. 6069.3)
- Acetic acid (Carl Roth, cat. No. T179.1)

- Dextran, Alexa Fluor™ 647; 10,000 MW, Anionic, Fixable (Invitrogen, cat. No. D22914)
- Tetramethylrhodamine isothiocyanate–Dextran (Sigma-Aldrich, cat. No. 52194)
- p-maleimidophenyl isocyanate (Thermo Fisher, cat. No. 28100)
- Methanol (Carl Roth, cat. No. 4627.6)
- Dithiothreitol (Sigma-Aldrich, cat. No.43815)
- Propidium Iodide (Sigma-Aldrich, cat. No.P4864)
- 3-[(3-cholamidopropyl)dimethylammonio]-1-propanesulfonate (Carl Roth, cat. No.1479.4)
- N-methyldiethanolamine (Sigma-Aldrich, cat. No.471828)
- Tween-20 (Sigma-Aldrich, cat. No. P9416-100ML)
- Sodium acetate (Sigma-Aldrich, cat. No. S2889)
- DMSO (Carl Roth, cat. No. A994.2)
- Triton X-100 (Sigma-Aldrich, cat. No. T8787)
- Ethanol (Merck, cat. No. 10098535000)
- 30% hydrogen peroxide solution (Honeywell, cat. No. 15693480)
- Tetrahydrofuran (Carl Roth, CP82.1)
- Dichloromethane (Carl Roth, cat. No. KK47.1)
- BABB (benzyl benzoate and benzyl alcohol at the volume ratio of 2 to 1, Sigma-Aldrich, cat. No. W213802, cat. No. 24122)
- Goat serum (GIBCO, cat. No. 16210072)
- O.C.T. Compound (Sakura Tissue-Tek, cat. No. M71484)
- Invitrogen™ ProLong™ Gold Antifade Mountant with DAPI (Thermo Fisher, cat. No. P36931)
- SARS-CoV-2 (COVID-19) Spike RBD Protein, B.1.1.7 / Alpha variant, His tag (active), Unconjugated (Biozol Diagnostica, cat. No. GTX136014-PRO-100)
- Coronavirus (COVID-19 Spike Protein; Full Length) Antigen (ECB-LA636-100, Enzo Life Sciences), Alexa Fluor 647 Conjugation Kit (Fast) - Lightning-Link&reg (ab269823, Abcam)
- DoubleStain IHC Kit: M&R on human tissue (DAB & FastRed) (Abcam, cat. No. ab210062)

Antibodies against SARS-CoV-2 (COVID-19) Spike (GeneTex, GTX135356, GTX632604), CD31 (Abcam, ab32457), Nucleocapsid (Invitrogen, PA1-41098), ACE2 (Invitrogen, PA5-20039), CD45 (14-0451-85, Thermo Fisher), Iba1 (019-19741, Wako). Goat anti-rabbit IgG Alexa Fluor 647 (Invitrogen, A-21245); goat anti-rabbit IgG Alexa Fluor 568 (Invitrogen, A-11036); goat anti-mouse IgG Alexa Fluor 568 (Invitrogen, A-11031); goat anti-mouse IgG Alexa Fluor 647 (Invitrogen, A-21235); goat anti-rat IgG Alexa Fluor 568 (Invitrogen, A-11077). Goat anti-rabbit IgG HRP antibody (Abcam, ab6721).

2.1.4 Computer and software

The computer for data analysis is a workstation with following configurations: Intel Xeon E5-2640 v3; 256 GB RAM; NVIDIA Quadro M5000.

The softwares used are:

ImSpector (Version 7.0.53, MiltenyiBioTec GmbH), Fiji (v.1.51, https:// fiji.sc/), Imaris (v.9.6, Bitplane), Vision4D (v.3.3 ×64, Arivis), Arivis converter (v.2.12.6, Arivis), MaxQuant (version 1.6.14.0), Perseus (version 1.6.14.0), DIA-NN 1.8, GraphpadPrism (version 8), IBM SPSS Statistics (version 22.0), R studio (Version 1.4.1717), Photoshop CS6 (v. 13.0, Adobe).

2.2 Methods

2.2.1 Spike protein labeling and tissue clearing for intact human kidney

After autopsy of the COVID-19 patient, the kidney artery opening was inserted with a tubing for perfusion with PBS and lectin Alexa-647, then the kidney was fixed in 4% PFA for 7 days. Next, we washed the kidney with PBS and injected 50 ml dextran solution (4.3 mg PMPI, 7.7 mg DTT and 2 mg dextran Alexa-647 in 50 ml PBS) through the artery opening, then the kidney was sealed in a plastic bag and kept at 37°C overnight.

Pre-treatment before antibody labelling: PBS wash 3 times for 3 hours each time, CHAPS/NMDEA solution (10% CHAPS and 25% NMDEA) for 10 days, PBS wash 3 times for 3 hours each time, dehydrate with EtOH/H_2O series: 50%, 70%, 100%, 100% for 2 days each step, DCM/MeOH for 3 days, rehydrate with EtOH/H_2O series: 100%, 70%, 50% for 2 days each step, diH_2O for 1 day, 0.5 M acetic acid solution for 2 days, wash with diH_2O for 8 hours, and guanidine solution (2% Triton X-100, 0.05 M sodium acetate, and 4 M guanidine hydrochloride in PBS) for 2 days, PBS wash for 8 hours, treat with blocking buffer (10% DMSO, 10% goat serum, and 0.2% Triton X-100 in PBS) for 1 day.

Antibody labeling for Spike protein: 400 uL FluoTag®-Q anti-SARS-CoV-2 Spike protein S1 (N3501-At565-L, NanoTag) was added in 2 L antibody incubation solution (5% goat serum, 3% DMSO and 0.2% Tween-20). The kidney was treated under active pumping for 7 days. PBS wash 3 times for 1 day each time.

Tissue clearing: Dehydrate with EtOH/dH_2O series 50%, 70%, 100%, 100% for 2 days each step. DCM for 2 days, change to refractive index matching solution BABB for 3 days.

2.2.2 Deep tissue immunolabelling of human tissue

Deep tissue labeling was performed according to the protocol known in our laboratory as the SHANEL protocol. Cut 1 cm thick slices of the desired human tissue for SHANEL pretreatment. The slices were then treated twice with CHAPS/NMDEA solution for 12 hours. PBS washing for 20 minutes each three times.Tissue was dehydrated by stepwise addition of ethanol (50% x1, 70% x1, 100% x1, 4 h for each). Then the solution was replaced with DCM/MeOH (2:1, v/v) for overnight. Tissues were rehydrated stepwise in diH_2O to remove ethanol (100% x1, 70% x1, 50% x1, 4 h for each step). After treating the tissue with a 0.5 M acetic acid solution overnight, wash it twice in diH_2O for 20 minutes. After 6 hours of guanidine solution treatment, wash the tissue twice with diH_2O. Block the tissue with 10% DMSO, 10% goat serum, and 0.2% Triton X-100 in PBS at 37°C overnight and then incubate it with propidium iodide (1:1000, Sigma, P4864) or antibodies against SARS-CoV-2 (COVID-19) Spike (1:1000, GeneTex, GTX135356, GTX632604), CD31 (1:1000, Abcam, ab32457), Nucleocapsid (1:1000, Invitrogen, PA1-41098), CD45 (1:1000, 14-0451-85, Thermo Fisher), Iba1 (1:1000, 019-19741, Wako), and ACE2 (1:1000, Invitrogen, PA5-20039) in antibody incubation solution (0.2% Tween-20, 5% goat serum, 3% DMSO) at 37°C for 5 days. After primary antibodies incubation, the tissue was washed three times in PBS for 2 hours each, and then secondary antibodies (Goat anti-rabbit IgG Alexa Fluor 647, Invitrogen A-21245; goat anti-rat IgG Alexa Fluor 568, Invitrogen, A-11077; goat anti-rabbit IgG Alexa Fluor 568, Invitrogen A-11036; goat anti-rat IgG Alexa Fluor 647, Invitrogen A-21235; and goat anti-mouse IgG Alexa Fluor 568, Invitrogen A-11031) were incubated at a concentration equal to that of each primary antibody for 5 days at 37°C. The tissues were then washed for 1 hour at room temperature to remove excess antibody. Dehydrate gradually in EtOH/H_2O (50% x1, 70% x1, 80% x1, 100% x2, 6 h for each step). Treat the sections with DCM for 1 h and finally immerse in BABB. The samples will be ready for imaging after 24 hours.

2.2.3 Spike S1 protein trafficking in the whole mouse

Protein preparation and injection

The Alexa Fluor 647 (AF647) was used to tag the Spike S1 protein according to the manufacturer's instructions (AlexaFluor 647 conjugation kit lightning link,

Abcam, ab269823). Briefly, Spike S1 protein (20 µg) supplied by the manufacturer (SARS-CoV-2 (COVID-19) Spike RBD Protein, B.1.1.7 / Alpha variant, His tag (active), Unconjugated, GTX136014-PRO-100) were dissolved in 0.1 M PBS (18 µl). The modifying reagent (1 µl) was added to the Spike S1 protein solution, and then mixed gently and transferred to a lyophilized material. The reaction was stopped after 15 minutes of incubation at room temperature by adding the quencher reagent (1 µl). The concentration of the fluorine-labeled protein is 1 mg ml^{-1}. The animals were given 4% isoflurane in a N_2O/O_2 mixture (70%/30%) to induce anesthesia, and 1.5% isoflurane was used to maintain it for the entire injection. 0.1 ml PBS solution containing 1 µg AF-647 of labeled Spike S1 protein was injected intravenously into the mouse tail vein. The Spike protein was allowed to circulate throughout the mouse for 30 minutes.

Perfusion

At the 30-minute time point, intraperitoneal injection of midazolam, medetomidine, and fentanyl (1 ml/100 g of body mass) was used to deeply anesthetize mice until they exhibited no pedal reflex response. Then, the mice were perfused intracardially for 5 minutes with PBS (10 U/ml of Heparin) to remove the blood, followed by a total volume of 20 ml of TRITC-dextran (5 mg/ml, MW 500000, Sigma, 52194) for vascular labeling. Mice were then perfused with 50 ml of 4% PFA for fixation. Then, after being post-fixed in 4% PFA for a day at 4°C, the bodies underwent three 10 minute room temperature washings with 0.1 M PBS.

Clearing the whole mouse using 3DISCO method

We performed tissue clearing based on the 3DISCO protocol for whole mice as previously described (109). For this purpose, mouse bodies were incubated in gradient of THF with gentle shaking in a fume hood: 50% x1, 70% x1, 80% x1, 100% x2, 12 hours each step, then 3 hours in DCM and lastly BABB solution until optical transparency.

2.2.4 Light-sheet microscopy imaging

A Blaze or II ultramicroscope (LaVision BioTec) with an axial resolution of 4 µm was used to capture image stacks. Entire mouse bodies were scanned with the 1.1x objective (LaVision BioTec MI PLAN 1.1x/0.1 NA [WD = 17 mm]). We imaged the ventral and dorsal sides to a depth of 11 mm, with a Z-step of 10 µm, and used tiling scan of 3x8 tiles with 25% overlap. The exposure time was set to

120 ms, and the laser power was changed in accordance with the brightness of the fluorescent signal. High-magnification tile scans for multiple organs (including brain, spinal cord, intestine, thymus, liver, lung, heart, spleen, kidney, testis, and ovary) were acquired individually.

The stitching plugin of Fiji was used to process the acquired raw pictures. Stitched images were loaded to Vision4D for volume fusion, and visualized in Imaris for 3D reconstruction, analysis, and video generation.

2.2.5 Laser capture microscopy

Human lung, kidney and brain tissues were dehydrated with 30% sucrose, embedded in OCT, then sectioned into 12 um slices with a cryostat, and adhered to the ZEISS Membrane Slides PEN for histochemical staining.

Tissue slices were first washed with PBS for 10 min, immersed with 0.2% Triton X-100 and 6% goat serum in PBS for 30 min, then incubated with SARS-CoV-2 Spike protein antibody (1:300 dilution) at 4°C overnight. After washing with PBS for three times, 10 min each, the slices were incubated in secondary antibody (1:500) for 1 hour, and visualized with DAB and FastRed according to the manufacturer's instruction (Abcam, ab210062).

Regarding microdissection of the Spike protein-positive regions, we laser-cut and isolated the selected samples using a laser microdissection system (Leica, LMD7000). Briefly, the sections were serially dehydrated with ethanol and air-dried under a fume hood for 15 minutes. The Spike protein-positive and protein-negative regions of the COVID-19 human tissue sections were selected with a closed-shape manual drawing tool and dissected using a UV laser. The excised regions were collected into a 0.5 ml tube and examined by camera. An accumulated area of 6 mm^2 was collected by laser cut and using 40x objective (HC PL FL L 40x/0.60 XT CORR). The tissues were quickly spun down and stored at -80°C.

2.2.6 Histology

Immunofluorescence and confocal microscopy

Briefly, frozen sections of human skulls were treated with 0.2% Triton X-100 for 15 minutes and 10% goat serum in PBST for 40 minutes at room temperature. Incubation with primary antibodies: SARS-CoV-2 (COVID-19) Spike (1:500, GeneTex, GTX135356, GTX632604), Nucleocapsid (1:500, Invitrogen, PA1-

41098), ACE2 (1:500, Invitrogen, PA5-20039), and NeuN (1:500, Invitrogen, PA5-78499) was performed overnight at 4°C. Next, the sections were washed for 15 min, incubated with secondary antibodies (1:1000, goat anti-mouse IgG Alexa Fluor 647, Invitrogen, A-21235; goat anti-rabbit IgG Alexa Fluor 647, Invitrogen, A21245; goat anti-rabbit IgG Alexa Fluor 568, Invitrogen, A-11036; goat anti-mouse IgG Alexa Fluor 568, Invitrogen, A-11031; goat anti-rat IgG Alexa Fluor 568, Invitrogen, A-11077) for 1 hour. After Hoechst 33342 staining, sections were mounted and a confocal microscope (ZEISS LSM880) was used to capture the images.

Immunohistochemistry (IHC)

Briefly, frozen sections were treated with 0.2% Triton X-100 for 10 min, 3% H_2O_2 for 10 min, 10% goat serum for 20 min, and incubated with primary antibody against SARS-CoV-2 (COVID-19) Spike (1:300, GeneTex, GTX135356) at room temperature for 1 h. Staining was detected with goat anti-rabbit IgG HRP antibody (1:300, Abcam, ab6721) and revealed by incubation with diaminobenzidine for 10-20 seconds (Vector, VEC-MP-7714). Hematoxylin (Sigma, 51275) was used as counterstaining. Prussian blue staining was performed according to manufacturer's instruction (NovaUltra, IW-3010).

2.2.7 SARS-CoV-2 RT-PCR test

Decalcified COVID-19 skull samples were minced in PBS; the tissue extract from the COVID-19 meninges samples was put through a 40 µm strainer after being ground in liquid nitrogen and reconstituted in PBS. RNA extraction was performed using RNeasy FFPE Kit (QIAGEN, 73504), followed by SARS-CoV-2 RT-PCR with the Seegene Allplex™ 2019-nCoV Assay (cat. no: RP10243X) on a CFX96 Real-time PCR Detection System-IVD (Bio-Rad).

2.2.8 Statistical analysis

Prism 8.0 (GraphPad) was used for statistical calculations. The data was analyzed with Shapiro-Wilk normality test and had Gaussian distribution. To compare two means, two-tailed *t* tests were performed. All figure legends list the statistical analyses that were conducted. The mean and standard deviation are displayed for each data point.

2.2.9 Proteomics

Sample preparation for mass spectrometry analysis

The human samples comprised eight post-mortem samples of human skull and meninges tissues from COVID-19 deceased and control donors. Protein extraction was carried out from 4% neutral buffered formalin fixed tissues. Briefly, the cells from the skull and the meninges tissues were isolated by mincing or grinding, and the tissue extract was passed through 40 µm strainer. The cell pellet was washed with PBS and reconstituted in SDS-lysis buffer (6% Sodium dodecyl sulfate, 500 mM TrisHCl, pH 8.5). The samples were heated at 95°C in a thermomixer for 45 min with 1000 rpm, then subjected to ultrasonication using a Bioruptor Pico sonication device operated at high frequency for 30 sec on and off for 30 cycles. After ultrasonication, the samples were again heated at 95°C for 45 min with 1000 rpm in a thermomixer. This was followed by proteins precipitation in ice-cold acetone (80% v/v) overnight in -80°C, and centrifugation for 15 min at 4°C. The proteins were resuspended in SDC solution and heated at 95°C for 10 minutes with 1000 rpm for reduction and alkylation. The samples were digested with trypsin and LysC at a ratio of enzyme to substrate of 1:50 at 37°C overnight, 1000 rpm in s thermomixer. Next, peptides were acidified using 1% TFA in 99% isopropanol in 1:1 v/v ratio. The peptides were subjected to in-house built StageTips made up of two layers of styrene divinylbenzene reversed-phase sulfonate (SDB-RPS; 3 M Empore) membranes. Peptides were loaded onto activated StageTips (100% ACN, 1% TFA in 30% Methanol, and 0.2% TFA), passed through the SDB-RPS membranes, and then washed with 1% TFA containing EtOAc, 1% TFA containing isopropanol, and 0.2% TFA, respectively. Peptide elution was carried out in 60 µL of 1.25% Ammonia, 80% ACN and dried for 40 min with SpeedVac (Eppendorf, Concentrator plus) at 45°C. Reconstitution of dried peptides was performed with 10 µL 2%ACN/0.1%TFA, the concentration was estimated using Pierce™ Quantitative Colorimetric Peptide Assay.

Liquid chromatography and mass spectrometry (LC-MS/MS)

The MS data was generated in both data dependent acquisition (DDA) as well as data independent acquisition (DIA) mode. Thermo Fisher Scientific's EASY-nLC 1200, together with an Orbitrap Exploris 480 mass spectrometer and a nano-electrospray ion source, were employed for the DDA analysis. With a flow rate of 300 nL/min, peptides were segregated via reversed-phase chromatography that used a binary buffer system containing 0.1% formic acid and a 120-minute gradient of 80% ACN in 0.1% formic acid (5-30% for 95 min, 30-65% for 5 min, 65-95% for 5 min, and wash with 95% for 5 min).

A data-dependent cycle time (1 second) scan approach was used to gather MS data. Full scan MS targets had an automatic gain control target percentage of 300 and were scanned in the 300–1650 *m/z* range. The data was acquired at 60000 resolution with a maximum injection time of 25 ms. Higher-energy C-trap dissociation with a normalized excitation energies at thirty pencent is used to fragment MS/MS scan precursor ions. The maximum injection time for MS/MS scan sets was 28 ms, with an AGC target of 100% and a 15000 resolution. For DIA mode, Thermo Fisher Scientific's EASY nanoLC 1200 was used for the LC-MS/MS analysis, together with a CaptiveSpray nano-electrospray ion source, quadrupole time-of-flight single cell proteomics mass spectrometer, and trapped ion mobility spectrometry. 50 ng of peptides was loaded onto a 25 cm Aurora Series UHPLC column with CaptiveSpray insert (75 µm ID, 1.6 µm C18) at 50°C and segregated using a gradient of 80% ACN in 0.1% formic acid at a flow rate of 300 nL/min for 50 min (5-20% for 30 min, 20-29% for 9 min, 29-45% for 6 min, 45-95% for 5 min, 95% for 5 min, 95-5% for 5 min). MS data were acquired in single-shot library-free DIA mode and the timsTOF SCP was run with DIA/parallel accumulation serial fragmentation (PASEF) using the high sensitivity detection-low sample amount mode. The ion accumulation and ramp time was set to 100 ms each. The collision energy scaled linearly from 59 eV at 1/K0 = 1.6 V-s cm^{-2} to 20 eV at 1/K0 = 0.6 V-s cm^{-2} as a function of the mobility. The isolation windows were defined as 24 X 25 Th from m/z 400 to 1000.

Proteomics data processing

The DDA files were handled with MaxQuant 1.6.14.0. Filtering at the level of proteins, peptides, and modifications was done using FDR 0.01. Acetylation (protein N-term) and oxidized methionine (M) were chosen as variable modifications, and carbamidomethyl (C) was taken as a fixed modification. Proteolytic cleavages using LysC and trypsin/P were included. The number of missed cleavages that permitted protein analysis was 2. Label free quantitation (LFQ) and "Match between runs" were enabled, and the human Uniprot database was used for all queries. DIA-NN was used to search the human Uniprot database against the diaPASEF raw files (128). The search of peptides with N-terminal acetylation was performed for a length range of seven amino acids. Cysteine carbamidomethylation was regarded as a fixed modification and methionine oxidation as a variable modification. Trypsin/P with two missed cleavages was the chosen enzyme specificity. The FASTA digest for the library-free search was enabled for predicting the library generation. The global and precursor levels of the FDR were both set to 1%. The "Robust LC (high precision)" quantification mode was selected, and the Match-between-runs (MBR) option was activated. Identification of the protein

group and PG was done using the Protein Group column in the DIA-NN report. The differential expression was calculated with MaxLFQ.

Proteomics downstream data analysis

The protein groups were filtered using Perseus and R studio such that only those proteins were considered for differential expression which were present in 3 out of 4 samples in each group with valid values. The values were log2 transformed and normalized with median centering the dataset. A Gaussian distribution with a range of 0.3 standard deviations and a downshift of 1.8 standard deviations was used to generate the missing values at random. The correlation heatmap was computed using the Pearson correlation coefficient. Differential protein expression of the COVID-19 compared to control groups was evaluated by student-*t* test. Multiple comparisons were adjusted using the Benjamini-Hochberg method. p-value less than 0.05 and a fold change greater than 1.5 were considered statistically significant unless specified. The gene ontology (GO) and pathway enrichment were performed in Cytoscape with ClueGO plug-in (129) or ClusterProfiler. PCA plot, volcano plot, GOChord plot, and heatmap were generated in R studio.

3. Results

3.1 Optimization of tissue clearing method for human organs

In comparison to organs from young experimental animals, human organs have substantially bigger volumes and include more complicated tissue constituents because of the effects of aging. This limits the post-staining methods that may be employed on human organs. To overcome the challenges in achieving transparency of whole human organs, we have standardized the SHANEL protocol and effectively cleared several human organs, such as the lung, heart, pancreas, kidney, and spleen (Fig. 4) (122).

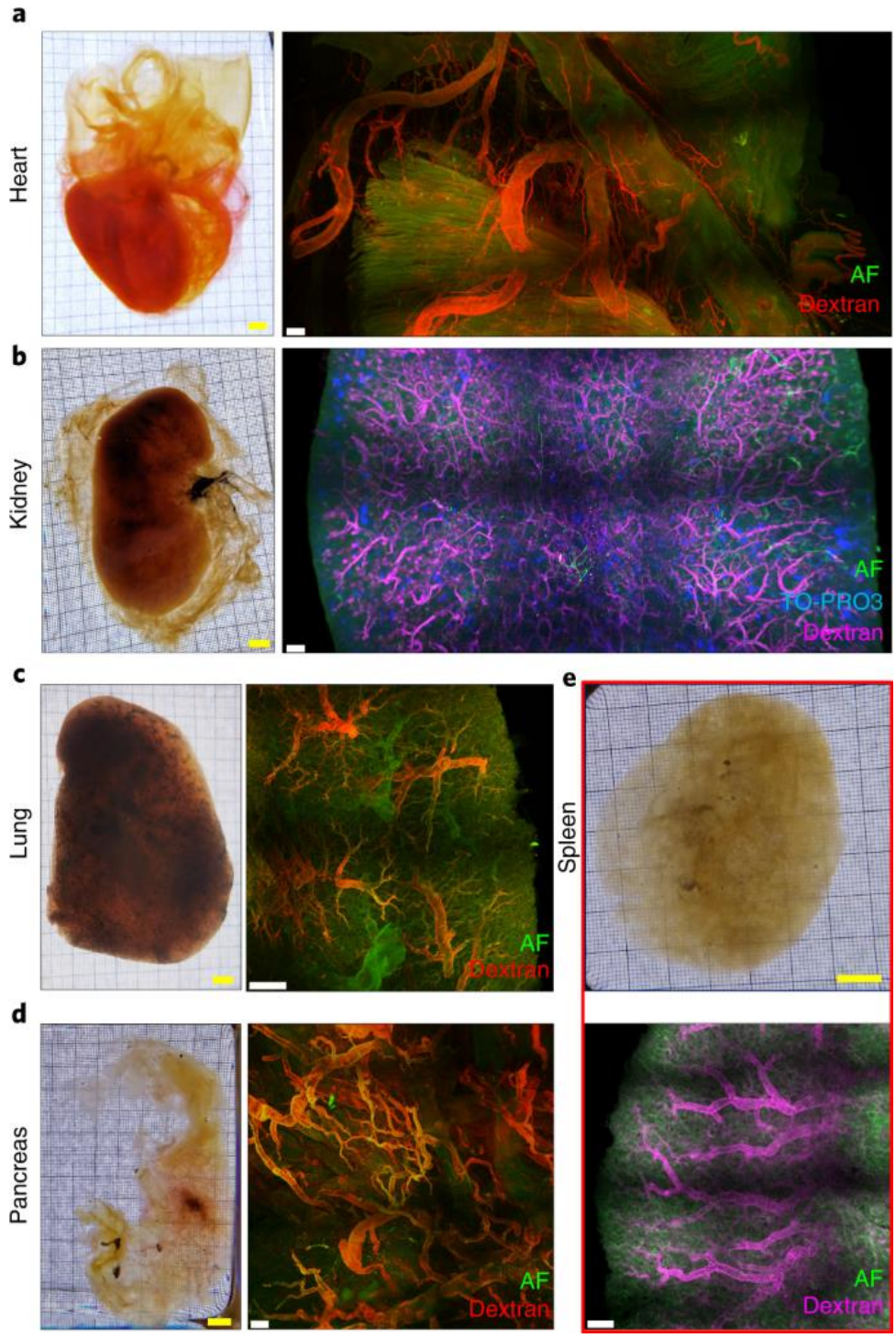

Figure 4. Tissue clearing and imaging of human organs with the SHANEL protocol (122)**:** TRITC-dextran was used to label the vasculature of human heart, kidney, lung, pancreas, and spleen. Tissue autofluorescence (AF) was imaged with excitation of 488 nm wavelength. Scale bars: 1 cm (yellow) and 2 mm (white).

3.2 Heterogenous infection patterns of COVID-19 patient organs

3.2.1 Volumetric investigation of SARS-CoV-2 Spike protein in lung, kidney, and brain of COVID-19 patients

We aim to inspect the lung tissue in a large-scale 3D view rather than in micrometer-thick sections. Therefore, 1 cm^3 lung tissue blocks were treated with SHANEL protocol and stained with antibodies including Spike protein, ACE2, and Iba1. We found the Spike protein distributed heterogeneously in the lung of COVID-19 patients, as we can see accumulation in some specific regions while other regions show minor infection, and there is a negative correlation between ACE2 level and Spike protein level. As a control, we did not find a signal of Spike protein in lungs from patients not infected with COVID-19 (Fig. 5).

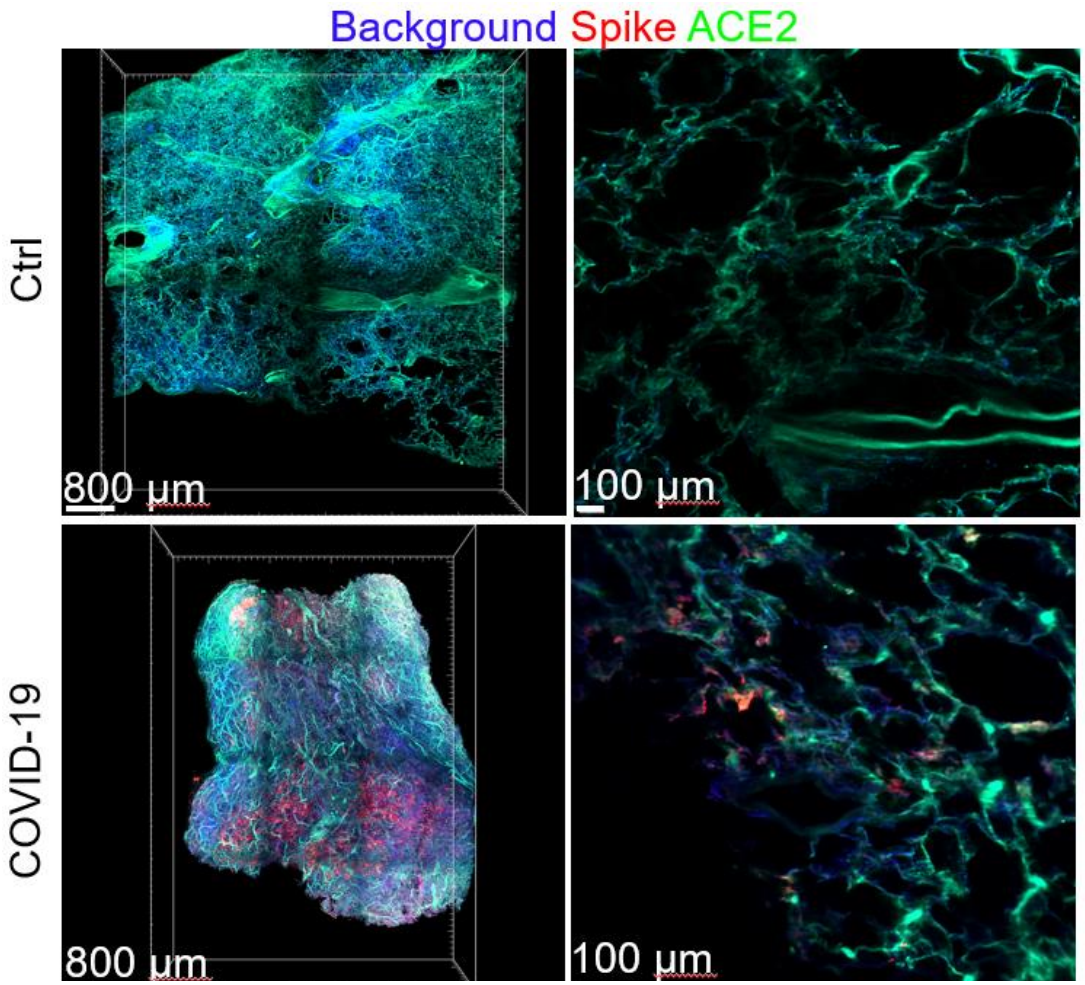

Figure 5. Heterogeneous SARS-CoV-2 infection in human lung. Representative images of Spike protein and ACE2 staining in human lung tissue block. Scale bars: 800 µm (3D reconstruction), 100 µm (2D section).

Using Iba1 antibody staining in lung tissue block, we identified massive macrophage infiltration in the lung of COVID-19 patients (Fig. 6).

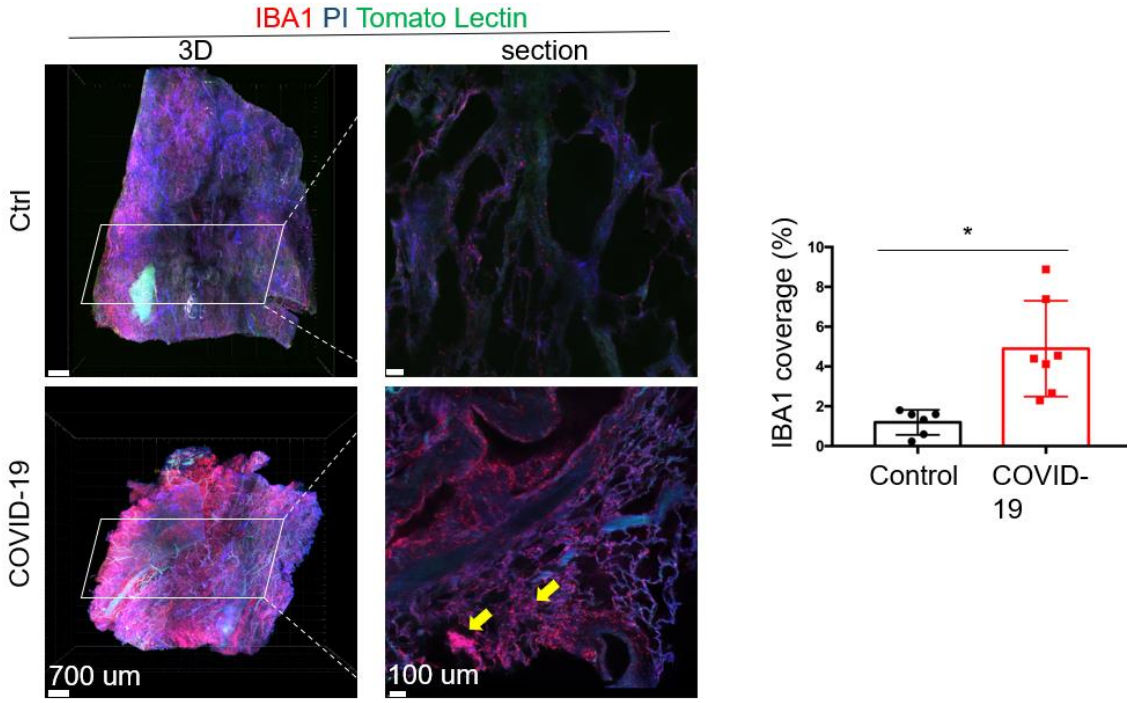

Figure 6. Massive macrophage infiltration in lung of COVID-19 patients. Representative images of Iba1 and PI staining in human lung tissue block. Scale bars: 700 µm (3D reconstruction), 100 µm (2D section). Quantification of the Iba1 positive area in 6 fields of view. *n* = 3. Data represent mean ± SD. Two-tailed unpaired Student's *t*-test. *p < 0.05.

Additionally, we confirmed Spike protein in the lung tissue of COVID-19 patients using traditional IHC staining, and detected evidence of lung fibrosis in the COVID-19 cases, which was determined by picrosirius red staining in lung sections (Fig. 7).

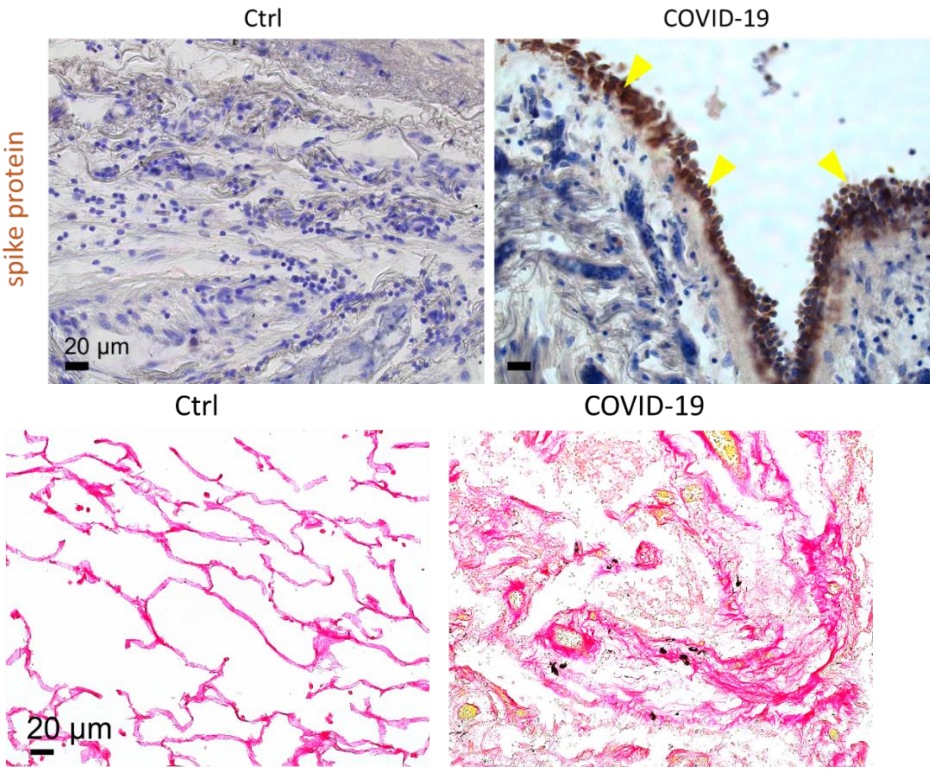

Figure 7. IHC staining of Spike protein and picrosirius red staining (PSR) in lung tissue. Spike protein is shown in brown, and cell nucleus in blue. Scale bars: 20 µm.

Meanwhile, we inspected one intact kidney from a COVID-19 patient by labeling the kidney with anti-SARS-CoV-2 Spike protein S1 nanobody and dextran following SHANEL protocol. After optical transparency, we scanned the kidney with a light-sheet microscope (Fig. 8).

The signal of Spike protein showed infection mainly in the cortex of the kidney, and by zooming-in to different regions, we can see the Spike protein enriched in some glomeruli and collecting ducts. This result is in line with research showing that SARS-CoV-2 directly infects human kidney tissues (53).

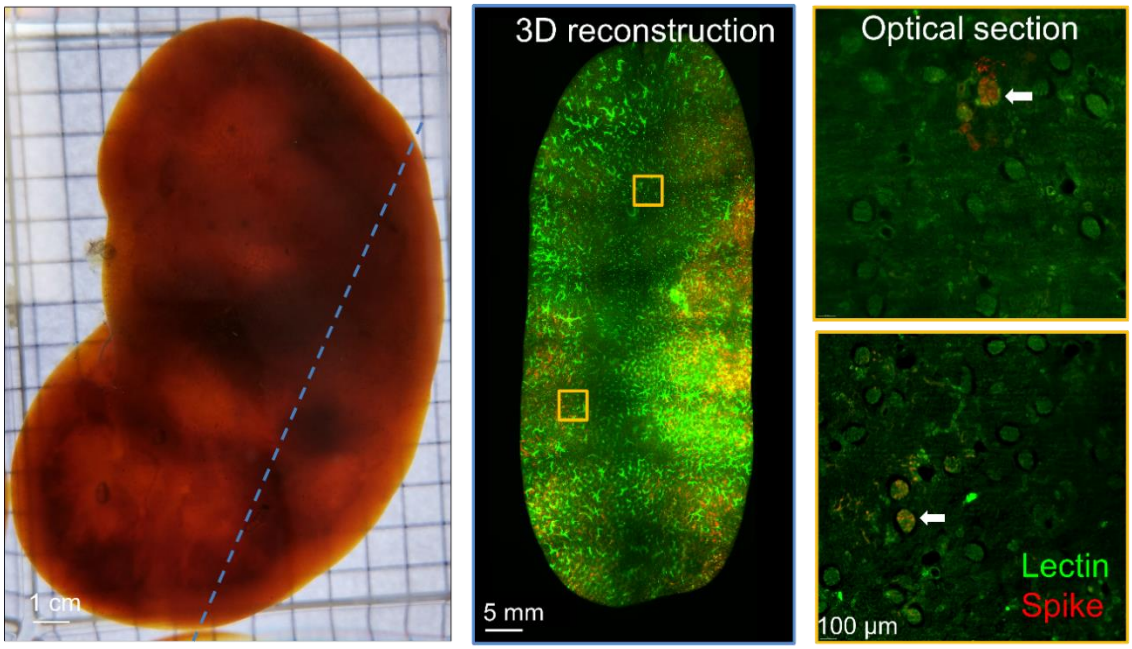

Figure 8. SHANEL enabled visualization of Spike protein in an intact kidney. The kidney was labeled with lectin for vasculature and SARS-CoV-2 Spike protein nanobody. The white arrow indicates the infected regions in this kidney. Scale bars: 1 cm, 5 mm (3D reconstruction), and 100 µm (2D section).

Since COVID-19 patients share common neurological and neuropsychiatric complications, we next investigated the effects of SARS-CoV-2 on the brain. Using volumetric imaging of cleared brain tissues of COVID-19 patients' prefrontal cortex, we found Spike protein in the brain parenchyma, some of which colocalized with the neurons as identified by Nissl staining. Interestingly, the meninges also harbor virus Spike protein (Fig. 9).

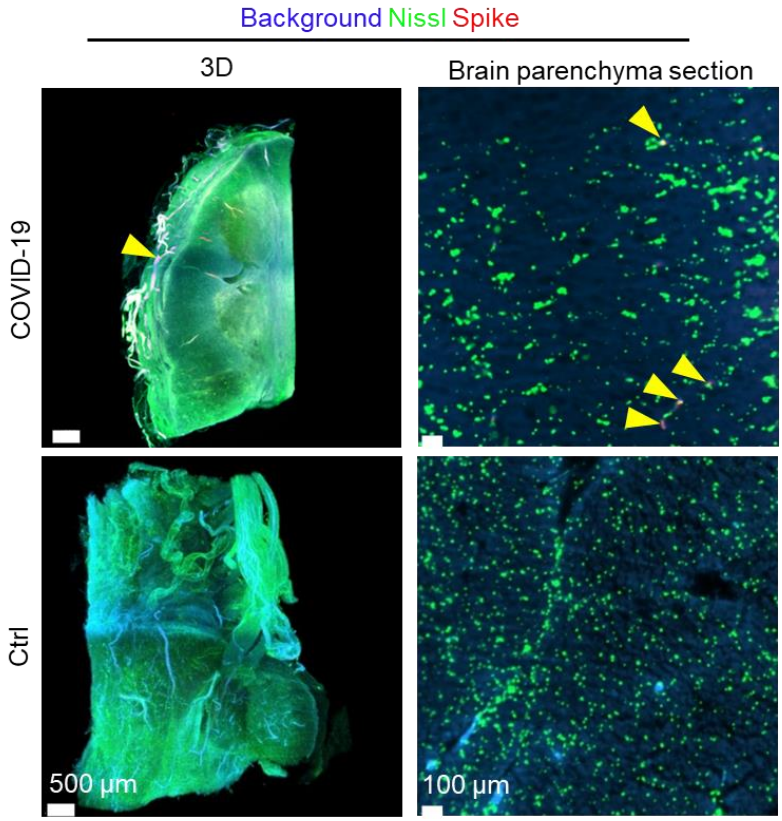

Figure 9. Spike protein and Nissl staining of brain tissue block. Representative images of Spike protein antibody and Nissl labeling in the human brain tissue block. Samples from patients not infected with COVID-19 were used as control. Yellow arrowheads indicate Spike protein in meninges (left) and colocalization with neurons (right). Scale bars: 500 µm (left), 100 µm (right).

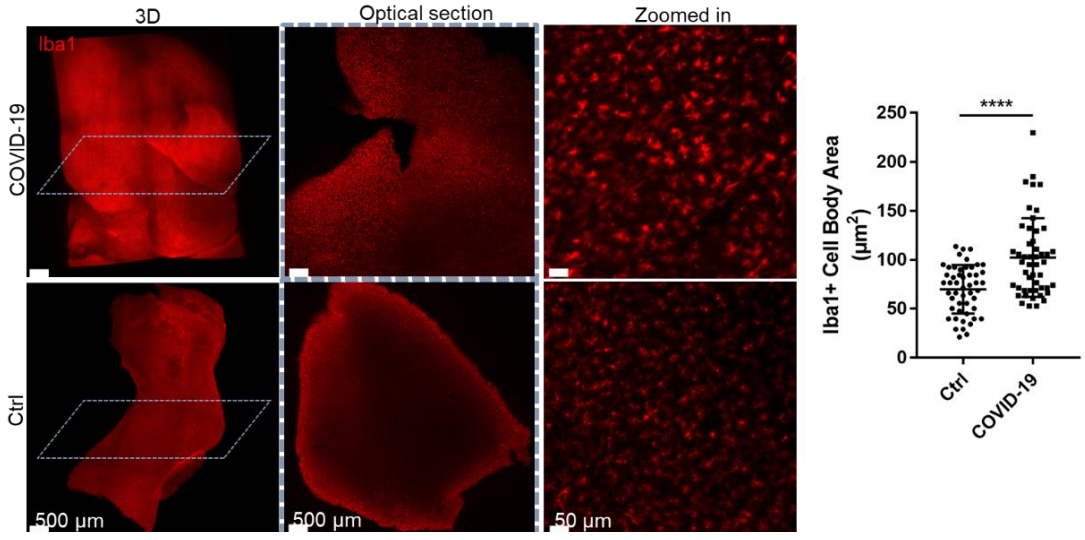

Figure 10. Iba1 staining of brain tissue block. Representative images of Iba1 antibody staining and light-sheet imaging of human brain cortex. Samples from patients not infected with COVID-19 were used as control. Scale bars: 500 µm (left and middle), 50 µm (right). Quantification of microglia cell body area, each filled dot represents the area of an individual microglia soma. *n* = 3 brain cortex blocks from two COVID-19 patients and one control. Graph displays mean ± SD. Two-tailed unpaired Student's *t* test, ****p < 0.0001.

Microglia are specialized macrophages in the central nervous system. They will retract the ramified processes and have an increased soma size when stimulated by infection or inflammation (130). Using Iba1 antibody staining, we identified activated microglia with enlarged cell body morphologies in the brain of COVID-19 patients (Fig. 10).

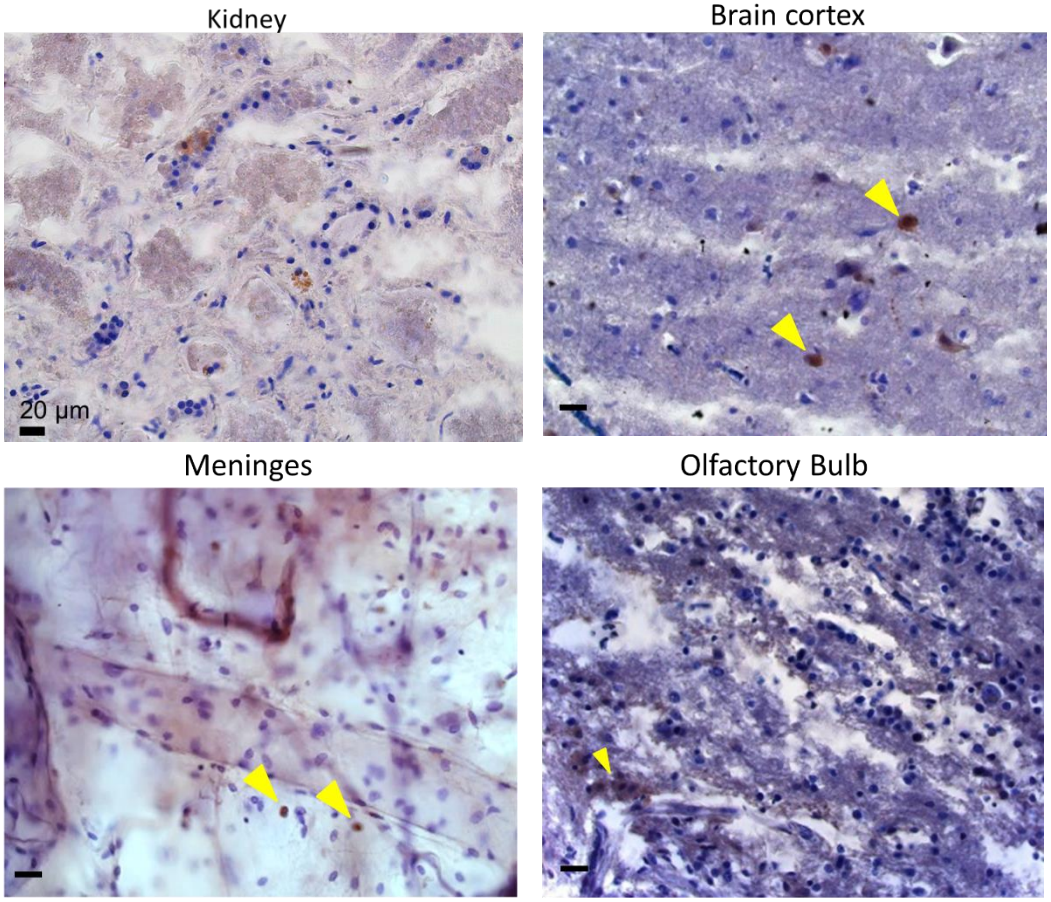

Figure 11. Immunohistochemistry of kidney and brain. Spike protein staining in kidney, brain and meninges sections, revealed with HRP-DAB in brown, cell nucleus in blue. Scale bars: 20 µm.

On the other hand, Spike protein was examined with traditional IHC methods and detected in the lung, olfactory bulb, brain cortex, and meninges tissue of COVID-19 patients (Fig. 11).

3.2.2 Spatial proteomics of lung, kidney, and brain of COVID-19 patients

To explore the molecular consequences of the lung, kidney, and brain tissue in the presence of Spike protein, we performed laser capture microdissection of the IHC Spike protein-positive and negative regions for proteomics analysis (Fig. 12).

We identified that ARG1, TIMP3, CXCL12, ALDOB, ACY1, and CLIC1, are up-regulated in the lung Spike positive region. ARG1 has been associated with the suppression of antiviral immune responses and could be a marker in the pathogenesis of COVID-19 (131). TIMP3 has been reported to interact with ACE2 (132).

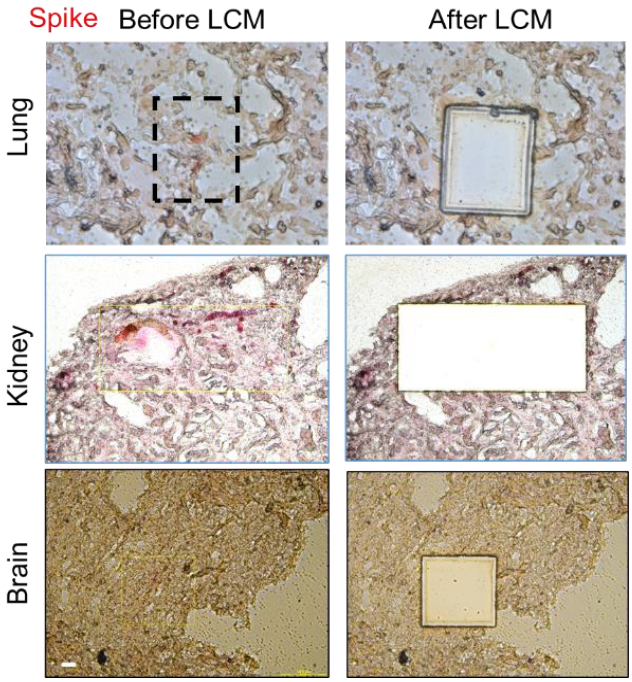

Figure 12. Overview of laser capture microdissection for proteomics study. Representative images showing the Spike protein positive region (red) before and after dissection. Scale bars: 20 µm.

CXCL12 is an inflammatory cytokine that has been reported to increase more than 10-fold in COVID-19 plasma compared to healthy donors (133) and is associated with T cell infiltration (134). The role of ALDOB and ACY1 in COVID-19 remains unclear. CLIC1 is required for the regulation of endolysosomal pH, and silencing of CLIC1 decreases infection by hepatitis C virus (135). It could be a possible target for antiviral strategies against SARS-CoV-2 (Fig. 13).

Gene ontology analysis suggests enrichment in the collagen-containing extracellular matrix, cell adhesion molecule binding, and cadherin binding are the evident changes in the Spike protein-positive lung region, correlating to the fibrosis we have observed in the lung tissue (136,137).

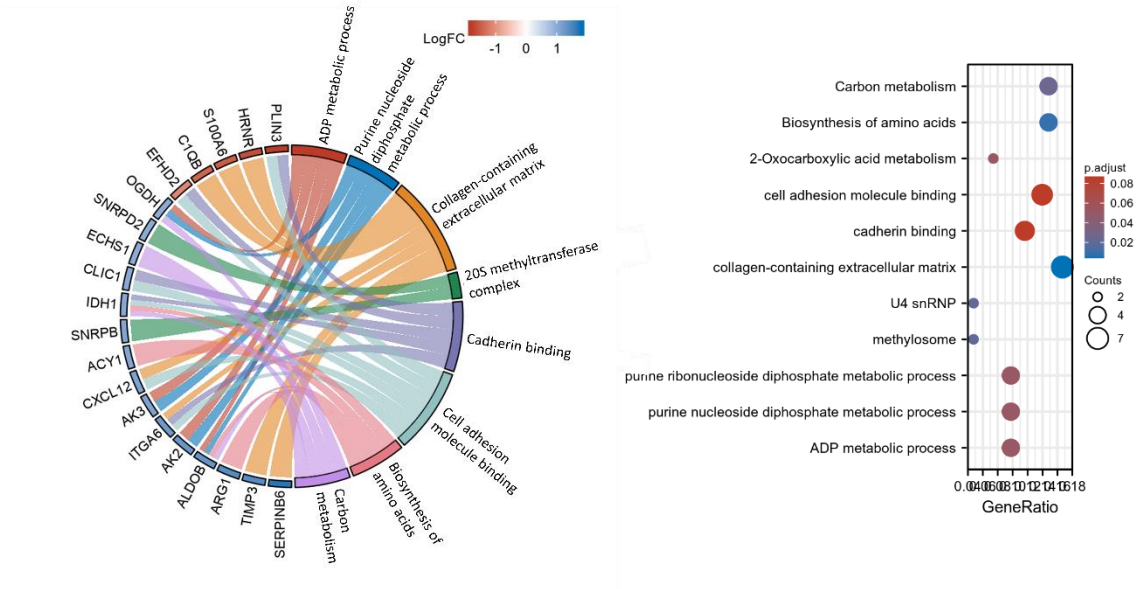

Figure 13. Proteomics analysis of lung tissue of COVID-19 patients. Dysregulated proteins and gene ontology registration of Spike protein positive lung region compared to Spike protein negative lung region. ($p < 0.05$, logFC = 1). *n* = 3 biological replicates.

In the kidney, dysregulated proteins in the Spike protein positive region compared to the Spike protein negative region consists of ribosomal subunit proteins like RPL5, RPL35, RPL4, RPL7, RPL8, RPS3, RPS5, and RPS8, they engage in interactions with viral non-structural proteins and are necessary for viral replication. Previous plasma proteomics study reported apolipoprotein APOD dysregulation in COVID-19 (138). Mitochondrial protein UQCRB is upregulated in COVID-19 bronchoalveolar lavage (139). In our study, we also identified some other dysregulated mitochondrial proteins in the kidney: COX7A2, UQCRQ, UQCRC1, NDUFA5, ATP5F1A, ATP5F1B, and ATP5F1C. It is reported that SARS-CoV-2 causes apoptosis in mitochondria from epithelial cells (140). Heat shock protein is involved in viral entry, replication, and viral exit from host cells (141). We found that HSPA8 and HSPA2 decreased in Spike protein-positive kidney tissue (Fig. 14).

Gene ontology analysis also identified changes in the cytosolic ribosome, structural constituent of ribosome, and focal adhesion, cadherin binding,these extracellular matrix changes are associated with fibrosis.

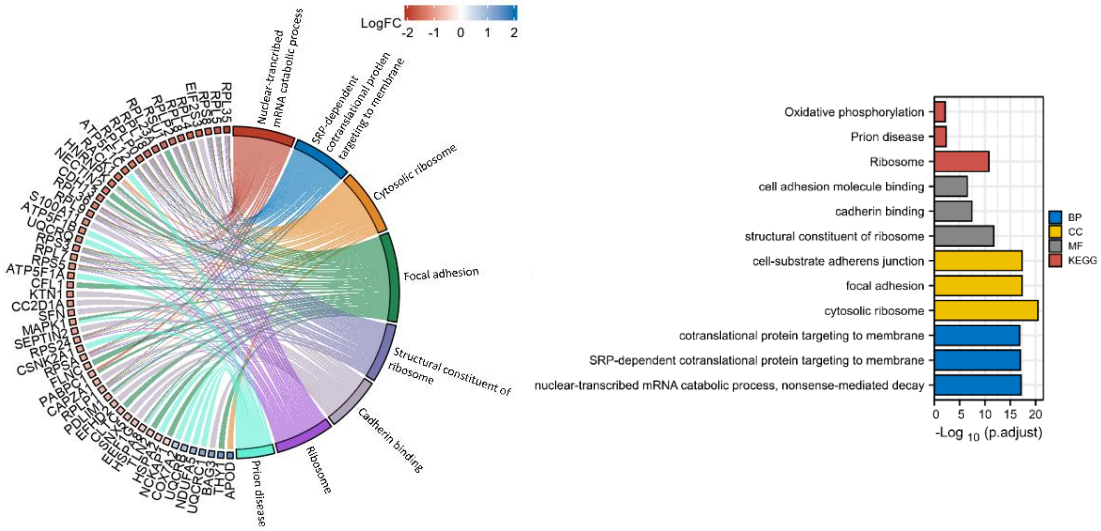

Figure 14. Proteomics analysis of kidney tissue of COVID-19 patients. Chord plot and gene ontology of dysregulated proteins between Spike protein-positive and negative kidney regions. ($p < 0.05$, logFC = 1). *n* = 3 biological replicates.

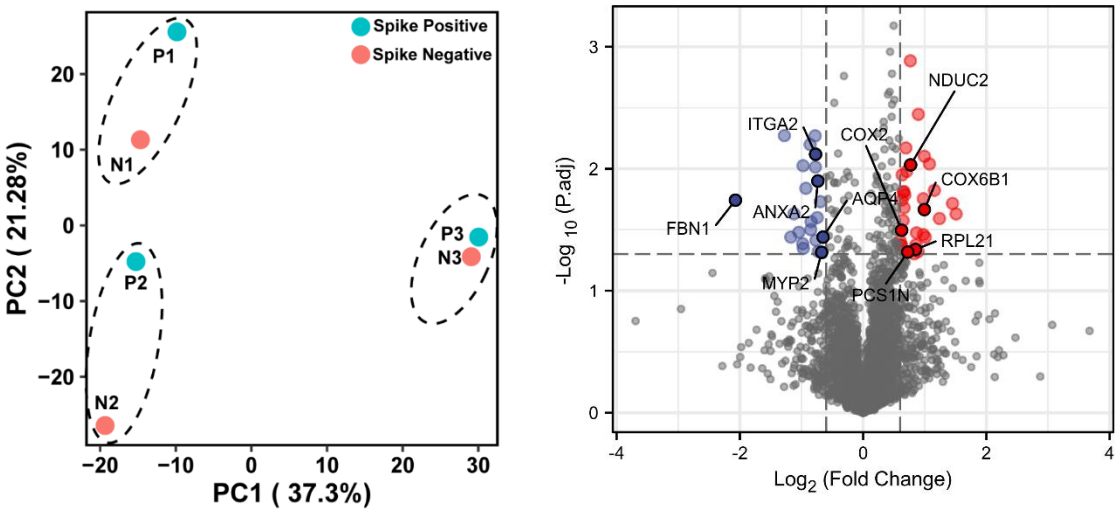

Figure 15. Proteomics analysis of brain tissue of COVID-19 patients. PCA plot of Spike protein positive and negative samples and volcano plot between Spike protein positive and negative brain regions. ($p < 0.05$, logFC = 1). *n* = 3 biological replicates.

Regarding proteomics, principal component analysis (PCA) showed clustering of samples from the same patient and a similar shift from Spike protein negative brain regions to Spike protein positive brain regions in all three patients (Fig. 15).

SARS-CoV-2 infection has been linked to mitochondrial dysfunction (142). We identified several upregulated mitochondrial proteins in our Spike-positive brain regions compared to the Spike-negative regions (Fig. 15). The list includes proteins such as NADH dehydrogenase [ubiquinone] 1 subunit C2 (NDUC2), Cytochrome c oxidase subunit 6B1 (QCR1) and Cytochrome c oxidase subunit 2 (COX2). However, their exact roles in COVID-19 pathogenesis have, to our knowledge, not been investigated in detail yet. The water-specific channel protein Aquaporin-4 (AQP4) was also identified as a downregulated protein. The expression of this protein could link COVID-19 to neurological disorders that may arise together with brain edema (143). Notably, patients with neuromyelitis optica present auto-antibodies against AQP4 (144). The extracellular matrix protein Fibrillin-1 (FBN1) was another downregulated protein. The expression levels of Annexin A2 (ANX2) predict mortality among hospitalized COVID-19 patients (145). Integrin alpha-2 (ITGA2) was also downregulated in the Spike-positive tissues. Integrins, in particular, have been implicated in the internalization of the SARS-CoV-2 (146).

3.3 A mouse model to study SARS-CoV-2 Spike protein S1 distribution

Recent studies showed the use of Spike protein subunit as a proxy to explore SARS-CoV-2 targeting and pathology in mice (147–149). We used intact transparent mice to map the distribution of the fluorescently labeled Spike S1 protein in order to determine all tissues that SARS-CoV-2 can infect. TRITC-dextran was injected intravenously together with Spike protein to visualize the blood vessels. After 30 minutes, we rendered the entire mouse body optically transparent using the 3DISCO method as described previously (109). We then used light-sheet microscopy to image the cell-level biodistribution of Spike protein throughout the transparent mouse bodies unbiasedly (Fig. 16).

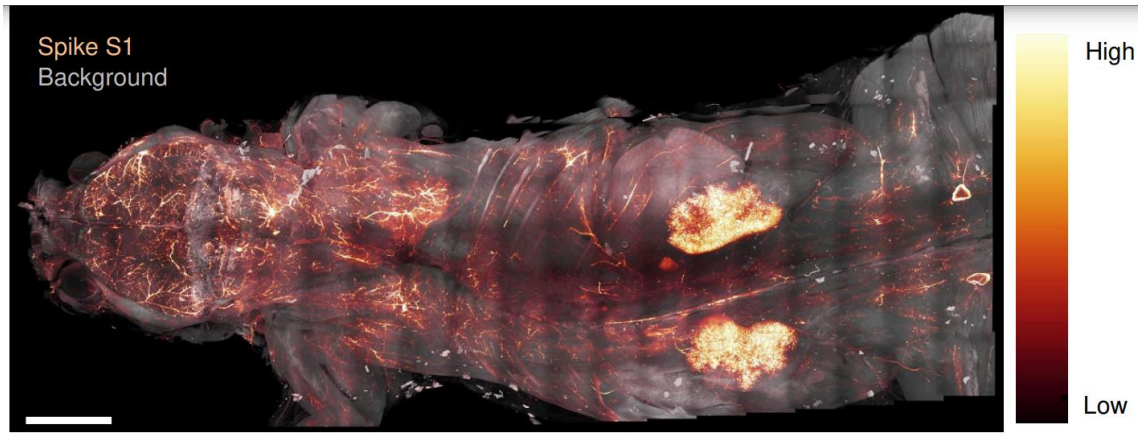

Figure 16. Spike S1 distribution in whole mouse body. S1 protein was graded colored by intensity. Scale bar: 4 mm.

We found Spike S1 protein binding in the heart, lung, liver, kidney, gut, thymus, spleen, and pancreas, among other organs (Fig. 17). The distribution within each organ was heterogeneous, with some regions of the organ depicting more Spike protein accumulation than others (Fig 1b, arrowheads vs. arrows). In particular, we found that the Spike S1 protein accumulated in and around areas with a high density of blood vessels in the liver, kidney, and lung, consistent with the known ACE2 expression pattern, an enzyme widely expressed in various organs in the body and serving as the receptor of SARS-CoV-2 (31,32). The fact that Spike S1 protein is present in all of these organs strongly suggests that multiple organ tropism of either the full virus or protein extrusions from the viral particles causes the widespread body pathology of SARS-CoV-2.

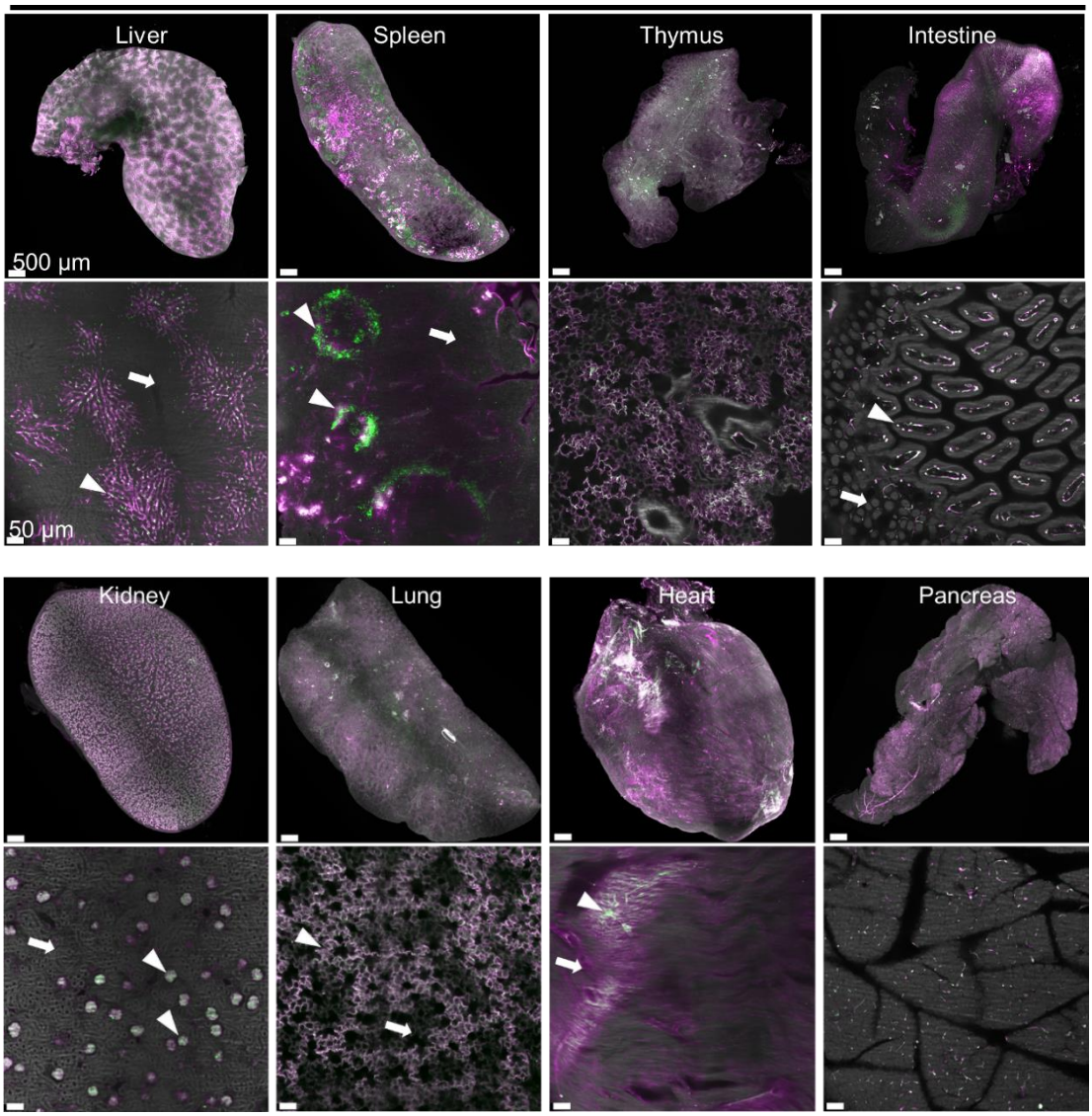

Figure 17. 3D reconstruction of main internal organs and representative high-resolution optical section view. Spike S1 protein in green and dextran in magenta. Arrow heads and arrows indicate regions with and without Spike S1 protein, respectively. Scale bars: 500 µm and 50 µm.

We found that most of the Spike S1 protein signal from the abdomen was in the capillary bed, and according to the morphological structure of tissues, we inferred that Spike S1 protein localized in liver Kupffer cells, spleen follicles, glomeruli, and alveoli.

Spike S1 protein was also found in the brain, spinal cord, and parenchyma of the testis and ovary (Fig. 18). It is worth mentioning that the presence of virions was also reported in human patient testis (150).

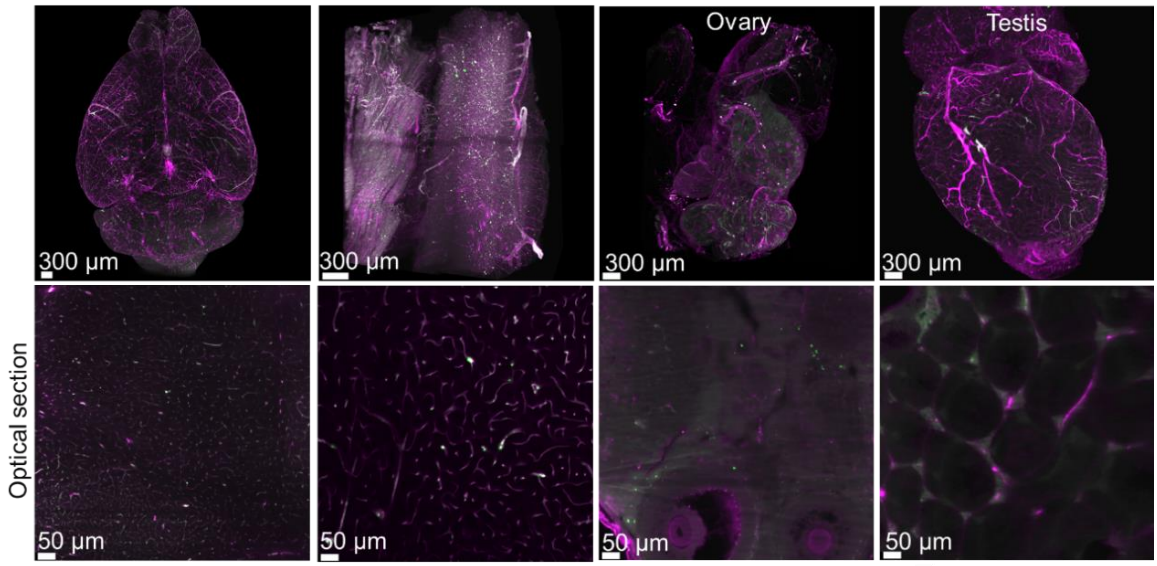

Figure 18. Spike S1 protein in the mouse central nervous system and reproductive system. Spike S1 protein in green and dextran in magenta. Scale bars: 300 µm and 50 µm.

To further confirm that the binding of the injected Spike protein to the ACE2 receptor is specific, we used ovalbumin as a control. Unlike Spike protein, ovalbumin is mainly detected in the kidney, liver, and spleen (Fig. 19). Interestingly, the pattern of ovalbumin and Spike is different in the kidney and spleen, the binding region in the kidney appears to be the renal collecting duct rather than glomeruli, and ovalbumin does not accumulate in spleen follicles. No ovalbumin is found in the brain, lung, pancreas, heart, or intestine.

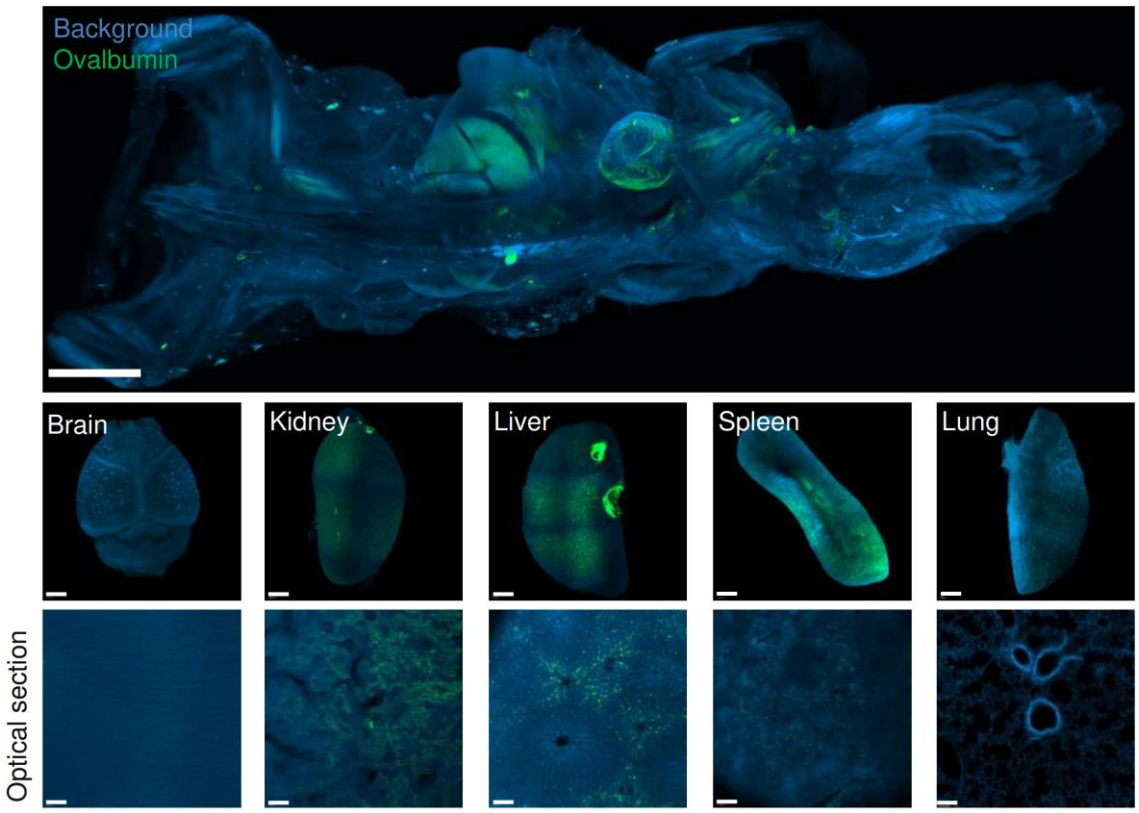

Figure 19. Tissue specificity of Spike S1 and ovalbumin binding to mouse organs. Fluorescently conjugated ovalbumin as a control for inspecting Spike S1 protein binding in intact mice. Scale bars: 4 mm (top), 500 µm (middle), 50 µm (bottom).

Next, to check whether this Spike S1 protein injection model mimics human infections, we stained the human tissue from COVID-19 patients with Spike antibodies, and compared the Spike S1 protein distribution in mouse models to the COVID-19 patient tissue. We found a similar pattern of Spike protein in different organs (Fig. 20). There are many proteins in the lung alveolar, and we found Spike protein mainly binding to glomeruli in the kidney. A few Spike proteins can be found in the brain perivascular space, confirming the validity of Spike S1 protein imaging in whole transparent mice as a proxy for human tissue investigation.

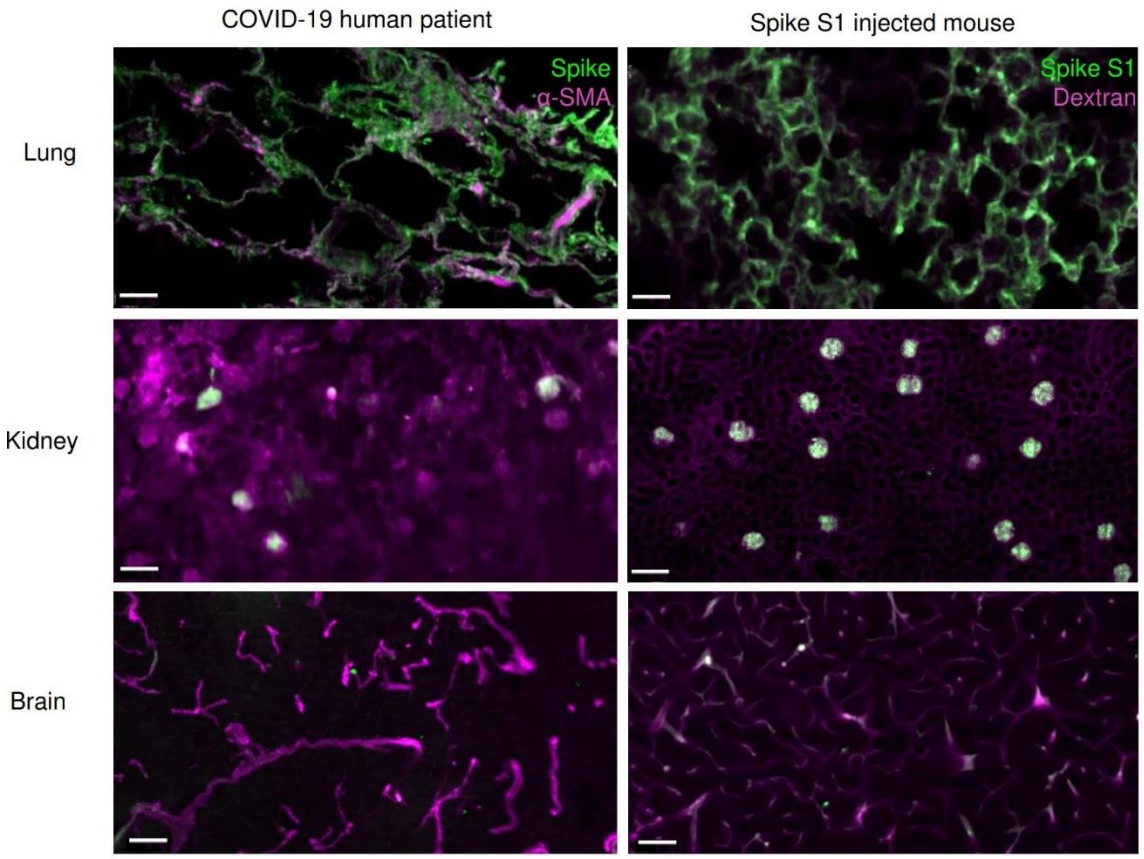

Figure 20. Comparison of the Spike protein in COVID-19 patient tissues and the Spike S1 protein in mouse tissues. Vasculature was labeled with αSMA antibody and dextran in human and mouse tissues. Scale bars: 100 μm (left), 50 μm (right).

We then addressed how SARS-CoV-2 might impact the brain by examining the heads of mice injected with Alexa-647-conjugated Spike S1 protein (Fig. 21). We found substantial Spike protein accumulation in the skull marrow niches. Notably, we detected the Spike protein in the channels connecting the skull bone marrow and the meninges, suggesting translocation of Spike S1 protein between the skull and meninges. Similarly, the Spike S1 protein accumulated in the marrow of other mouse bones including the tibia and femur, indicating its capacity to reach bone marrow niches in general (Fig. 22). As control, ovalbumin was not detected in brain or bone marrow.

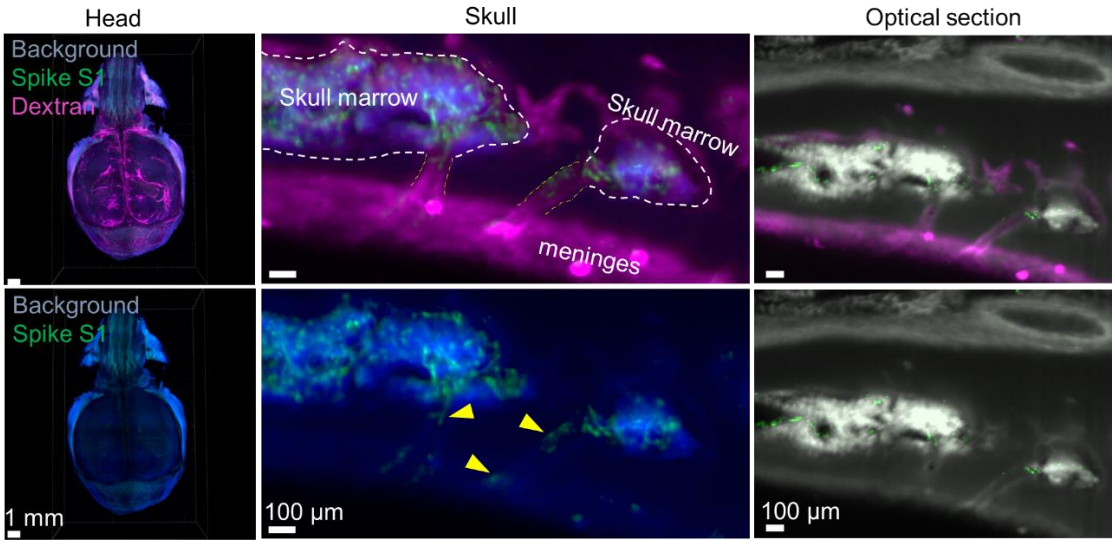

Figure 22. Spike S1 protein homes in mouse CNS borders: skull marrow and meninges. Visualization of Spike S1 protein in the intact mouse head. Scale bars: 1 mm. Representative sagittal images of the skull bone marrow, SMCs, and meninges. Arrow heads indicate Spike S1 protein in SMCs. Arrow heads indicate Spike S1 protein in SMCs. Scale bars: 100 µm.

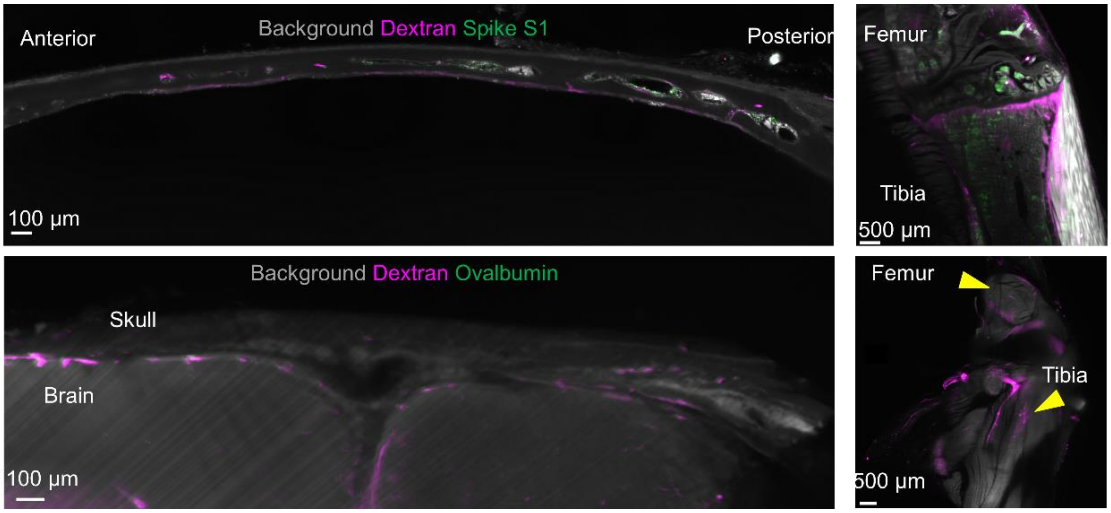

Figure 21. Spike S1 protein homes in mouse bone marrow. Representative images of mouse skull marrow and bone marrow of tibia and femur. Scale bars: 100 µm and 500 µm respectively.

3.4 SARS-CoV-2 homing in human skull marrow and meninges niches

The skull bone marrow has been characterized as a myeloid cell reservoir for the meninges and CNS parenchyma, enabled by the channels between the skull marrow and meninges (151–153). In another mouse model with bacteria-induced meningitis, a small amount of bacteria transit from perivascular CSF through skull

channels into marrow cavities (154). Therefore, we hypothesized that the skull marrow and meninges channel may also facilitate SARS-CoV-2 virus entrance into the brain.

We looked at the distributions of SARS-CoV-2 and Spike proteins in COVID-19 human tissues and confirmed our finding in mouse model that the Spike S1 protein accumulates at the CNS borders and in the brain (n = 11 different COVID-19 cases, Table 1).

We dissected the skull with the underlying dura from COVID-19 human patients and stained with the Spike protein antibody and PI using SHANEL protocol (121). We identified the Spike protein in COVID-19 human skull bone marrow niches, SMC, and meninges using three-dimensional reconstruction corroborating the mouse data (Fig. 23). There was no Spike protein labeling in control individuals without SARS-CoV-2 infection.

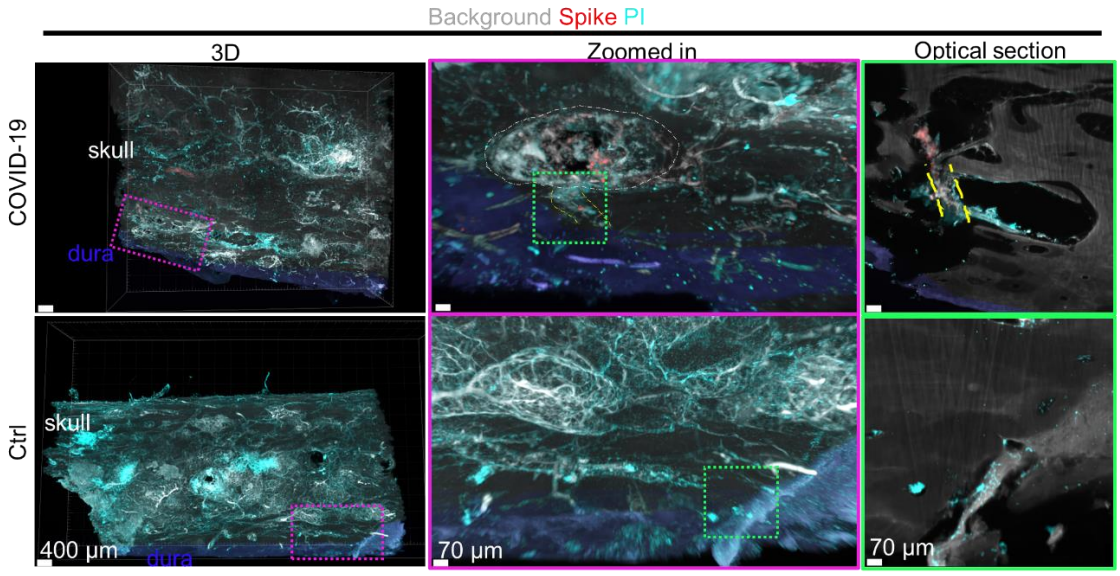

Figure 23. Spike protein in COVID-19 patient skull and meninges. Representative images of Spike protein antibody and PI labeling in the COVID-19 patient skull with meninges. The dura mater is segmented manually based on autofluorescence and imported for 3D reconstruction in Imaris. Non-COVID-19 sample is used as a control. Scale bars: 400 µm (left), 70 µm (middle and right).

Imaging vessels via CD31 labeling, we found that about half of Spike protein accumulated outside of the blood vessels in the skull marrow niches (Fig. 24), suggesting the homing of Spike protein to the patient's skull marrow.

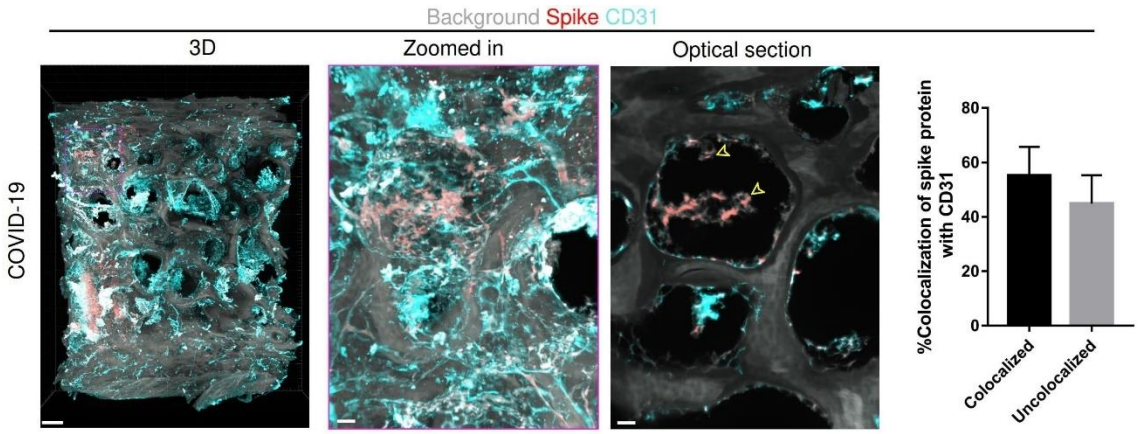

Figure 24. Spike protein homes in COVID-19 patient skull and meninges. Representative images of Spike protein antibody and CD31 labeling in the COVID-19 patient skull with meninges. Arrowheads indicate Spike protein homing in the skull marrow niche. Scale bars: 500 µm (left), 50 µm (middle and right). Quantification of Spike protein colocalization with CD31 signal in 6 optical sections. Data are mean ± SEM.

Given the potential for infected cells to release a significant number of free soluble Spike protein subunits (155), we aimed to check whether the immunostaining of Spike protein in the skull and meninges only resulted from the circulating peptide or the presence of virus particle. The examination of SARS-CoV-2 RNA by RT-PCR in tissues from infected patients showed positive results only in 2/10 skull and 2/5 meninges of patients who died from COVID-19. In these PCR-positive samples, we confirmed the virus infection by coronavirus structural protein nucleocapsid staining (Fig. 25) as complementation to Spike protein staining. In contrast, we found viral Spike protein in all skull and meninges samples evaluated using confocal microscopy. These findings demonstrated that the skull and meninges were infected with SARS-CoV-2. The presence of Spike protein in the skull and meninges tissues in the absence of viral load (PCR negative) shows that Spike protein has a longer half-life than SARS-CoV-2 in the skull marrow niches.

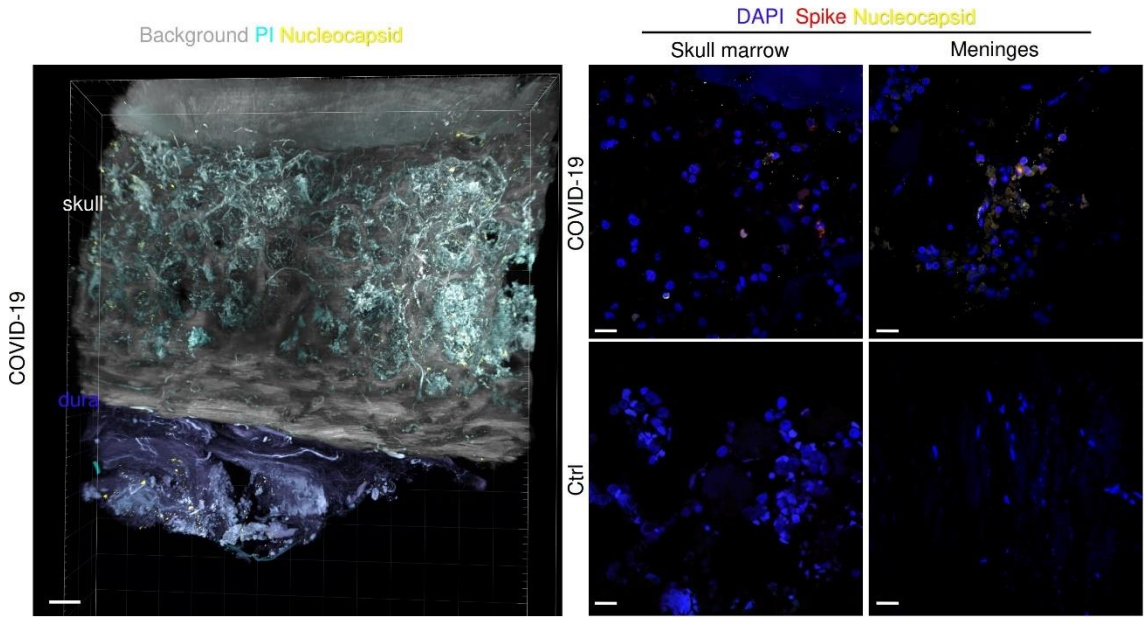

Figure 25. SARS-CoV-2 infection in human skull and meninges. Representative image of nucleocapsid protein in COVID-19 patient skull with meninges. Scale bar: 400 µm. Representative confocal images of Spike protein and nucleocapsid protein in human skull marrow and meninges. Scale bars: 20 µm.

In addition, we identified co-expression of ACE2 and Spike protein in the COVID-19 cases (Fig. 26). The level of ACE2 decreased in the Spike protein-positive regions of COVID-19 patient meninges compared to control meninges, which is consistent with a report that SARS-CoV-2 Spike protein affects endothelial function by reducing ACE2 (156).

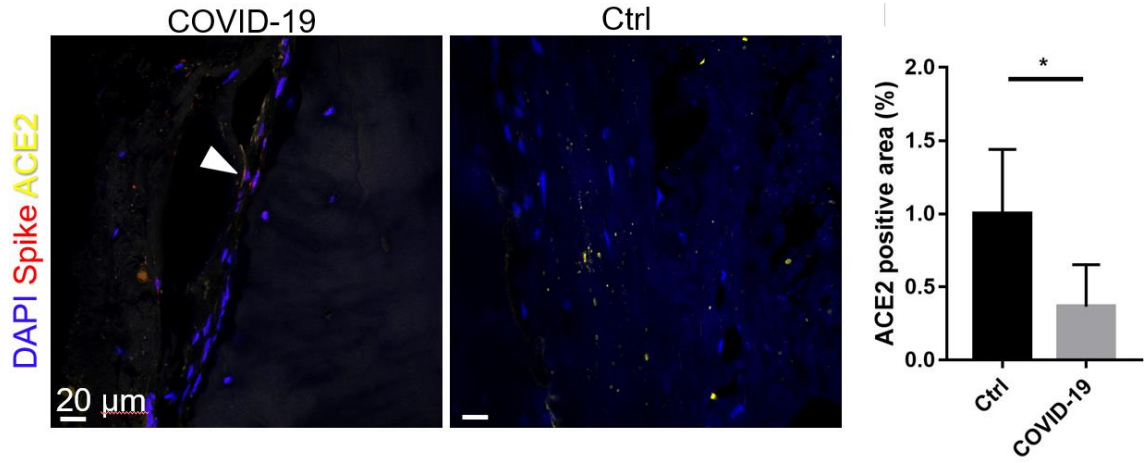

Figure 26. Colocalization of Spike protein with ACE2. Representative confocal images of Spike protein antibody and ACE2 antibody labeling in the COVID-19 patient and control meninges.

Scale bars: 20 µm. Quantification of the ACE2 positive region in 6 fields of view. n = 3. Data represent mean ± SD. Two-tailed unpaired Student's *t*-test (p = 0.0142). *p < 0.05.

To investigate the effects of SARS-CoV-2 infection and Spike protein accumulation at the CNS borders, we performed mass spectrometry-based label-free quantitative proteomics analysis on region matched tissues from COVID-19 vs. control (non-COVID-19) human tissues. The clinical samples were comprised of 8 post-mortem samples of human skull and meninges tissues from the COVID-19 deceased victims and control donors. The MS data were generated in data-independent acquisition mode, and DIA-NN was used to analyse the raw data against the Human Uniprot database. 5975 protein groups were identified across the skull marrow samples from COVID-19 and control, with Pearson correlation values ranging from 0.36 to 0.92 between the two groups (Fig. 27). PCA plot showed the clear segregation of the skull marrow samples from COVID-19 and control group.

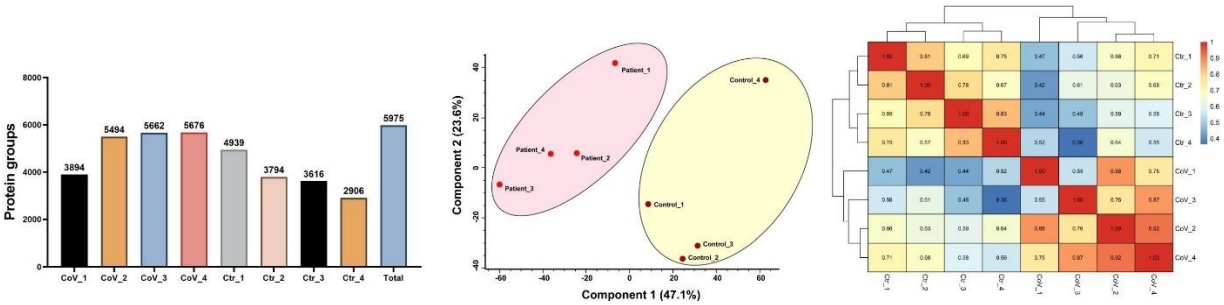

Figure 27. Proteomics information of COVID-19 patient and control skull marrow. Protein numbers, PCA plot and Pearson correlation map of skull marrow samples are listed here.

Out of the 519 proteins differentially expressed in the COVID-19 skull marrow, we identified 271 upregulated proteins and 248 downregulated proteins (Fig. 28). Some of the SARS-CoV-2 host-cell entry factors including neuropilin 1 (NRP1), neuropilin 2 (NRP2) (102) and dipeptidyl peptidase 4 (DPP4, also known as CD26) (157,158), were significantly decreased in COVID-19 skull marrow. While other coronavirus entry factors such as basignin (BSG, also known as CD147) and alanyl aminopeptidase (ANPEP, also known as CD13) (157), and cathepsin B (CTSB) (33) were not changed. Using KEGG pathway analysis to relate the dysregulated proteins to biological processes whose activity is modulated in response to SARS-CoV-2, we discovered the most significantly dysregulated proteins were involved in the coronavirus disease pathway or in the complement and coagulation cascades (Fig. 28). The majority of the coronavirus disease

pathway's proteins were upregulated in COVID-19 patients' skull marrow, this includes various large and small ribosomal subunit proteins and suggests COVID-19 related immune response due to virus hijacked human cells and replication in the skull marrow of COVID-19 patients.

We discovered that the complement components were significantly downregulated, C1, C3, C4, C5, C8, and factor H in the skull marrow of these non-survivor COVID-19 patients were decreased compared to controls (Fig. 28).

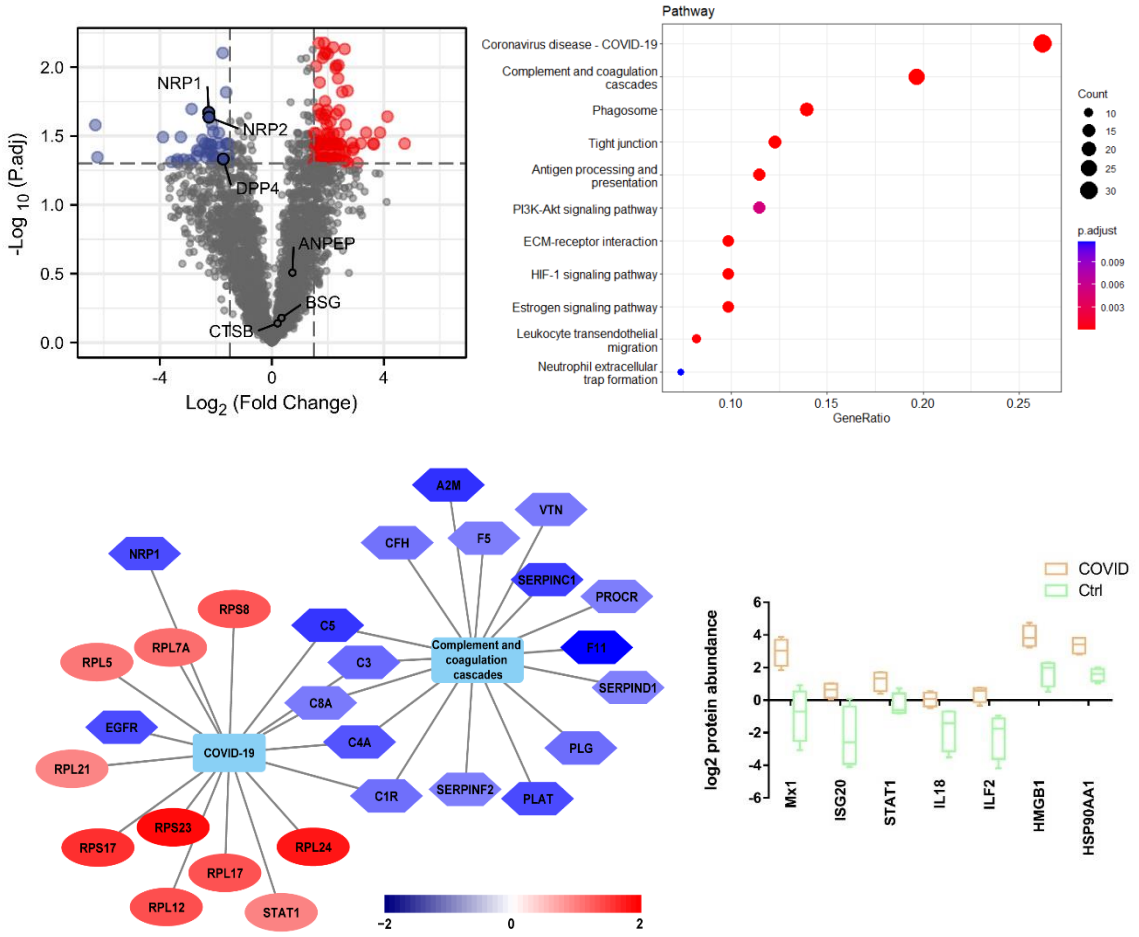

Figure 28. Dysregulated proteins and enriched pathways in COVID-19 patient skull marrow. Volcano plot between COVID-19 and control skull marrow ($p < 0.05$, LogFC = 1). n = 4 biological replicates.

We also identified some of the key regulators of Interferon alpha/beta signaling cascades, for example, Interferon-stimulated gene 20 kDa protein (ISG20), Interferon-induced GTP-binding protein Mx1 (MX1), and Signal transducer and activator of transcription 1-alpha/beta (STAT1), an important regulator of IL-6 signaling were all upregulated in the skull marrow of COVID-19 patients (Fig. 29), thereby indicating the active antiviral inflammatory response in skull marrow of

COVID-19 patients. Such inflammatory response induces the cytokine storms in COVID-19 cases, which is further associated with increased accumulation and degranulation of neutrophils (159,160). Some of the proteins involved in neutrophil degranulation such as Interleukin-18 (IL-18), Interleukin enhancer-binding factor 2 (ILF2), Heat shock protein HSP 90-alpha (HSP90AA1), High mobility group protein B1 (HMGB1) were also upregulated in the skull marrow of COVID-19 patients.

Furthermore, we found expression changes in proteins related to the VEGFA-VEGFR2 and PI3K-AKT signaling pathways, which are implicated in COVID-19 infections and are associated with coagulopathies, e.g., HSP90AA1, HSP90AB1, and GNB1 which were upregulated and EGFR, IGF2, FN1 which were downregulated (Fig. 29).

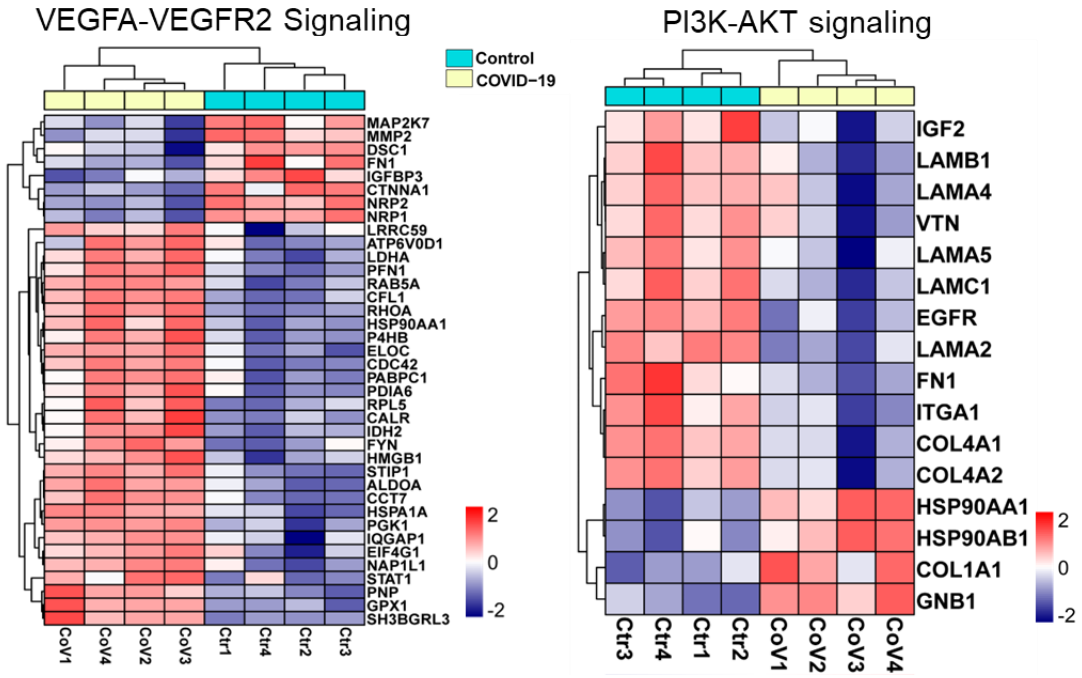

Figure 29. Dysregulated VEGFA-VEGFR2 signaling pathway and PI3K-AKT signaling pathway in COVID-19 patient skull marrow.

In the meninges, we identified 4171 protein groups across all samples with Pearson correlation coefficients between 0.41 and 0.98. The PCA plot clearly distinguished the meninges samples from the COVID-19 group and the control group (Fig. 30).

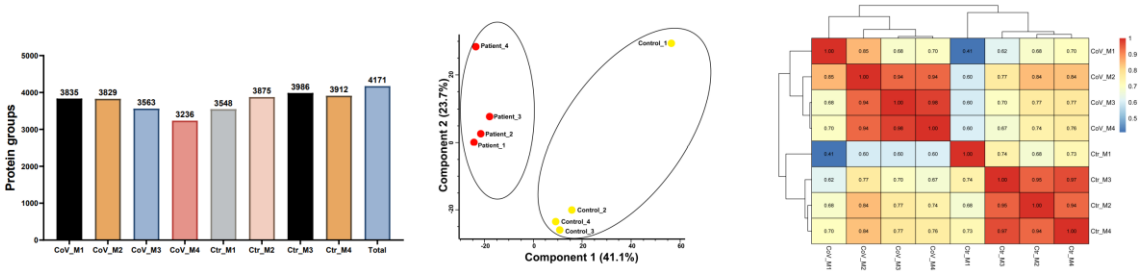

Figure 30. Proteomics analysis of COVID-19 patient and control meninges. Protein numbers, PAC plot and Pearson correlation map of meninges samples are listed here.

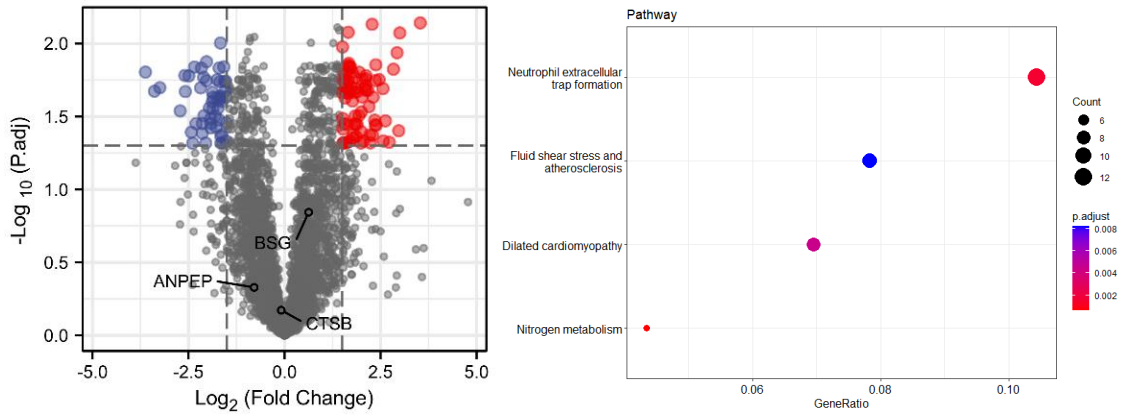

Figure 31. Dysregulated protein and pathways in COVID-19 patient meninges. Volcano plot between COVID-19 and control meninges ($p < 0.05$, LogFC = 1.5). n = 4 biological replicates. KEGG pathway analysis shows the most dysregulated pathway in COVID-19 meninges when comparing to controls.

218 differentially expressed proteins were identified, with 126 upregulated and 92 downregulated in the meninges (Fig. 31). Neutrophil migration directly from the channels that link skull marrow and meninges has been reported in the inflammatory events (151). Our pathway analysis discovered that proteins associated with the neutrophil extracellular traps (NETs) formation were significantly upregulated in the meninges of COVID-19 patients (Fig. 31). These include fibrinogen (FGA, FGB, FGG), cathepsin G (CTSG), and myeloperoxidase (MPO) (Fig. 32). FGA, FGB, and FGG not only play a role in NETs but also in the formation of blood clots. The NETs increase in COVID-19 meninges could be due to the upregulation of HMGB1 in the skull marrow niches, as extracellular HMGB1 stimulates NETs formation (161).

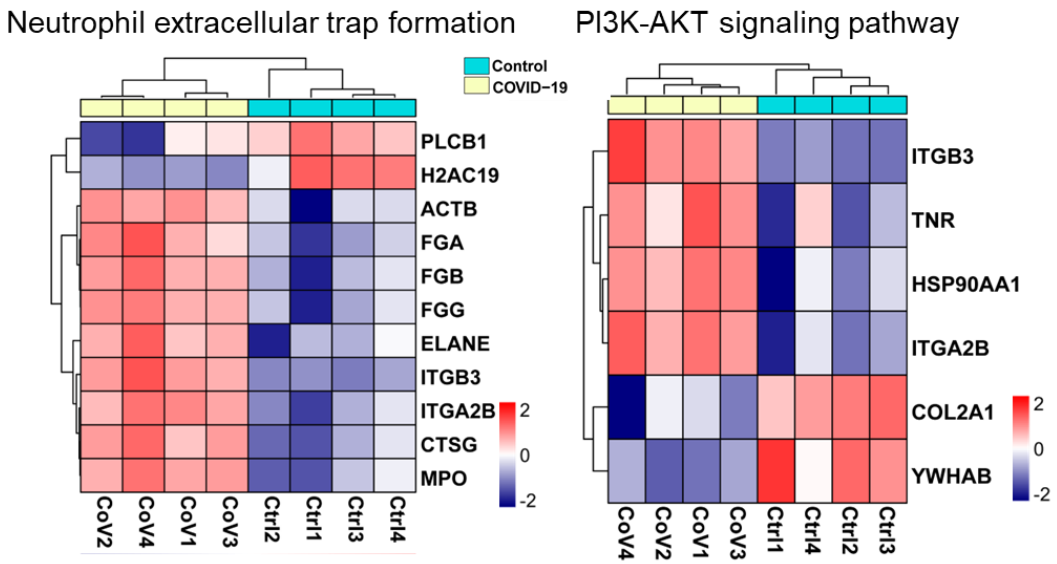

Figure 32. Dysregulated Neutrophil extracellular trap formation and PI3K-AKT signaling pathway in COVID-19 patient meninges.

We also noticed the overexpression of calprotectin (S100A8/A9) proteins in the meninges, which play a pro-inflammatory role in the migration of neutrophils (Fig. 33). Specifically, S100A8 has recently been hypothesized to be involved in hyper-inflammation in severe COVID-19 (162). Higher inflammation would induce thrombosis (163). We also identified upregulation of platelet factor 4 (PF4) and Platelet basic protein (PPBP) in the meninges tissue (Fig. 33).

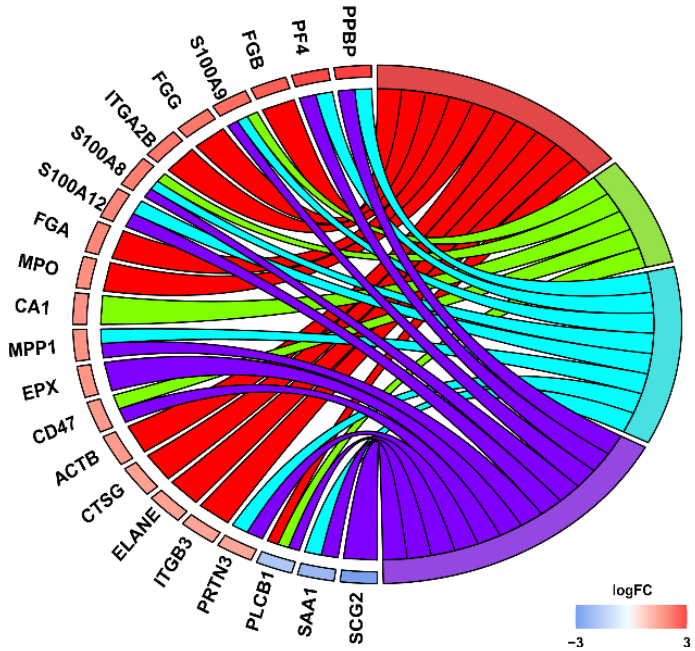

Figure 33. Chord diagram showing the most enriched biological processes with their differentially expressed proteins in the meninges of COVID-19 patients.

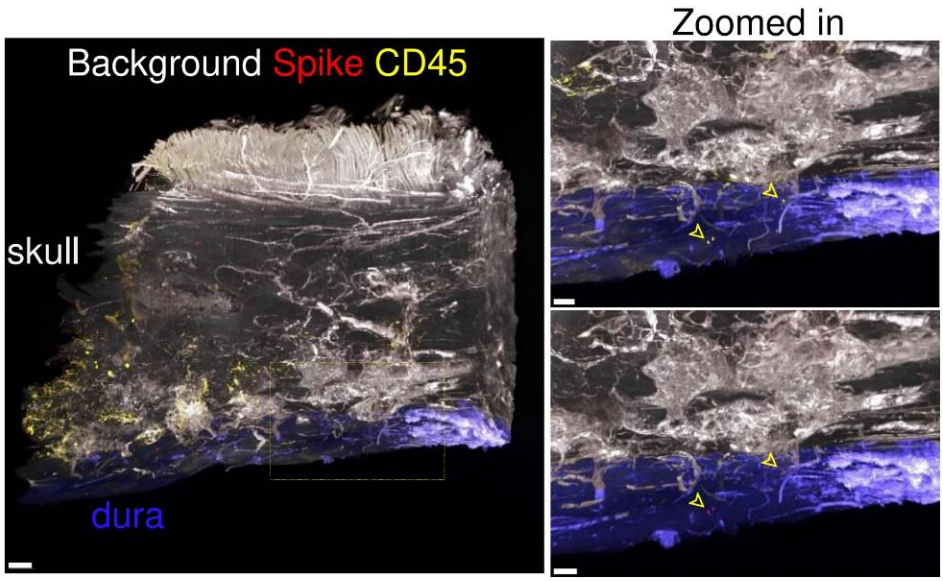

Figure 34. Representative images of Spike protein and CD45 antibody labeling in COVID-19 patient skull with meninges. Yellow arrow indicates the colocalization of Spike protein and CD45. Scale bars: 300 µm (left), 150 µm (right).

These data demonstrate that neutrophils, constituting the predominant cell population in the skull bone marrow niches (164), might be moving into the meninges and inducing both formation of NETs and a pro-inflammatory response. Indeed, neutrophil migration directly from channels between skull marrow and meninges has been reported in inflammatory events (151,152). We examined skull samples of COVID-19 patients with general immune cell marker CD45 and with the Spike protein (Fig. 34). Our data clearly showed colocalization of immune cells with the Spike protein, confirmed that the Spike protein interacts with the immune cells in skull marrow and meninges, suggesting a potential immune activation via protein binding. Spike protein accumulation in skull-meninges niches and gene expression changes in the brain

Through staining Spike protein and vasculature in the meninges attached to the brain tissues of COVID-19 patients, we identified the Spike protein both in the meninges and brain tissues (Fig. 35). However, we could not detect the nucleocapsid protein in the patient brain tissue (Fig. 36) again suggesting a longer half-life of Spike protein compared to SARS-CoV-2.

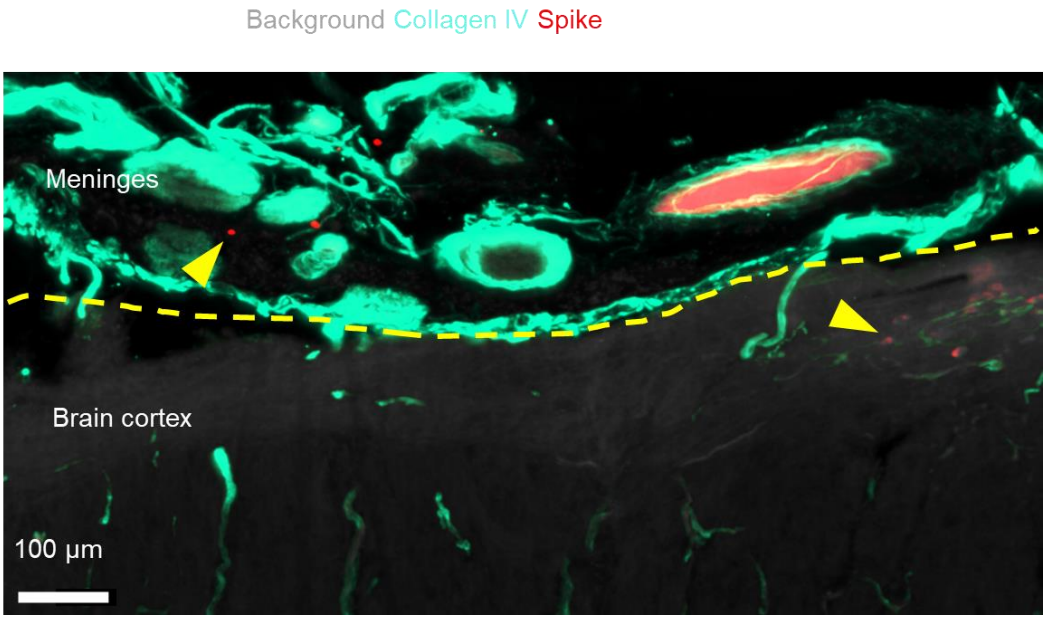

Figure 35. Representative image of Spike protein and collagen IV antibody staining in COVID-19 patient brain with meninges. The yellow arrow indicates Spike protein in meninges and brain parenchyma. Scale bar: 1000 µm.

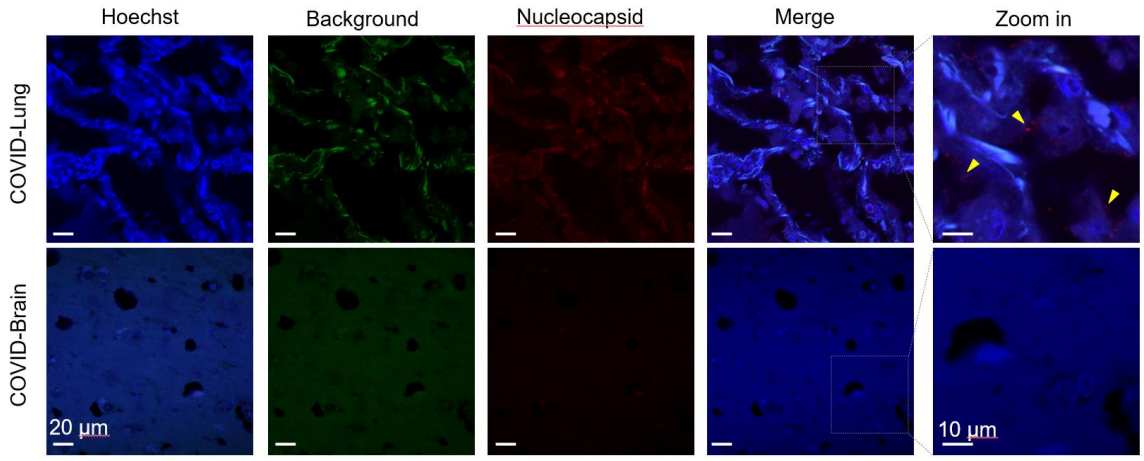

Figure 36. Representative confocal images of nucleocapsid staining in COVID-19 patient lung and brain tissue. Scale bars: 20 µm (left), 10 µm (right, zoom-in).

Proteomics study of brain tissues (COVID-19 cases vs. controls) showed clear segregation of the brain samples from the COVID-19 and control group in the PCA plot (Fig. 37). The predominant dysregulated pathways were the VEGFA-VEGFR2 signaling pathway, neutrophil degranulation, COVID-19, and PI3K-AKT pathways (Fig. 38), pathways that were also differentially expressed in the skull marrow.

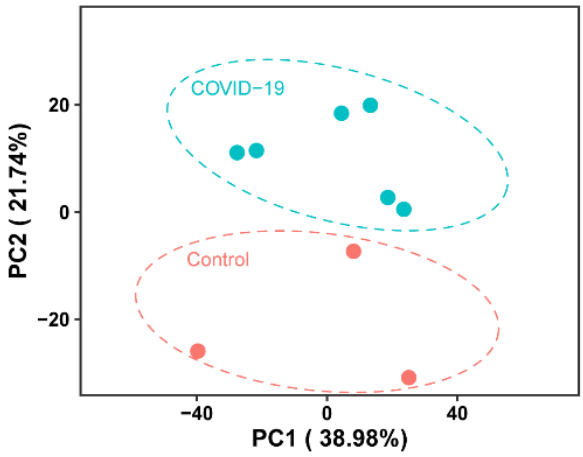

Figure 37. PCA plot of COVID-19 patient and control brain proteomics.

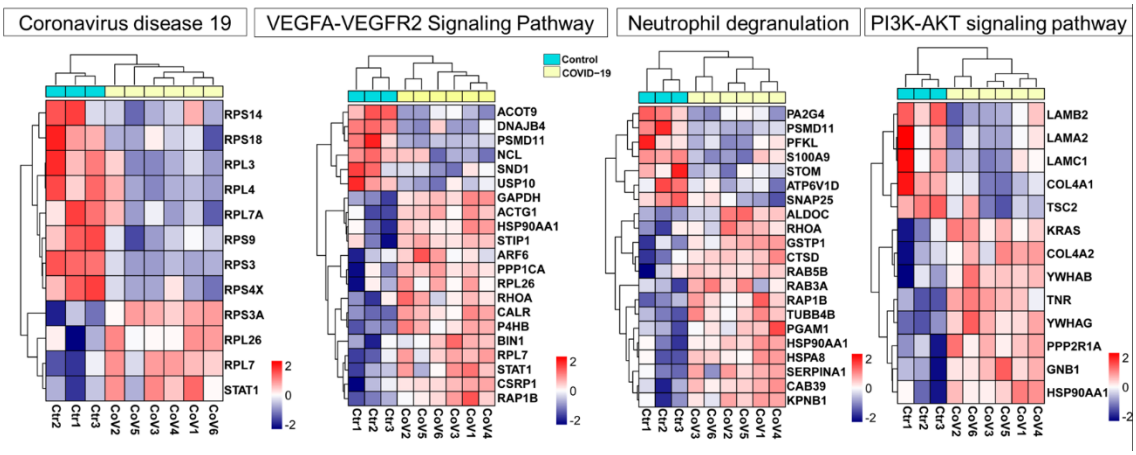

Figure 38. The dysregulated proteins in the brain of COVID-19 patients are enriched in the VEGFA-VEGFR2 signaling pathway, Coronavirus disease 19, neutrophil degranulation and PI3K-AKT pathway.

The proteins related to the VEGFA-VEGFR2 signaling pathway that were commonly differentially expressed in the skull marrow and brain samples include: RHOA, P4HB, HSP90AA1, CALR, STIP1, and STAT1 (Fig. 29 and 38). The Ras homolog family member RHOA was upregulated in the brain and skull tissues. Reportedly, the viral Spike protein leads to the activation of RHOA, which triggers the disruption of the blood-brain barrier (165). It has been suggested that PI3K

regulates the RHOA GTPase (166) and activates RHOA in the neutrophil degranulation pathway. This GTPase and other protein family members in human neutrophils regulate actin dynamics and cell migration (166). Protein disulfide-isomerase (P4HB) was also common to the skull and brain tissues, upregulation of this protein was associated with thrombosis in COVID-19 patients (167). The heat shock protein HSP90AA1 was upregulated in the skull and brain samples. Earlier reports suggested a positive correlation in this gene expression with SARS-CoV-2 RNA and associated with the disease progression (168). This protein may assist in the protein folding of newly synthesized viral proteins. Notably, HSP90AA1 is also listed as related to the neutrophil degranulation pathway in KEGG. In response to HSP90AA1, calreticulin (CALR) is known to be one of the heat shock proteins that greatly enhance viral Spike accumulation and immunobiological activity (169). The Stress-induced-phosphoprotein 1 (STIP1), an HSP90AA1 co-chaperone (170), was upregulated in both tissues. It has been found that the protein interacts with SARS-CoV-2 proteins Nsp12, Orf3a, Orf8, and E (171). The transcription factor STAT1 is another common upregulated protein between skull marrow and brain; reportedly, SARS-CoV-2 blocks STAT1 translocating into cell nucleus and reduces transcription of interferon response-related genes (172).

Among the VEGFA-VEGFR2 signaling pathway-related proteins, ADP-ribosylation factor 6 ARF6 was identified only in the brain tissue as an upregulated protein. A recent report suggested that ARF6 mediates viral entry by regulating endocytosis (173). Actin Gamma 1 (ACTG1) was also upregulated in the brain tissue. Its expression was reported to correlate with disease severity (174). We identified a subunit of 19S regulatory complex PSMD11 as a downregulated protein in brain samples of COVID-19 patients. Myc box-dependent-interacting protein 1 (BIN1), an Alzheimer's disease risk gene was also identified as an upregulated protein in the brain tissue (175). However, detailed functional association of PSMD11 and BIN1 proteins in COVID-19 pathogenesis was not performed at the time of writing.

In the PI3K-AKT signaling pathway, which was differentially regulated in all three tissue types investigated here, six proteins were commonly identified in the brain and skull tissues: COL4A1, COL4A2, GNB1, HSP90AA1, LAMA2, LAMC1 (Fig. 29 and 38). The brain and skull both had decreased levels of collagen alpha-1(IV) chain (COL4A1), but collagen alpha-2(IV) chain (COL4A2) had increased levels in the brain but decreased levels in the tissues of the skull. COL4A1 protein has a role in regulating cerebrovascular homeostasis, although a role in COVID-19 pathogenesis has not been reported yet (176). At the transcript level, COL4A2 was downregulated in COVID-19 brain samples (177). Guanine nucleotide-binding protein G(I)/G(S)/G(T) subunit beta-1 (GNB1) was upregulated in the post-

mortem brain tissue of COVID-19 patients and has been associated with intellectual disability (178), but no associations have—to our knowledge—been made with respect to COVID-19 pathogenesis previously. Components of the extracellular matrix were reported to be downregulated in COVID-19 lung tissues (179). We observed downregulated expression of laminin subunit alpha-2 (LAMA2), laminin subunit beta-2 (LAMB2), and laminin subunit gamma-1 (LAMC1), indicating a loss of structural integrity of the infected tissues. Activation of the proteasome-mediated protein degradation pathways in COVID-19 infection is well established (180). Heat shock protein HSPA1B was reported to be upregulated at the transcript level and we also observed the same in our dataset along with other HSPs, including HSPA8, HSP90AA1, HSP90B1and HSP90AB1 (181). These proteins may assist in the protein folding of newly synthesized viral proteins. As reported earlier, the RNA binding protein PA2G4 was also upregulated in COVID-19 conditions (182). A potential strategy to target SARS-CoV-2 has been through targeting RNA binding proteins among others (183). Another upregulated protein was GTPase KRas (KRAS), which was only identified in the brain tissue. Interestingly, a drug screen previously identified drugs used to treat KRAS-mutated cancers as potential drugs to inhibit replication of SARS-CoV-2 (184). We identified TSC2, an autophagy initiation-related molecule among the downregulated proteins. The downregulation of the autophagy pathway during SARS-CoV-2 has been reported earlier (185). Overall, in the brain parenchyma sample, we observed dysregulation of the regulators of protein homeostasis and maintenance of the blood-brain barrier.

In addition, we examined micro-bleeds and found in all four brain tissues of COVID-19 patients analyzed using Prussian blue staining, compared to only one out of four in control brain tissues (Fig. 39).

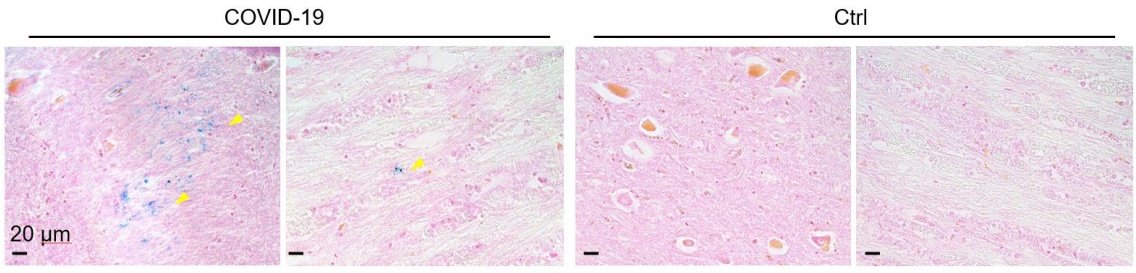

Figure 39. Representative images of Prussian blue staining in COVID-19 patient and control brain. Cell nucleus in red. Scale bars: 20 µm.

In summary, we discovered SARS-CoV-2 infection in the skull marrow and meninges. Our proteomics data suggest a correlated inflammatory state associated

with complement, coagulation, and neutrophil as well as dysregulated VEGF signaling pathway between the skull marrow and brain of COVID-19 patients (Fig. 40). Brain inflammation and probable vascular injury may be a result of virus homing and Spike protein shedding that accumulates at the brain border.

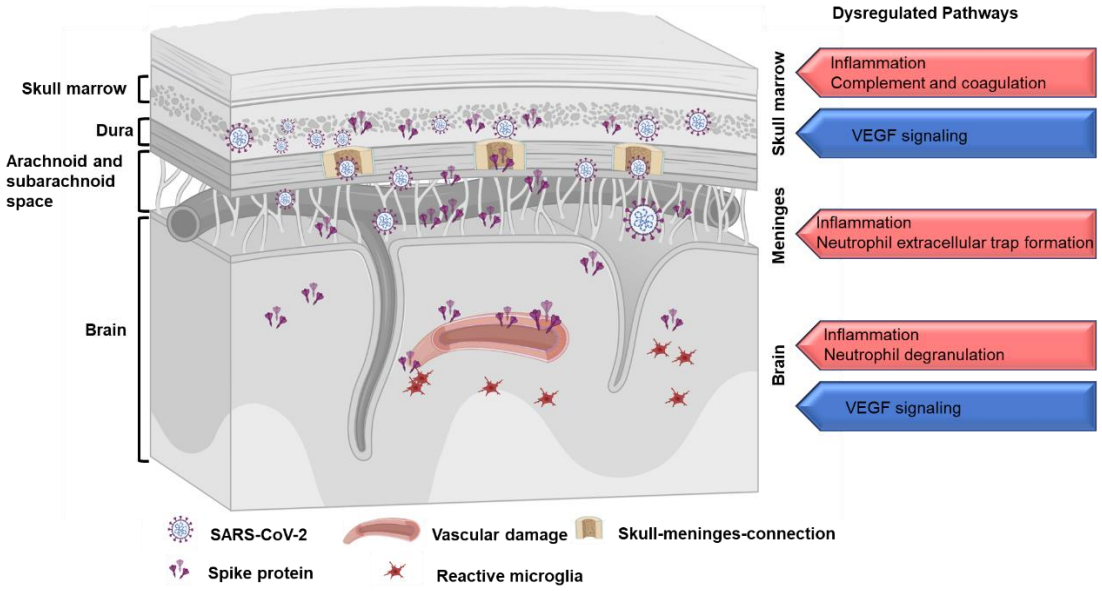

Figure 40. Model of SARS-CoV-2 Spike protein accumulation in the CNS borders and Spike-induced molecular changes.

4. Discussion

4.1 Whole mouse clearing as a platform to study the long-term effect of SARS-CoV-2 infection and inspect specific biodistribution of Spike protein

The SARS-CoV-2 virus infects cells by binding to the ACE2 receptor on their surface. Human and mouse ACE2 both have 805 amino acids, eight crucial residues in human ACE2 are involved in its ability to bind to viral Spike protein, however five of these amino acids are different in mouse ACE2 (186). Similarly, mouse ACE2 was reported to bind the S1 domain of SARS-CoV less efficiently than human ACE2 (187). Therefore, the binding of Spike S1 in wild-type mice would be lower than that in human ACE2 transgenic mice (188). The K18-hACE2 mouse model has been generated since the SARS-CoV outbreak in 2003 (189) and is also widely used as a model to study SARS-CoV-2 (190). There are other lineages of transgenic mice that express humanized ACE2, including CMV-hACE2 (191) and Syn-hACE2 (192) mice, as well as hACE2 knock-in (hACE2-KI) mice (193), mice transduced with adenovirus type 5-expressing hACE2 (Ad5-hACE2) (194).

Here, we used the S1 protein from SARS-CoV-2 Alpha variant, which consists of the N501Y mutation and has been shown to infect wild-type mice through binding with mouse ACE2 (195,196), to identify all potential SARS-CoV-2 tissue targets. In addition to the expected target organs such as the lung and kidney (197,198), our results showed an accumulation of virus and Spike protein in the skull marrow and brain meninges. The localization of the Spike protein in optically transparent mice brain tissues recapitulated the tissue distribution we observed in various post-mortem organs from COVID-19 patients. We can still improve this experimental model by using real SARS-CoV-2 virus infection in an hACE2 mouse.

With a biosafety level three laboratory, we can test and compare the infection of different variants of virus in different mouse model at different dosage and time points, and whole-body tissue clearing to study the distribution. The delivery route is also important to simulate human infection. For example, intranasal or aerosol infection would be better than intravenous injection to study the virus tropism.

To better understand how SARS-CoV-2 infection will progress over time and because COVID-19's long-term consequences are still a significant concern, we could utilize this method with the combination of different reporter mouse strains to study different organ systems.

Our unbiased assessment of the fluorescently labeled Spike protein in whole mouse bodies provides clues of tissues that could potentially be targeted by SARS-CoV-2 infection. However, other cellular factors might limit the ability of the virus to enter a replicate cycle in different cell types. We identified several candidate proteins with no previous association with COVID-19, especially those earlier associated with neurological diseases, supporting the power of combining unbiased imaging with molecular analysis. Our findings in the mouse model reproduce our findings in the human brain, emphasizing the relevance of our mouse model.

4.2 Spike protein accumulation in skull-meninges niches links to brain proteomics change

Even in mild COVID-19 cases, significant brain tissue loss urges a quick exploration of the mechanisms of brain damage caused by SARS-CoV-2 (199).

SARS-CoV-2 Spike protein was detected in the human skull bone marrow, meninges, and brain tissues and accumulated along with the viral nucleocapsid protein in the human skull bone marrow niches, SMC, and meninges suggesting that the virus infects the skull bone marrow and meninges. In contrast, only the Spike protein was detected in the brain parenchyma. The detected Spike protein could be either a residual viral infection in the brain that has been cleared, or it could have infiltrated the brain from the cerebral circulation. Either case suggests that the Spike protein could have a long lifetime in the body (200). A recent preprint supports this notion in medRxiv that suggests the persistence of Spike protein in plasma samples up to 12 months post-diagnosis (201).

Although many studies in humans, animal, and cell line models addressed the molecular underpinning of SARS-CoV-2 infection, very few currently link the brain-associated pathologies evident in severe COVID-19 cases with the changes in the host proteome of the brain and adjacent tissues (202). In this study, the spatial proteomics datasets of COVID-19 infected brain samples provide leads to study Spike-specific changes in the brain. Our study benefited from the simultaneous analysis of compartments adjacent to COVID-19 infected individuals, namely the skull marrow and the meninges.

The 29 proteins that the SARS-CoV-2 viral genome encodes (203) directly or indirectly regulate the expression of many host proteins. Our molecular analysis suggests activation of immune response in the skull-meninges-brain axis, potentially via recruiting and increasing the activity of neutrophils similar to what

has been reported in the respiratory tract (139,204). Individual viral proteins have been suggested to exert physiological effects in the absence of other viral components, especially the Spike protein which has e.g. been reported to induce the expression of inflammatory cytokines and chemokines in macrophages and lung epithelial cells and to compromise endothelial function (148,156,205–208).

Trying to understand the changes in host cell expression, we find that certain host processes are most consistently dysregulated in individual tissues. In the skull marrow, predominant dysregulated pathways were the coronavirus disease pathway and complement and coagulation cascades as reported previously for peripheral organs of patients with severe COVID-19 (209). The increased expression of pro-inflammatory proteins, including calprotectin and proteins associated with thrombosis such as PF4 and PPBP, illustrate that the viral proteins act as an inflammatory stimulus that leads to the development of a significant immune response in the brain, although we cannot distinguish between direct effects by viral factors and systemic effects of the disease.

In the meninges, we find that a major consequence of the inflammatory state is an upregulation of proteins involved in the release of chromatin webs and lytic proteins by neutrophils in the extracellular space to form NETs, a process known as NETosis to contain the infection. The upregulation of NET proteins such as FGA, FGB and FGG supports presumably leads to the formation of high levels of NETs in the skull-meninges-brain axis and the infiltration of circulating neutrophils into the meninges. The presence of NETs could further propagates the inflammation (161), potentially inducing tissue damage, including endothelium damage (210), leading to pathologies such as thrombosis and alterations in the coagulation process (211).

In the brain, the neutrophil degranulation pathway was the most prominent pathway that was only upregulated in the brain, suggesting an active immune response in the brain parenchyma.

The dysregulation of the VEGFA-VEGFR2 and PI3K-AKT pathways was detected in both the skull marrow and the brain. The upregulation of these pathways might explain the observed propensity of COVID-19 patients to develop mini-infracts in the brain parenchyma (212,213) and our observation of an increase level of micro-bleeds in COVID-19 patients, potentially contributing to the observed brain damage in the COVID-19 patients in acute and chronic stages. Alternatively, the upregulation of the VEGFA-VEGFR2 pathway could also reflect the initiation of tissue repair after the virus-induced vascular injury.

A common feature of all three tissues is the activation of neutrophil related pathways, in the form of neutrophil degranulation in the brain and the skull marrow or in the form of NET formation in the meninges. This common feature suggests that neutrophils may play a key role in maintaining inflammatory responses in and around the central nervous system.

We identified a number of candidate proteins with no previous association with COVID-19, especially those earlier associated with neurological diseases such as Ras-related protein Rab-8B (RAB8B), Ras-related protein Rab-6 (RAB6A, RAB6B) and EF-hand domain-containing protein D2 (EFHD2). Notably, role of these proteins have been associated with disorders such as Parkinson's disease, Alzheimer’s disease and dementia (214,215). This clearly supports the power of combining unbiased imaging with molecular analysis.

The proteins and pathways identified to be differentially regulated in the brain, skull marrow and meninges provide leads to investigate the molecular mechanisms of immediate and long-term consequences of SARS-CoV-2 infections for the human brain. The common dysregulation of neutrophil activation and PI3K-AKT pathways in the skull, meninges, and brain tissue demonstrated a common effect of SARS-CoV-2 infections on immune system along the skull-meninges-brain axis. These molecules or molecular pathways can be leveraged as therapeutic targets to prevent or treat brain related complications in COVID-19.

Our data may also suggest a mechanism for the virus into the central nervous system. In both mouse and COVID-19 human tissues we find Spike protein in the SMCs, which the virus or virus components could use to travel from the skull marrow to meninges and from there to the brain parenchyma (151–153,216). Of course, the virus might take other routes to reach the brain in a not mutually exclusive way. E.g. the virus could directly traverse the cerebrovasculature to reach the brain parenchyma or be carried there by immune cells (e.g., via neutrophils or phagocytic cells). More data will be needed to establish the most common route of brain invasion by SARS-CoV-2, which might differ between different parts of the brain. Brain invasion of virus-shed Spike protein found in some COVID-19 cases has been linked to a compromised blood-brain-barrier (100,99), and to trafficking along the olfactory nerve or vagus nerve (101). Here, we suggest an alternative scenario wherein SARS-CoV-2 Spike protein reaches first the skull marrow and then the meninges before entering the brain.

Spike-induced alterations in the skull-meninges-brain axis presents diagnostic and therapeutic opportunities as both skull and meninges are easier to access

than brain parenchyma. Panels of such proteins tested in plasma samples of COVID-19 patients might provide an early prognosis of brain-related complications.

4.3 mRNA vaccine encoded Spike protein may contribute to adverse effects

The first company that received emergency validation from the WHO since the pandemic was Pfizer/BioNTech after the mRNA vaccine was authorized against COVID-19 for emergency use on December 31, 2020. By January 2021, nine vaccinations in all had received international approval for emergency use (217).

Of note, mRNA Vaccine encoded the Spike protein of SARS-CoV-2 to stimulate the body to establish immunity. Although adverse effects of COVID-19 vaccine are rare, some recent studies demonstrated that vaccination recipients had a higher risk of cardiac and neurological issues (218–220), leading to the Spike hypothesis that the vaccine-encoded antigen can contribute to adverse effects (221). There are reports that Spike protein alone could result in vascular endothelial damage (148,156). The half-life of Spike protein and its potential impact on the vascular system needs further study.

How the vaccine product would distribute in the body of vaccinated individuals, remain elusive. Similarly to our study, lipid nanoparticles conveying mRNA encoding the Spike protein can be injected into the mouse to evaluate the biodistribution of Spike protein in the whole body through different routes, dosages, and time points. In this context, the whole mouse tissue clearing technology offers an invaluable and powerful tool to assess the efficacy of vaccines and examine their long-term effects.

5. Summary

COVID-19 is a pandemic that has had a profound impact on lives and communities around the world. In addition to the clinical manifestations of patients during the acute phase, symptoms not directly related to the respiratory system still appear several months or even years after the recovery. The present study aims to explore the sites of SARS-CoV-2 virus infection throughout the body, and to understand the mechanism of COVID-19 related neurological complications.

We demonstrated that various internal organs can be bound by the SARS-CoV-2 Spike protein, the skull bone marrow and meninges are also susceptible sites to the virus; elevated inflammatory responses and compromised vascular homeostasis were found in the skull bone marrow of COVID-19 patients. The accumulation of virus and Spike protein in the skull marrow can spread to the meninges through the reported skull-meninges connections and potentially facilitate brain access. The Spike protein can be detected even though viral load was not detectable by RT-PCR in the examined brain samples of COVID-19 patients, suggesting the persistence of viral shedding proteins in the brain tissue. And it is worth noting that the Spike protein itself can also cause tissue damage.

Using proteomic analysis, we discovered the consistent inflammatory response in the skull marrow, meninges and brain tissue of COVID-19 patients, which is highlighted by the complement activation, neutrophil extracellular trap formation and neutrophil degranulation. Proteins involved in the PI3K-AKT pathway were commonly dysregulated in the skull marrow, meninges and brain tissue of COVID-19 patients. We also identified a number of dysregulated proteins with no previous association with COVID-19 in the brain, especially those earlier associated with neurological diseases such as RAB8B, RAB6A, RAB6B and EFHD2. These pathways and protein candidates could be potential targets to prevent or treat the neurological complications of COVID-19.

References

1. Wang C, Horby PW, Hayden FG, Gao GF. A novel coronavirus outbreak of global health concern. The Lancet. 2020 Feb 15;395(10223):470–3.

2. Liu NQ, Dekker LJM, Stingl C, Güzel C, De Marchi T, Martens JWM, et al. Quantitative Proteomic Analysis of Microdissected Breast Cancer Tissues: Comparison of Label-Free and SILAC-based Quantification with Shotgun, Directed, and Targeted MS Approaches. J Proteome Res. 2013 Oct 4;12(10):4627–41.

3. Stephenson E, Reynolds G, Botting RA, Calero-Nieto FJ, Morgan MD, Tuong ZK, et al. Single-cell multi-omics analysis of the immune response in COVID-19. Nat Med. 2021 May;27(5):904–16.

4. Lam SM, Zhang C, Wang Z, Ni Z, Zhang S, Yang S, et al. A multi-omics investigation of the composition and function of extracellular vesicles along the temporal trajectory of COVID-19. Nat Metab. 2021 Jul;3(7):909–22.

5. Shu T, Ning W, Wu D, Xu J, Han Q, Huang M, et al. Plasma Proteomics Identify Biomarkers and Pathogenesis of COVID-19. Immunity. 2020 Nov;53(5):1108-1122.e5.

6. Melms JC, Biermann J, Huang H, Wang Y, Nair A, Tagore S, et al. A molecular single-cell lung atlas of lethal COVID-19. Nature. 2021 Jul;595(7865):114–9.

7. Liao M, Liu Y, Yuan J, Wen Y, Xu G, Zhao J, et al. Single-cell landscape of bronchoalveolar immune cells in patients with COVID-19. Nat Med. 2020 Jun;26(6):842–4.

8. Rendeiro AF, Ravichandran H, Bram Y, Chandar V, Kim J, Meydan C, et al. The spatial landscape of lung pathology during COVID-19 progression. Nature. 2021 May 27;593(7860):564–9.

9. Witkowski M, Tizian C, Ferreira-Gomes M, Niemeyer D, Jones TC, Heinrich F, et al. Untimely TGFβ responses in COVID-19 limit antiviral functions of NK cells. Nature. 2021 Dec;600(7888):295–301.

10. Wu P, Chen D, Ding W, Wu P, Hou H, Bai Y, et al. The trans-omics landscape of COVID-19. Nat Commun. 2021 Jul 27;12(1):4543.

11. Yang AC, Kern F, Losada PM, Agam MR, Maat CA, Schmartz GP, et al. Dysregulation of brain and choroid plexus cell types in severe COVID-19. Nature. 2021 Jul;595(7868):565–71.

12. Wanner N, Andrieux G, Badia-i-Mompel P, Edler C, Pfefferle S, Lindenmeyer MT, et al. Molecular consequences of SARS-CoV-2 liver tropism. Nat Metab. 2022 Mar;4(3):310–9.

13. Huang C, Wang Y, Li X, Ren L, Zhao J, Hu Y, et al. Clinical features of patients infected with 2019 novel coronavirus in Wuhan, China. Lancet. 2020;395(10223):497–506.

14. Backer JA, Klinkenberg D, Wallinga J. Incubation period of 2019 novel coronavirus (2019-nCoV) infections among travellers from Wuhan, China, 20–28 January 2020. Euro Surveill. 2020 Feb 6;25(5):2000062.

15. Linton NM, Kobayashi T, Yang Y, Hayashi K, Akhmetzhanov AR, Jung S mok, et al. Incubation Period and Other Epidemiological Characteristics of 2019 Novel Coronavirus Infections with Right Truncation: A Statistical Analysis of Publicly Available Case Data. J Clin Med. 2020 Feb 17;9(2):538.

16. Alimohamadi Y, Taghdir M, Sepandi M. Estimate of the Basic Reproduction Number for COVID-19: A Systematic Review and Meta-analysis. J Prev Med Public Health. 2020 May;53(3):151–7.

17. Mizumoto K, Kagaya K, Zarebski A, Chowell G. Estimating the asymptomatic proportion of coronavirus disease 2019 (COVID-19) cases on board the Diamond Princess cruise ship, Yokohama, Japan, 2020. Euro Surveill. 2020 Mar;25(10).

18. Nishiura H, Kobayashi T, Miyama T, Suzuki A, Jung S mok, Hayashi K, et al. Estimation of the asymptomatic ratio of novel coronavirus infections (COVID-19). International Journal of Infectious Diseases. 2020 May 1;94:154–5.

19. Chen N, Zhou M, Dong X, Qu J, Gong F, Han Y, et al. Epidemiological and clinical characteristics of 99 cases of 2019 novel coronavirus pneumonia in Wuhan, China: a descriptive study. The Lancet. 2020 Feb 15;395(10223):507–13.

20. Wang D, Hu B, Hu C, Zhu F, Liu X, Zhang J, et al. Clinical Characteristics of 138 Hospitalized Patients With 2019 Novel Coronavirus–Infected Pneumonia in Wuhan, China. JAMA. 2020 Mar 17;323(11):1061–9.

21. Guan W jie, Ni Z yi, Hu Y, Liang W hua, Ou C quan, He J xing, et al. Clinical Characteristics of Coronavirus Disease 2019 in China. N Engl J Med. 2020 Apr 30;382(18):1708–20.

22. Wu Z, McGoogan JM. Characteristics of and Important Lessons From the Coronavirus Disease 2019 (COVID-19) Outbreak in China: Summary of a Report of 72 314 Cases From the Chinese Center for Disease Control and Prevention. JAMA. 2020 Apr 7;323(13):1239–42.

23. Figliozzi S, Masci PG, Ahmadi N, Tondi L, Koutli E, Aimo A, et al. Predictors of adverse prognosis in COVID-19: A systematic review and meta-analysis. European Journal of Clinical Investigation. 2020;50(10):e13362.

24. Kim D, Lee JY, Yang JS, Kim JW, Kim VN, Chang H. The Architecture of SARS-CoV-2 Transcriptome. Cell. 2020 May 14;181(4):914-921.e10.

25. Korber B, Fischer WM, Gnanakaran S, Yoon H, Theiler J, Abfalterer W, et al. Tracking Changes in SARS-CoV-2 Spike: Evidence that D614G Increases Infectivity of the COVID-19 Virus. Cell. 2020 Aug 20;182(4):812-827.e19.

26. Tao K, Tzou PL, Nouhin J, Gupta RK, de Oliveira T, Kosakovsky Pond SL, et al. The biological and clinical significance of emerging SARS-CoV-2 variants. Nat Rev Genet. 2021 Dec;22(12):757–73.

27. Cao Y, Wang J, Jian F, Xiao T, Song W, Yisimayi A, et al. Omicron escapes the majority of existing SARS-CoV-2 neutralizing antibodies. Nature. 2022 Feb;602(7898):657–63.

28. Nyberg T, Ferguson NM, Nash SG, Webster HH, Flaxman S, Andrews N, et al. Comparative analysis of the risks of hospitalisation and death associated with SARS-CoV-2 omicron (B.1.1.529) and delta (B.1.617.2) variants in England: a cohort study. The Lancet. 2022 Apr 2;399(10332):1303–12.

29. Yamasoba D, Kimura I, Nasser H, Morioka Y, Nao N, Ito J, et al. Virological characteristics of the SARS-CoV-2 Omicron BA.2 spike. Cell. 2022 Jun 9;185(12):2103-2115.e19.

30. Cao Y, Yisimayi A, Jian F, Song W, Xiao T, Wang L, et al. BA.2.12.1, BA.4 and BA.5 escape antibodies elicited by Omicron infection. Nature. 2022 Aug;608(7923):593–602.

31. Hamming I, Timens W, Bulthuis M, Lely A, Navis G, van Goor H. Tissue distribution of ACE2 protein, the functional receptor for SARS coronavirus. A first step in understanding SARS pathogenesis. J Pathol. 2004 Jun;203(2):631–7.

32. Beyerstedt S, Casaro EB, Rangel ÉB. COVID-19: angiotensin-converting enzyme 2 (ACE2) expression and tissue susceptibility to SARS-CoV-2 infection. Eur J Clin Microbiol Infect Dis. 2021 May;40(5):905–19.

33. Hoffmann M, Kleine-Weber H, Schroeder S, Krüger N, Herrler T, Erichsen S, et al. SARS-CoV-2 Cell Entry Depends on ACE2 and TMPRSS2 and Is Blocked by a Clinically Proven Protease Inhibitor. Cell. 2020 Apr 16;181(2):271-280.e8.

34. Khan M, Yoo SJ, Clijsters M, Backaert W, Vanstapel A, Speleman K, et al. Visualizing in deceased COVID-19 patients how SARS-CoV-2 attacks the respiratory and olfactory mucosae but spares the olfactory bulb. Cell. 2021 Nov 24;184(24):5932-5949.e15.

35. Xu Z, Shi L, Wang Y, Zhang J, Huang L, Zhang C, et al. Pathological findings of COVID-19 associated with acute respiratory distress syndrome. The Lancet Respiratory Medicine. 2020 Apr 1;8(4):420–2.

36. Jensen S, Thomsen AR. Sensing of RNA Viruses: a Review of Innate Immune Receptors Involved in Recognizing RNA Virus Invasion. J Virol. 2012 Mar;86(6):2900–10.

37. Delorey TM, Ziegler CGK, Heimberg G, Normand R, Yang Y, Segerstolpe Å, et al. COVID-19 tissue atlases reveal SARS-CoV-2 pathology and cellular targets. Nature. 2021 Jul;595(7865):107–13.

38. Hu B, Huang S, Yin L. The cytokine storm and COVID-19. Journal of Medical Virology. 2021;93(1):250–6.

39. Lucas C, Wong P, Klein J, Castro TBR, Silva J, Sundaram M, et al. Longitudinal analyses reveal immunological misfiring in severe COVID-19. Nature. 2020 Aug;584(7821):463–9.

40. Qin C, Zhou L, Hu Z, Zhang S, Yang S, Tao Y, et al. Dysregulation of Immune Response in Patients With Coronavirus 2019 (COVID-19) in Wuhan, China. Clinical Infectious Diseases. 2020 Jul 28;71(15):762–8.

41. Tan L, Wang Q, Zhang D, Ding J, Huang Q, Tang YQ, et al. Lymphopenia predicts disease severity of COVID-19: a descriptive and predictive study. Sig Transduct Target Ther. 2020 Mar 27;5(1):1–3.

42. Afzali B, Noris M, Lambrecht BN, Kemper C. The state of complement in COVID-19. Nat Rev Immunol. 2022 Feb;22(2):77–84.

43. Mathew D, Giles JR, Baxter AE, Oldridge DA, Greenplate AR, Wu JE, et al. Deep immune profiling of COVID-19 patients reveals distinct immunotypes with therapeutic implications. Science. 2020 Sep 4;369(6508):eabc8511.

44. Sinkovits G, Mező B, Réti M, Müller V, Iványi Z, Gál J, et al. Complement Overactivation and Consumption Predicts In-Hospital Mortality in SARS-CoV-2 Infection. Frontiers in Immunology [Internet]. 2021 [cited 2022 Apr 13];12. Available from: https://www.frontiersin.org/article/10.3389/fimmu.2021.663187

45. Zinellu A, Mangoni AA. Serum Complement C3 and C4 and COVID-19 Severity and Mortality: A Systematic Review and Meta-Analysis With Meta-Regression. Frontiers in Immunology [Internet]. 2021 [cited 2022 Apr 7];12. Available from: https://www.frontiersin.org/article/10.3389/fimmu.2021.696085

46. Aid M, Busman-Sahay K, Vidal SJ, Maliga Z, Bondoc S, Starke C, et al. Vascular Disease and Thrombosis in SARS-CoV-2-Infected Rhesus Macaques. Cell. 2020 Nov 25;183(5):1354-1366.e13.

47. Goshua G, Pine AB, Meizlish ML, Chang CH, Zhang H, Bahel P, et al. Endotheliopathy in COVID-19-associated coagulopathy: evidence from a single-centre, cross-sectional study. Lancet Haematol. 2020 Aug;7(8):e575–82.

48. Varga Z, Flammer AJ, Steiger P, Haberecker M, Andermatt R, Zinkernagel AS, et al. Endothelial cell infection and endotheliitis in COVID-19. Lancet. 2020;395(10234):1417–8.

49. Wu Z, Hu R, Zhang C, Ren W, Yu A, Zhou X. Elevation of plasma angiotensin II level is a potential pathogenesis for the critically ill COVID-19 patients. Crit Care. 2020 Jun 5;24(1):290.

50. Senchenkova EY, Russell J, Almeida-Paula LD, Harding JW, Granger DN. Angiotensin II–Mediated Microvascular Thrombosis. Hypertension. 2010 Dec;56(6):1089–95.

51. Borczuk AC, Salvatore SP, Seshan SV, Patel SS, Bussel JB, Mostyka M, et al. COVID-19 pulmonary pathology: a multi-institutional autopsy cohort from Italy and New York City. Mod Pathol. 2020 Nov;33(11):2156–68.

52. Zhang L, Yan X, Fan Q, Liu H, Liu X, Liu Z, et al. D-dimer levels on admission to predict in-hospital mortality in patients with Covid-19. Journal of Thrombosis and Haemostasis. 2020;18(6):1324–9.

53. Puelles VG, Lütgehetmann M, Lindenmeyer MT, Sperhake JP, Wong MN, Allweiss L, et al. Multiorgan and Renal Tropism of SARS-CoV-2. N Engl J Med. 2020 Aug 6;383(6):590–2.

54. Wang Y, Liu S, Liu H, Li W, Lin F, Jiang L, et al. SARS-CoV-2 infection of the liver directly contributes to hepatic impairment in patients with COVID-19. Journal of Hepatology. 2020 Oct 1;73(4):807–16.

55. Natarajan A, Zlitni S, Brooks EF, Vance SE, Dahlen A, Hedlin H, et al. Gastrointestinal symptoms and fecal shedding of SARS-CoV-2 RNA suggest prolonged gastrointestinal infection. Med [Internet]. 2022 Apr 12 [cited 2022 May 12];0(0). Available from: https://www.cell.com/med/abstract/S2666-6340(22)00167-2

56. Zollner A, Koch R, Jukic A, Pfister A, Meyer M, Rössler A, et al. Post-acute COVID-19 is characterized by gut viral antigen persistence in inflammatory bowel diseases. Gastroenterology. 2022 Apr 28;S0016-5085(22)00450-4.

57. Kudose S, Batal I, Santoriello D, Xu K, Barasch J, Peleg Y, et al. Kidney Biopsy Findings in Patients with COVID-19. JASN. 2020 Sep 1;31(9):1959–68.

58. Nie X, Qian L, Sun R, Huang B, Dong X, Xiao Q, et al. Multi-organ proteomic landscape of COVID-19 autopsies. Cell. 2021 Feb;184(3):775-791.e14.

59. Helms J, Kremer S, Merdji H, Clere-Jehl R, Schenck M, Kummerlen C, et al. Neurologic Features in Severe SARS-CoV-2 Infection. N Engl J Med. 2020 Jun 4;382(23):2268–70.

60. Paterson RW, Brown RL, Benjamin L, Nortley R, Wiethoff S, Bharucha T, et al. The emerging spectrum of COVID-19 neurology: clinical, radiological and laboratory findings. Brain. 2020 Oct 1;143(10):3104–20.

61. Matschke J, Lütgehetmann M, Hagel C, Sperhake JP, Schröder AS, Edler C, et al. Neuropathology of patients with COVID-19 in Germany: a post-mortem case series. The Lancet Neurology. 2020 Nov 1;19(11):919–29.

62. Ellul MA, Benjamin L, Singh B, Lant S, Michael BD, Easton A, et al. Neurological associations of COVID-19. The Lancet Neurology. 2020 Sep 1;19(9):767–83.

63. Taquet M, Geddes JR, Husain M, Luciano S, Harrison PJ. 6-month neurological and psychiatric outcomes in 236 379 survivors of COVID-19: a retrospective cohort study using electronic health records. The Lancet Psychiatry. 2021 May 1;8(5):416–27.

64. Rogers JP, Watson CJ, Badenoch J, Cross B, Butler M, Song J, et al. Neurology and neuropsychiatry of COVID-19: a systematic review and meta-analysis of the early literature reveals frequent CNS manifestations and key emerging narratives. J Neurol Neurosurg Psychiatry. 2021 Sep 1;92(9):932–41.

65. Kumar S, Veldhuis A, Malhotra T. Neuropsychiatric and Cognitive Sequelae of COVID-19. Frontiers in Psychology [Internet]. 2021 [cited 2022 Mar 25];12. Available from: https://www.frontiersin.org/article/10.3389/fpsyg.2021.577529

66. Wu P, Duan F, Luo C, Liu Q, Qu X, Liang L, et al. Characteristics of Ocular Findings of Patients With Coronavirus Disease 2019 (COVID-19) in Hubei Province, China. JAMA Ophthalmol. 2020 May 1;138(5):575–8.

67. Shen C, Wang Z, Zhao F, Yang Y, Li J, Yuan J, et al. Treatment of 5 Critically Ill Patients With COVID-19 With Convalescent Plasma. JAMA. 2020 Apr 28;323(16):1582–9.

68. Xu X, Han M, Li T, Sun W, Wang D, Fu B, et al. Effective treatment of severe COVID-19 patients with tocilizumab. Proc Natl Acad Sci U S A. 2020 May 19;117(20):10970–5.

69. Plotkin SA. Updates on immunologic correlates of vaccine-induced protection. Vaccine. 2020 Feb 24;38(9):2250–7.

70. Polack FP, Thomas SJ, Kitchin N, Absalon J, Gurtman A, Lockhart S, et al. Safety and Efficacy of the BNT162b2 mRNA Covid-19 Vaccine. New England Journal of Medicine. 2020 Dec 31;383(27):2603–15.

71. Baden LR, El Sahly HM, Essink B, Kotloff K, Frey S, Novak R, et al. Efficacy and Safety of the mRNA-1273 SARS-CoV-2 Vaccine. New England Journal of Medicine. 2021 Feb 4;384(5):403–16.

72. Olliaro P, Torreele E, Vaillant M. COVID-19 vaccine efficacy and effectiveness—the elephant (not) in the room. The Lancet Microbe. 2021 Jul 1;2(7):e279–80.

73. Lauring AS, Tenforde MW, Chappell JD, Gaglani M, Ginde AA, McNeal T, et al. Clinical severity of, and effectiveness of mRNA vaccines against, covid-19 from omicron, delta, and alpha SARS-CoV-2 variants in the United States: prospective observational study. BMJ. 2022 Mar 9;376:e069761.

74. Knoll MD, Wonodi C. Oxford–AstraZeneca COVID-19 vaccine efficacy. The Lancet. 2021 Jan 9;397(10269):72–4.

75. Gupta A, Madhavan MV, Sehgal K, Nair N, Mahajan S, Sehrawat TS, et al. Extrapulmonary manifestations of COVID-19. Nat Med. 2020 Jul;26(7):1017–32.

76. Hirsch JS, Ng JH, Ross DW, Sharma P, Shah HH, Barnett RL, et al. Acute kidney injury in patients hospitalized with COVID-19. Kidney Int. 2020 Jul;98(1):209–18.

77. Zubair AS, McAlpine LS, Gardin T, Farhadian S, Kuruvilla DE, Spudich S. Neuropathogenesis and Neurologic Manifestations of the Coronaviruses in the Age of Coronavirus Disease 2019: A Review. JAMA Neurol. 2020 Aug 1;77(8):1018–27.

78. Ayoubkhani D, Khunti K, Nafilyan V, Maddox T, Humberstone B, Diamond I, et al. Post-covid syndrome in individuals admitted to hospital with covid-19: retrospective cohort study. BMJ. 2021 Mar 31;372:n693.

79. Lopez-Leon S, Wegman-Ostrosky T, Perelman C, Sepulveda R, Rebolledo PA, Cuapio A, et al. More than 50 long-term effects of COVID-19: a systematic review and meta-analysis. Sci Rep. 2021 Aug 9;11(1):16144.

80. Hama Amin BJ, Kakamad FH, Ahmed GS, Ahmed SF, Abdulla BA, mohammed SH, et al. Post COVID-19 pulmonary fibrosis; a meta-analysis study. Ann Med Surg (Lond). 2022 Apr 6;77:103590.

81. Rysz S, Al-Saadi J, Sjöström A, Farm M, Campoccia Jalde F, Plattén M, et al. COVID-19 pathophysiology may be driven by an imbalance in the renin-angiotensin-aldosterone system. Nat Commun. 2021 Apr 23;12(1):2417.

82. Xie Y, Xu E, Bowe B, Al-Aly Z. Long-term cardiovascular outcomes of COVID-19. Nat Med. 2022 Mar;28(3):583–90.

83. Long JD, Strohbehn I, Sawtell R, Bhattacharyya R, Sise ME. COVID-19 Survival and its impact on chronic kidney disease. Translational Research. 2022 Mar 1;241:70–82.

84. Bowe B, Xie Y, Xu E, Al-Aly Z. Kidney Outcomes in Long COVID. JASN. 2021 Nov 1;32(11):2851–62.

85. Dan JM, Mateus J, Kato Y, Hastie KM, Yu ED, Faliti CE, et al. Immunological memory to SARS-CoV-2 assessed for up to 8 months after infection. Science. 2021 Feb 5;371(6529):eabf4063.

86. Turner JS. SARS-CoV-2 infection induces long-lived bone marrow plasma cells in humans. :15.

87. Huang L, Yao Q, Gu X, Wang Q, Ren L, Wang Y, et al. 1-year outcomes in hospital survivors with COVID-19: a longitudinal cohort study. The Lancet. 2021 Aug 28;398(10302):747–58.

88. Al-Aly Z, Xie Y, Bowe B. High-dimensional characterization of post-acute sequelae of COVID-19. Nature. 2021 Jun;594(7862):259–64.

89. Huang L, Li X, Gu X, Zhang H, Ren L, Guo L, et al. Health outcomes in people 2 years after surviving hospitalisation with COVID-19: a longitudinal cohort study. The Lancet Respiratory Medicine [Internet]. 2022 May 11 [cited 2022 May 16];0(0). Available from: https://www.thelancet.com/journals/lanres/article/PIIS2213-2600(22)00126-6/fulltext

90. Asadi-Pooya AA, Akbari A, Emami A, Lotfi M, Rostamihosseinkhani M, Nemati H, et al. Long COVID syndrome-associated brain fog. Journal of Medical Virology. 2022;94(3):979–84.

91. Hugon J, Msika EF, Queneau M, Farid K, Paquet C. Long COVID: cognitive complaints (brain fog) and dysfunction of the cingulate cortex. J Neurol. 2022 Jan 1;269(1):44–6.

92. Ceban F, Ling S, Lui LMW, Lee Y, Gill H, Teopiz KM, et al. Fatigue and cognitive impairment in Post-COVID-19 Syndrome: A systematic review and meta-analysis. Brain, Behavior, and Immunity. 2022 Mar 1;101:93–135.

93. Premraj L, Kannapadi NV, Briggs J, Seal SM, Battaglini D, Fanning J, et al. Mid and long-term neurological and neuropsychiatric manifestations of post-COVID-19 syndrome: A meta-analysis. J Neurol Sci. 2022 Jan 29;434:120162.

94. Gwenaamp#x000EB lle D. SARS-CoV-2 is associated with changes in brain structure in UK Biobank. :32.

95. Iadecola C, Anrather J, Kamel H. Effects of COVID-19 on the Nervous System. Cell. 2020 Oct 1;183(1):16-27.e1.

96. Song E, Zhang C, Israelow B, Lu-Culligan A, Prado AV, Skriabine S, et al. Neuroinvasion of SARS-CoV-2 in human and mouse brain [Internet]. Microbiology; 2020 Jun [cited 2021 Jul 19]. Available from: http://biorxiv.org/lookup/doi/10.1101/2020.06.25.169946

97. Gomes I, Karmirian K, Oliveira JT, Pedrosa C da SG, Mendes MA, Rosman FC, et al. SARS-CoV-2 infection of the central nervous system in a 14-month-old child: A case report of a complete autopsy. The Lancet Regional Health - Americas. 2021 Oct 1;2:100046.

98. Song E, Zhang C, Israelow B, Lu-Culligan A, Prado AV, Skriabine S, et al. Neuroinvasion of SARS-CoV-2 in human and mouse brain. bioRxiv. 2020 Sep 8;2020.06.25.169946.

99. Zhang L, Zhou L, Bao L, Liu J, Zhu H, Lv Q, et al. SARS-CoV-2 crosses the blood–brain barrier accompanied with basement membrane disruption without tight junctions alteration. Sig Transduct Target Ther. 2021 Sep 6;6(1):1–12.

100. Krasemann S, Haferkamp U, Pfefferle S, Woo MS, Heinrich F, Schweizer M, et al. The blood-brain barrier is dysregulated in COVID-19 and serves as a CNS entry route for SARS-CoV-2. Stem Cell Reports. 2022 Feb 8;17(2):307–20.

101. Meinhardt J, Radke J, Dittmayer C, Franz J, Thomas C, Mothes R, et al. Olfactory transmucosal SARS-CoV-2 invasion as a port of central nervous system entry in individuals with COVID-19. Nat Neurosci. 2021 Feb;24(2):168–75.

102. Cantuti-Castelvetri L, Ojha R, Pedro LD, Djannatian M, Franz J, Kuivanen S, et al. Neuropilin-1 facilitates SARS-CoV-2 cell entry and infectivity. Science. 2020 Nov 13;370(6518):856–60.

103. Daly JL, Simonetti B, Klein K, Chen KE, Williamson MK, Antón-Plágaro C, et al. Neuropilin-1 is a host factor for SARS-CoV-2 infection. Science. 2020 Nov 13;370(6518):861–5.

104. Butowt R, Meunier N, Bryche B, von Bartheld CS. The olfactory nerve is not a likely route to brain infection in COVID-19: a critical review of data from humans and animal models. Acta Neuropathol. 2021 Jun 1;141(6):809–22.

105. Bilinska K, von Bartheld CS, Butowt R. Expression of the ACE2 Virus Entry Protein in the Nervus Terminalis Reveals the Potential for an Alternative Route to Brain Infection in COVID-19. Frontiers in Cellular Neuroscience [Internet]. 2021 [cited 2022 Mar 24];15. Available from: https://www.frontiersin.org/article/10.3389/fncel.2021.674123

106. Ueda HR, Dodt HU, Osten P, Economo MN, Chandrashekar J, Keller PJ. Whole-Brain Profiling of Cells and Circuits in Mammals by Tissue Clearing and Light-Sheet Microscopy. Neuron. 2020 May 6;106(3):369–87.

107. Hama H, Kurokawa H, Kawano H, Ando R, Shimogori T, Noda H, et al. Scale: a chemical approach for fluorescence imaging and reconstruction of transparent mouse brain. Nat Neurosci. 2011 Nov;14(11):1481–8.

108. Susaki EA, Tainaka K, Perrin D, Kishino F, Tawara T, Watanabe TM, et al. Whole-Brain Imaging with Single-Cell Resolution Using Chemical Cocktails and Computational Analysis. Cell. 2014 Apr 24;157(3):726–39.

109. Three-dimensional imaging of solvent-cleared organs using 3DISCO | Nature Protocols [Internet]. [cited 2022 Apr 30]. Available from: https://www.nature.com/articles/nprot.2012.119

110. Chung K, Deisseroth K. CLARITY for mapping the nervous system. Nat Methods. 2013 Jun;10(6):508–13.

111. Dodt HU, Leischner U, Schierloh A, Jährling N, Mauch CP, Deininger K, et al. Ultramicroscopy: three-dimensional visualization of neuronal networks in the whole mouse brain. Nat Methods. 2007 Apr;4(4):331–6.

112. Liu AKL, Hurry MED, Ng O t. W, DeFelice J, Lai HM, Pearce RKB, et al. Bringing CLARITY to the human brain: visualization of Lewy pathology in three dimensions. Neuropathology and Applied Neurobiology. 2016;42(6):573–87.

113. Lai HM, Liu AKL, Ng HHM, Goldfinger MH, Chau TW, DeFelice J, et al. Next generation histology methods for three-dimensional imaging of fresh and archival human brain tissues. Nat Commun. 2018 Mar 14;9(1):1066.

114. Hildebrand S, Schueth A, Herrler A, Galuske R, Roebroeck A. Scalable Labeling for Cytoarchitectonic Characterization of Large Optically Cleared Human Neocortex Samples. Sci Rep. 2019 Jul 26;9(1):10880.

115. Tainaka K, Murakami TC, Susaki EA, Shimizu C, Saito R, Takahashi K, et al. Chemical Landscape for Tissue Clearing Based on Hydrophilic Reagents. Cell Reports. 2018 Aug 21;24(8):2196-2210.e9.

116. Murray E, Cho JH, Goodwin D, Ku T, Swaney J, Kim SY, et al. Simple, Scalable Proteomic Imaging for High-Dimensional Profiling of Intact Systems. Cell. 2015 Dec 3;163(6):1500–14.

117. Park YG, Sohn CH, Chen R, McCue M, Yun DH, Drummond GT, et al. Protection of tissue physicochemical properties using polyfunctional crosslinkers. Nat Biotechnol. 2019 Jan;37(1):73–83.

118. Ku T, Guan W, Evans NB, Sohn CH, Albanese A, Kim JG, et al. Elasticizing tissues for reversible shape transformation and accelerated molecular labeling. Nat Methods. 2020 Jun;17(6):609–13.

119. Free-of-Acrylamide SDS-based Tissue Clearing (FASTClear) for three dimensional visualization of myocardial tissue - PubMed [Internet]. [cited 2022 Aug 14]. Available from: https://pubmed.ncbi.nlm.nih.gov/28701763/

120. CUBIC pathology: three-dimensional imaging for pathological diagnosis | Scientific Reports [Internet]. [cited 2022 Aug 14]. Available from: https://www.nature.com/articles/s41598-017-09117-0

121. Zhao S, Todorov MI, Cai R, Al -Maskari R, Steinke H, Kemter E, et al. Cellular and Molecular Probing of Intact Human Organs. Cell. 2020 Feb 20;180(4):796-812.e19.

122. Mai H, Rong Z, Zhao S, Cai R, Steinke H, Bechmann I, et al. Scalable tissue labeling and clearing of intact human organs. Nat Protoc. 2022 Jul 20;1–35.

123. Ong SE, Foster LJ, Mann M. Mass spectrometric-based approaches in quantitative proteomics. Methods. 2003 Feb 1;29(2):124–30.

124. Aebersold R, Mann M. Mass spectrometry-based proteomics. Nature. 2003 Mar;422(6928):198–207.

125. Doerr A. DIA mass spectrometry. Nat Methods. 2015 Jan;12(1):35–35.

126. Meier F, Park MA, Mann M. Trapped Ion Mobility Spectrometry and Parallel Accumulation–Serial Fragmentation in Proteomics. Molecular & Cellular Proteomics [Internet]. 2021 Jan 1 [cited 2022 Aug 15];20. Available from: https://www.mcponline.org/article/S1535-9476(21)00110-9/abstract

127. Liu J, Li Y, Liu Q, Yao Q, Wang X, Zhang H, et al. SARS-CoV-2 cell tropism and multiorgan infection. Cell Discov. 2021 Mar 23;7(1):1–4.

128. Demichev V, Messner CB, Vernardis SI, Lilley KS, Ralser M. DIA-NN: neural networks and interference correction enable deep proteome coverage in high throughput. Nat Methods. 2020 Jan;17(1):41–4.

129. Bindea G, Mlecnik B, Hackl H, Charoentong P, Tosolini M, Kirilovsky A, et al. ClueGO: a Cytoscape plug-in to decipher functionally grouped gene ontology and pathway annotation networks. Bioinformatics. 2009 Apr 15;25(8):1091–3.

130. Torres-Platas SG, Comeau S, Rachalski A, Bo GD, Cruceanu C, Turecki G, et al. Morphometric characterization of microglial phenotypes in human cerebral cortex. Journal of Neuroinflammation. 2014 Jan 21;11(1):12.

131. Derakhshani A, Hemmat N, Asadzadeh Z, Ghaseminia M, Shadbad MA, Jadideslam G, et al. Arginase 1 (Arg1) as an Up-Regulated Gene in COVID-19 Patients: A Promising Marker in COVID-19 Immunopathy. J Clin Med. 2021 Mar 4;10(5):1051.

132. Xu J, Xu X, Jiang L, Dua K, Hansbro PM, Liu G. SARS-CoV-2 induces transcriptional signatures in human lung epithelial cells that promote lung fibrosis. Respiratory Research. 2020 Jul 14;21(1):182.

133. Xu ZS, Shu T, Kang L, Wu D, Zhou X, Liao BW, et al. Temporal profiling of plasma cytokines, chemokines and growth factors from mild, severe and fatal COVID-19 patients. Sig Transduct Target Ther. 2020 Jun 19;5(1):1–3.

134. Ackermann M, Mentzer SJ, Kolb M, Jonigk D. Inflammation and intussusceptive angiogenesis in COVID-19: everything in and out of flow. Eur Respir J. 2020 Nov 12;56(5):2003147.

135. Igloi Z, Mohl BP, Lippiat JD, Harris M, Mankouri J. Requirement for Chloride Channel Function during the Hepatitis C Virus Life Cycle. J Virol. 2015 Jan 21;89(7):4023–9.

136. Herrera J, Henke CA, Bitterman PB. Extracellular matrix as a driver of progressive fibrosis. J Clin Invest. 128(1):45–53.

137. Paine R, Ward PA. Cell adhesion molecules and pulmonary fibrosis 1 2. The American Journal of Medicine. 1999 Sep 1;107(3):268–79.

138. Carapito R, Li R, Helms J, Carapito C, Gujja S, Rolli V, et al. Identification of driver genes for critical forms of COVID-19 in a deeply phenotyped young patient cohort. Science Translational Medicine. 2021 Oct 26;14(628):eabj7521.

139. Zhou Z, Ren L, Zhang L, Zhong J, Xiao Y, Jia Z, et al. Heightened Innate Immune Responses in the Respiratory Tract of COVID-19 Patients. Cell Host & Microbe. 2020 Jun 10;27(6):883-890.e2.

140. Yang Y, Wu Y, Meng X, Wang Z, Younis M, Liu Y, et al. SARS-CoV-2 membrane protein causes the mitochondrial apoptosis and pulmonary edema via targeting BOK. Cell Death Differ. 2022 Jul;29(7):1395–408.

141. Makhoba XH, Makumire S. The capture of host cell's resources: The role of heat shock proteins and polyamines in SARS-COV-2 (COVID-19) pathway to viral infection. Biomolecular Concepts. 2022 Jan 1;13(1):220–9.

142. Shang C, Liu Z, Zhu Y, Lu J, Ge C, Zhang C, et al. SARS-CoV-2 Causes Mitochondrial Dysfunction and Mitophagy Impairment. Front Microbiol. 2021;12:780768.

143. Pajo AT, Espiritu AI, Apor ADAO, Jamora RDG. Neuropathologic findings of patients with COVID-19: a systematic review. Neurol Sci. 2021 Apr 1;42(4):1255–66.

144. Cabal-Herrera AM, Mateen FJ. COVID-19 in a patient treated with eculizumab for aquaporin-4 neuromyelitis optica. J Neurol. 2021 Dec;268(12):4479–82.

145. Zuniga M, Gomes C, Carsons SE, Bender MT, Cotzia P, Miao QR, et al. Autoimmunity to annexin A2 predicts mortality among hospitalised COVID-19 patients. Eur Respir J. 2021 Oct;58(4):2100918.

146. Liu J, Lu F, Chen Y, Plow E, Qin J. Integrin mediates cell entry of the SARS-CoV-2 virus independent of cellular receptor ACE2. J Biol Chem. 2022 Mar;298(3):101710.

147. Rhea EM, Logsdon AF, Hansen KM, Williams LM, Reed MJ, Baumann KK, et al. The S1 protein of SARS-CoV-2 crosses the blood–brain barrier in mice. Nat Neurosci. 2021 Mar;24(3):368–78.

148. Nuovo GJ, Magro C, Shaffer T, Awad H, Suster D, Mikhail S, et al. Endothelial cell damage is the central part of COVID-19 and a mouse model induced by injection of the S1 subunit of the spike protein. Annals of Diagnostic Pathology. 2021 Apr 1;51:151682.

149. Biancatelli RMLC, Solopov PA, Sharlow ER, Lazo JS, Marik PE, Catravas JD. The SARS-CoV-2 spike protein subunit S1 induces COVID-19-like acute lung injury in K18-hACE2 transgenic mice and barrier dysfunction in human endothelial cells. American Journal of Physiology-Lung Cellular and Molecular Physiology [Internet]. 2021 Aug 10 [cited 2022 Apr 30]; Available from: https://journals.physiology.org/doi/full/10.1152/ajplung.00223.2021

150. Ma X. Pathological and molecular examinations of postmortem testis biopsies reveal SARS-CoV-2 infection in the testis and spermatogenesis damage in COVID-19 patients. :3.

151. Herisson F. Direct vascular channels connect skull bone marrow and the brain surface enabling myeloid cell migration. Nature Neuroscience. 2018;21:14.

152. Cai R, Pan C, Ghasemigharagoz A, Todorov MI, Förstera B, Zhao S, et al. Panoptic imaging of transparent mice reveals whole-body neuronal projections and skull–meninges connections. Nat Neurosci. 2019 Feb;22(2):317–27.

153. Cugurra A, Mamuladze T, Rustenhoven J, Dykstra T, Beroshvili G, Greenberg ZJ, et al. Skull and vertebral bone marrow are myeloid cell reservoirs for the meninges and CNS parenchyma. 2021;13.

154. Pulous FE, Cruz-Hernández JC, Yang C, Kaya Z, Wojtkiewicz G, Capen D, et al. Cerebrospinal fluid outflow through skull channels instructs cranial hematopoiesis [Internet]. bioRxiv; 2021 [cited 2022 Apr 12]. p. 2021.08.27.457954. Available from: https://www.biorxiv.org/content/10.1101/2021.08.27.457954v1

155. Letarov AV, Babenko VV, Kulikov EE. Free SARS-CoV-2 Spike Protein S1 Particles May Play a Role in the Pathogenesis of COVID-19 Infection. Biochemistry Moscow. 2021 Mar 1;86(3):257–61.

156. Lei Y, Zhang J, Schiavon CR, He M, Chen L, Shen H, et al. SARS-CoV-2 Spike Protein Impairs Endothelial Function via Downregulation of ACE 2. Circulation Research. 2021 Apr 30;128(9):1323–6.

157. Vankadari N, Wilce JA. Emerging COVID-19 coronavirus: glycan shield and structure prediction of spike glycoprotein and its interaction with human CD26. Emerging Microbes & Infections. 2020 Jan 1;9(1):601–4.

158. Qi F, Qian S, Zhang S, Zhang Z. Single cell RNA sequencing of 13 human tissues identify cell types and receptors of human coronaviruses. Biochem Biophys Res Commun. 2020 May 21;526(1):135–40.

159. Vanderbeke L, Van Mol P, Van Herck Y, De Smet F, Humblet-Baron S, Martinod K, et al. Monocyte-driven atypical cytokine storm and aberrant neutrophil activation as key mediators of COVID-19 disease severity. Nat Commun. 2021 Jul 5;12(1):4117.

160. Rosa BA, Ahmed M, Singh DK, Choreño-Parra JA, Cole J, Jiménez-Álvarez LA, et al. IFN signaling and neutrophil degranulation transcriptional signatures are induced during SARS-CoV-2 infection. Commun Biol. 2021 Mar 5;4(1):1–14.

161. Activated platelets present high mobility group box 1 to neutrophils, inducing autophagy and promoting the extrusion of neutrophil extracellular traps - Maugeri - 2014 - Journal of Thrombosis and Haemostasis - Wiley Online Library [Internet]. [cited 2022 Apr 30]. Available from: https://onlinelibrary.wiley.com/doi/10.1111/jth.12710

162. S100A8 may govern hyper‐inflammation in severe COVID‐19 - Deguchi - 2021 - The FASEB Journal - Wiley Online Library [Internet]. [cited 2022 Apr 30]. Available from: https://faseb.onlinelibrary.wiley.com/doi/10.1096/fj.202101013

163. Stark K, Massberg S. Interplay between inflammation and thrombosis in cardiovascular pathology. Nat Rev Cardiol. 2021 Sep;18(9):666–82.

164. Zhao E, Xu H, Wang L, Kryczek I, Wu K, Hu Y, et al. Bone marrow and the control of immunity. Cell Mol Immunol. 2012 Jan;9(1):11–9.

165. DeOre BJ, Tran KA, Andrews AM, Ramirez SH, Galie PA. SARS-CoV-2 Spike Protein Disrupts Blood–Brain Barrier Integrity via RhoA Activation. J Neuroimmune Pharmacol. 2021 Dec 1;16(4):722–8.

166. McCormick B, Chu JY, Vermeren S. Cross-talk between Rho GTPases and PI3K in the neutrophil. Small GTPases. 2019 May;10(3):187–95.

167. Ercan H, Schrottmaier WC, Pirabe A, Schmuckenschlager A, Pereyra D, Santol J, et al. Platelet Phenotype Analysis of COVID-19 Patients Reveals Progressive Changes in the Activation of Integrin αIIbβ3, F13A1, the SARS-CoV-2 Target EIF4A1 and Annexin A5. Front Cardiovasc Med. 2021;8:779073.

168. Wyler E, Mösbauer K, Franke V, Diag A, Gottula LT, Arsiè R, et al. Transcriptomic profiling of SARS-CoV-2 infected human cell lines identifies HSP90 as target for COVID-19 therapy. iScience. 2021 Mar 19;24(3):102151.

169. Qiu X, Hong C, Li Y, Bao W, Gao XM. Calreticulin as a hydrophilic chimeric molecular adjuvant enhances IgG responses to the spike protein of severe acute respiratory syndrome coronavirus. Microbiol Immunol. 2012 Aug;56(8):554–61.

170. Bhattacharya K, Weidenauer L, Luengo TM, Pieters EC, Echeverría PC, Bernasconi L, et al. The Hsp70-Hsp90 co-chaperone Hop/Stip1 shifts the proteostatic balance from folding towards degradation. Nat Commun. 2020 Nov 25;11(1):5975.

171. Wang JY, Zhang W, Roehrl VB, Roehrl MW, Roehrl MH. An Autoantigenome from HS-Sultan B-Lymphoblasts Offers a Molecular Map for Investigating Autoimmune Sequelae of COVID-19. bioRxiv. 2021 Apr 6;2021.04.05.438500.

172. Miorin L, Kehrer T, Sanchez-Aparicio MT, Zhang K, Cohen P, Patel RS, et al. SARS-CoV-2 Orf6 hijacks Nup98 to block STAT nuclear import and antagonize interferon signaling. Proc Natl Acad Sci U S A. 2020 Nov 10;117(45):28344–54.

173. Zhou YQ, Wang K, Wang XY, Cui HY, Zhao Y, Zhu P, et al. SARS-CoV-2 pseudovirus enters the host cells through spike protein-CD147 in an Arf6-dependent manner. Emerg Microbes Infect. 2022 Dec;11(1):1135–44.

174. Messner CB, Demichev V, Wendisch D, Michalick L, White M, Freiwald A, et al. Ultra-High-Throughput Clinical Proteomics Reveals Classifiers of COVID-19 Infection. Cell Syst. 2020 Jul 22;11(1):11-24.e4.

175. Voskobiynyk Y, Roth JR, Cochran JN, Rush T, Carullo NV, Mesina JS, et al. Alzheimer's disease risk gene BIN1 induces Tau-dependent network hyperexcitability. Elife. 2020 Jul 13;9:e57354.

176. Role of COL4A1 in Small-Vessel Disease and Hemorrhagic Stroke | NEJM [Internet]. [cited 2022 May 3]. Available from: https://www.nejm.org/doi/full/10.1056/NEJMoa053727

177. Zou M, Su X, Wang L, Yi X, Qiu Y, Yin X, et al. The Molecular Mechanism of Multiple Organ Dysfunction and Targeted Intervention of COVID-19 Based on Time-Order Transcriptomic Analysis. Front Immunol. 2021;12:729776.

178. Da Silva JD, Costa MD, Almeida B, Lopes F, Maciel P, Teixeira-Castro A. Case Report: A Novel GNB1 Mutation Causes Global Developmental Delay With Intellectual Disability and Behavioral Disorders. Front Neurol. 2021;12:735549.

179. Leng L, Cao R, Ma J, Mou D, Zhu Y, Li W, et al. Pathological features of COVID-19-associated lung injury: a preliminary proteomics report based on clinical samples. Sig Transduct Target Ther. 2020 Dec;5(1):240.

180. Alfaro E, Díaz-García E, García-Tovar S, Zamarrón E, Mangas A, Galera R, et al. Upregulated Proteasome Subunits in COVID-19 Patients: A Link with Hypoxemia, Lymphopenia and Inflammation. Biomolecules. 2022 Mar;12(3):442.

181. Sun G, Cui Q, Garcia G, Wang C, Zhang M, Arumugaswami V, et al. Comparative transcriptomic analysis of SARS-CoV-2 infected cell model systems reveals differential innate immune responses. Sci Rep. 2021 Aug 25;11(1):17146.

182. Kamel W, Noerenberg M, Cerikan B, Chen H, Järvelin AI, Kammoun M, et al. Global analysis of protein-RNA interactions in SARS-CoV-2-infected cells reveals key regulators of infection. Molecular Cell. 2021 Jul 1;81(13):2851-2867.e7.

183. Li Z, Yao Y, Cheng X, Chen Q, Zhao W, Ma S, et al. A computational framework of host-based drug repositioning for broad-spectrum antivirals against RNA viruses. iScience [Internet]. 2021 Mar 19 [cited 2022 May 3];24(3). Available from: https://www.cell.com/iscience/abstract/S2589-0042(21)00116-4

184. Derosa L, Melenotte C, Griscelli F, Gachot B, Marabelle A, Kroemer G, et al. The immuno-oncological challenge of COVID-19. Nat Cancer. 2020 Oct;1(10):946–64.

185. Gassen NC, Papies J, Bajaj T, Emanuel J, Dethloff F, Chua RL, et al. SARS-CoV-2-mediated dysregulation of metabolism and autophagy uncovers host-targeting antivirals. Nat Commun. 2021 Jun 21;12(1):3818.

186. Soldatov VO, Kubekina MV, Silaeva YY, Bruter AV, Deykin AV. On the way from SARS-CoV-sensitive mice to murine COVID-19 model. Research Results in Pharmacology. 2020 May 4;6(2):1–7.

187. Li W, Greenough TC, Moore MJ, Vasilieva N, Somasundaran M, Sullivan JL, et al. Efficient Replication of Severe Acute Respiratory Syndrome Coronavirus in Mouse Cells Is Limited by Murine Angiotensin-Converting Enzyme 2. Journal of Virology. 2004 Oct 15;78(20):11429–33.

188. Sun SH, Chen Q, Gu HJ, Yang G, Wang YX, Huang XY, et al. A Mouse Model of SARS-CoV-2 Infection and Pathogenesis. Cell Host & Microbe. 2020 Jul 8;28(1):124-133.e4.

189. McCray PB, Pewe L, Wohlford-Lenane C, Hickey M, Manzel L, Shi L, et al. Lethal infection of K18-hACE2 mice infected with severe acute respiratory syndrome coronavirus. J Virol. 2007 Jan;81(2):813–21.

190. Dong W, Mead H, Tian L, Park JG, Garcia JI, Jaramillo S, et al. The K18-Human ACE2 Transgenic Mouse Model Recapitulates Non-severe and Severe COVID-19 in Response to an Infectious Dose of the SARS-CoV-2 Virus. J Virol. 2022 Jan 12;96(1):e0096421.

191. Yoshikawa N, Yoshikawa T, Hill T, Huang C, Watts DM, Makino S, et al. Differential Virological and Immunological Outcome of Severe Acute Respiratory Syndrome Coronavirus Infection in Susceptible and Resistant Transgenic Mice Expressing Human Angiotensin-Converting Enzyme 2. J Virol. 2009 Jun;83(11):5451–65.

192. Feng Y, Xia H, Cai Y, Halabi CM, Becker LK, Santos RAS, et al. Brain-selective overexpression of human Angiotensin-converting enzyme type 2 attenuates neurogenic hypertension. Circ Res. 2010 Feb 5;106(2):373–82.

193. Zhou B, Thao TTN, Hoffmann D, Taddeo A, Ebert N, Labroussaa F, et al. SARS-CoV-2 spike D614G change enhances replication and transmission. Nature. 2021 Apr;592(7852):122–7.

194. Sun J, Zhuang Z, Zheng J, Li K, Wong RLY, Liu D, et al. Generation of a Broadly Useful Model for COVID-19 Pathogenesis, Vaccination, and Treatment. Cell. 2020 Aug 6;182(3):734-743.e5.

195. Niu Z, Zhang Z, Gao X, Du P, Lu J, Yan B, et al. N501Y mutation imparts cross-species transmission of SARS-CoV-2 to mice by enhancing receptor binding. Sig Transduct Target Ther. 2021 Jul 27;6(1):1–3.

196. Shuai H, Chan JFW, Yuen TTT, Yoon C, Hu JC, Wen L, et al. Emerging SARS-CoV-2 variants expand species tropism to murines. eBioMedicine [Internet]. 2021 Nov 1 [cited 2022 Apr 19];73. Available from: https://www.thelancet.com/journals/ebiom/article/PIIS2352-3964(21)00436-9/fulltext

197. Braun F, Lütgehetmann M, Pfefferle S, Wong MN, Carsten A, Lindenmeyer MT, et al. SARS-CoV-2 renal tropism associates with acute kidney injury. The Lancet. 2020 Aug 29;396(10251):597–8.

198. Jansen J, Reimer KC, Nagai JS, Varghese FS, Overheul GJ, de Beer M, et al. SARS-CoV-2 infects the human kidney and drives fibrosis in kidney organoids. Cell Stem Cell. 2022 Feb 3;29(2):217-231.e8.

199. Douaud G, Lee S, Alfaro-Almagro F, Arthofer C, Wang C, McCarthy P, et al. SARS-CoV-2 is associated with changes in brain structure in UK Biobank. Nature. 2022 Mar 7;1–17.

200. George S, Pal AC, Gagnon J, Timalsina S, Singh P, Vydyam P, et al. Evidence for SARS-CoV-2 Spike Protein in the Urine of COVID-19 Patients. Kidney360. 2021 Jun 24;2(6):924–36.

201. Swank Z, Senussi Y, Alter G, Walt DR. Persistent circulating SARS-CoV-2 spike is associated with post-acute COVID-19 sequelae [Internet]. medRxiv; 2022 [cited 2022 Jun 24]. p. 2022.06.14.22276401. Available from: https://www.medrxiv.org/content/10.1101/2022.06.14.22276401v1

202. Qiu Y, Wu D, Ning W, Xu J, Shu T, Huang M, et al. Post-mortem tissue proteomics reveals the pathogenesis of multi-organ injuries of COVID-19. National Science Review. 2021 Nov 1;8(11):nwab143.

203. Gordon DE, Jang GM, Bouhaddou M, Xu J, Obernier K, White KM, et al. A SARS-CoV-2 protein interaction map reveals targets for drug repurposing. Nature. 2020 Jul;583(7816):459–68.

204. Liao M, Liu Y, Yuan J, Wen Y, Xu G, Zhao J, et al. Single-cell landscape of bronchoalveolar immune cells in patients with COVID-19. Nat Med. 2020 Jun;26(6):842–4.

205. Raghavan S, Kenchappa DB, Leo MD. SARS-CoV-2 Spike Protein Induces Degradation of Junctional Proteins That Maintain Endothelial Barrier Integrity. Frontiers in Cardiovascular Medicine [Internet]. 2021 [cited 2022 Jun 28];8. Available from: https://www.frontiersin.org/article/10.3389/fcvm.2021.687783

206. Kim ES, Jeon MT, Kim KS, Lee S, Kim S, Kim DG. Spike Proteins of SARS-CoV-2 Induce Pathological Changes in Molecular Delivery and Metabolic Function in the Brain Endothelial Cells. Viruses. 2021 Oct;13(10):2021.

207. DeOre BJ, Tran KA, Andrews AM, Ramirez SH, Galie PA. SARS-CoV-2 Spike Protein Disrupts Blood-Brain Barrier Integrity via RhoA Activation. J Neuroimmune Pharmacol. 2021 Dec;16(4):722–8.

208. Khan S, Shafiei MS, Longoria C, Schoggins JW, Savani RC, Zaki H. SARS-CoV-2 spike protein induces inflammation via TLR2-dependent activation of the NF-κB pathway. Schiffer JT, Taniguchi T, Allen C, editors. eLife. 2021 Dec 6;10:e68563.

209. Ghebrehiwet B, Peerschke EI. Complement and coagulation: key triggers of COVID-19–induced multiorgan pathology. J Clin Invest. 2020 Nov 2;130(11):5674–6.

210. Pramitasuri TI, Laksmidewi AAAP, Putra IBK, Dalimartha FA. Neutrophil Extracellular Traps in Coronavirus Disease-19-Associated Ischemic Stroke: A Novel Avenue in Neuroscience. Exp Neurobiol. 2021 Feb 28;30(1):1–12.

211. Jorch SK, Kubes P. An emerging role for neutrophil extracellular traps in noninfectious disease. Nat Med. 2017 Mar;23(3):279–87.

212. Li J, Long X, Zhu C, Hu S, Lin Z, Li J, et al. A case of COVID-19 pneumonia with cerebral hemorrhage. Thrombosis Research. 2020 Sep 1;193:22–4.

213. Leasure AC, Khan YM, Iyer R, Elkind MSV, Sansing LH, Falcone GJ, et al. Intracerebral Hemorrhage in Patients With COVID-19. Stroke. 2021 Jul;52(7):e321–3.

214. Lai YC, Kondapalli C, Lehneck R, Procter JB, Dill BD, Woodroof HI, et al. Phosphoproteomic screening identifies Rab GTPases as novel downstream targets of PINK1. EMBO J. 2015 Nov 12;34(22):2840–61.

215. Borger E, Herrmann A, Mann DA, Spires-Jones T, Gunn-Moore F. The calcium-binding protein EFhd2 modulates synapse formation in vitro and is linked to human dementia. J Neuropathol Exp Neurol. 2014 Dec;73(12):1166–82.

216. Brioschi S, Wang WL, Peng V, Wang M, Shchukina I, Greenberg ZJ, et al. Heterogeneity of meningeal B cells reveals a lymphopoietic niche at the CNS borders. Science. 2021 Jul 23;373(6553):eabf9277.

217. Kaur RJ, Dutta S, Bhardwaj P, Charan J, Dhingra S, Mitra P, et al. Adverse Events Reported From COVID-19 Vaccine Trials: A Systematic Review. Indian J Clin Biochem. 2021 Oct;36(4):427–39.

218. Patone M, Handunnetthi L, Saatci D, Pan J, Katikireddi SV, Razvi S, et al. Neurological complications after first dose of COVID-19 vaccines and SARS-CoV-2 infection. Nat Med. 2021 Dec;27(12):2144–53.

219. Montgomery J, Ryan M, Engler R, Hoffman D, McClenathan B, Collins L, et al. Myocarditis Following Immunization With mRNA COVID-19 Vaccines in Members of the US Military. JAMA Cardiology. 2021 Oct 1;6(10):1202–6.

220. Li X, Lai FTT, Chua GT, Kwan MYW, Lau YL, Ip P, et al. Myocarditis Following COVID-19 BNT162b2 Vaccination Among Adolescents in Hong Kong. JAMA Pediatrics. 2022 Jun 1;176(6):612–4.

221. Adverse effects of COVID-19 mRNA vaccines: the spike hypothesis: Trends in Molecular Medicine [Internet]. [cited 2022 Aug 14]. Available from: https://www.cell.com/trends/molecular-medicine/fulltext/S1471-4914(22)00103-4

Appendix A:

I have also contributed to another study exploring the mechanism of Alzheimer's disease with tissue clearing technology in the whole mouse brain. The manuscript was submitted to bioRxiv, DOI:10.1101/2021.11.02.466753, and has been accepted for publication at Cell.

With the help of intact brain imaging, we found the earliest dense core amyloid plaques occurring at five weeks old 5xFAD mouse hippocampus. After 3D reconstruction and positioning of the brain, we could dissect the plaques with spatial information and proceed with proteomics analysis. Briefly, 4 to 6 weeks old 5xFAD mouse brains were stained with Iba1 antibody and Congo red with SHANEL protocol. We identified some proteins associated with amyloid pathology and some novel molecules which might help learn the progression of Alzheimer's disease at the initial stage.

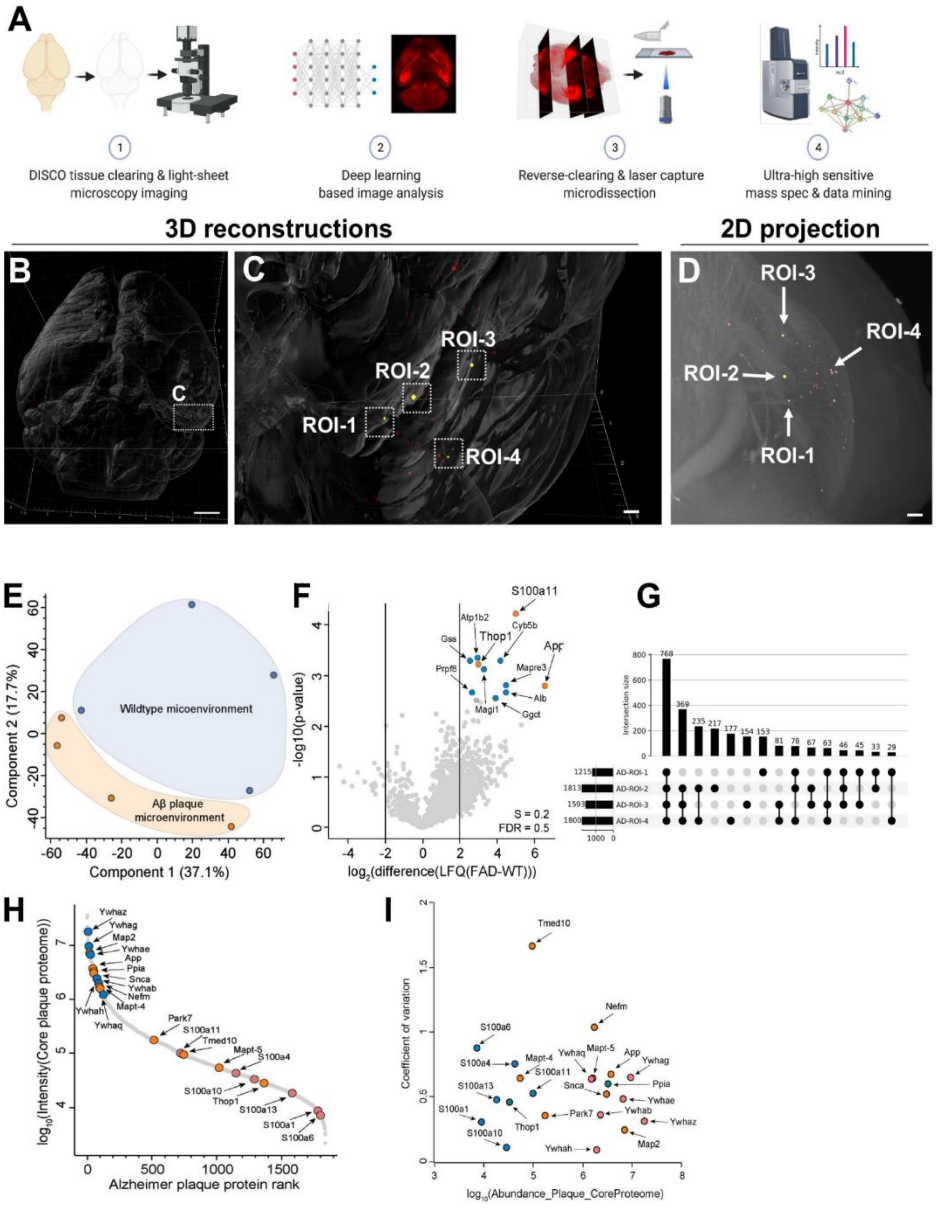

Acknowledgments

This dissertation would not be completed without many people's support.

To begin with, I wish to sincerely acknowledge my supervisor Prof. Dr. Ali Ertürk, for the valuable opportunity to study as a doctorate candidate in an international team with diverse backgrounds. From the topic selection to the research plan implementation, this project has been finished under his careful supervision. Additionally, I would like to thank the rest of my thesis advisory committee: Prof. Dr. Nikolaus Plesnila and Prof. Dr. Dominik Paquet, for their constructive suggestions and fruitful discussion.

I am also very grateful to Dr. Farida Hellal, who has offered great help to me and given lots of excellent advice in the progress of my project. Her extensive scientific knowledge and strong logical reasoning have tremendously impressed me and served as a great model for my future scientific studies. Another special thanks to Hongcheng Mai, the main partner of my research project. We have many people with different expertise in the lab, which is a great place for interdisciplinary scientific research. We have been working on several projects, and it is always delightful to overcome challenges together. And of course, I want to thank all the colleagues in the Institute of Tissue Engineering and Regenerative Medicine and the Institute for Stroke and Dementia research for the friendly, inspiring, and cooperative working environment.

Besides, I would like to thank all collaborators from the University of Leipzig, University Medical Center Hamburg-Eppendorf, and the Technical University of Munich for their solid input and technical support.

My biggest appreciation to my parents and family for always encouraging me and supporting me to make decisions independently. I have spent the last four years getting to know a lot of wonderful people, experiencing diverse cultures, and visiting a lot of interesting destinations, which has been an incredible and unique experience for me.

Affidavit

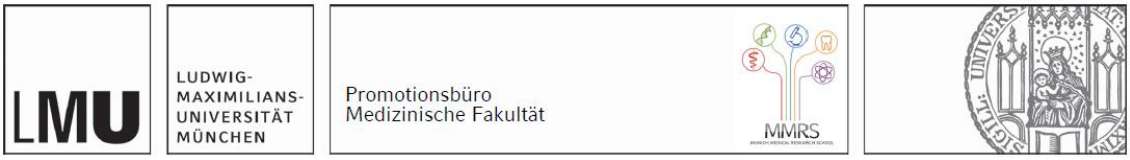

Affidavit

Rong, Zhouyi
Surname, first name

Feodor-Lynen-Str 17
Street

81377, Munich, Germany
Zip code, town, country

I hereby declare, that the submitted thesis entitled:

Unraveling proteomic changes of heterogeneous SARS-CoV-2 infection identified by panoptic imaging
……

is my own work. I have only used the sources indicated and have not made unauthorised use of services of a third party. Where the work of others has been quoted or reproduced, the source is always given.

I further declare that the submitted thesis or parts thereof have not been presented as part of an examination degree to any other university.

Munich, 15.05.2023 — Zhouyi Rong

place, date — Signature doctoral candidate

Confirmation of congruency

LMU LUDWIG-MAXIMILIANS-UNIVERSITÄT MÜNCHEN

Promotionsbüro Medizinische Fakultät

MMRS

Confirmation of congruency between printed and electronic version of the doctoral thesis

Rong, Zhouyi

Surname, first name

Feodor-Lynen-Str 17

Street

81377, Munich, Germany

Zip code, town, country

I hereby declare, that the submitted thesis entitled:

Unraveling proteomic changes of heterogeneous SARS-CoV-2 infection identified by panoptic imaging

……

is congruent with the printed version both in content and format.

Munich, 15.05.2023

place, date

Zhouyi Rong

Signature doctoral candidate

List of publications

1. Mai, H., **Rong, Z**., Zhao, S., Cai, R., Steinke, H., Bechmann, I., & Ertürk, A. (2022). Scalable tissue labeling and clearing of intact human organs. *Nature Protocols*, 1-35. https://doi.org/10.1038/s41596-022-00712-8
2. **Rong, Z**., Cheng, B., Zhong, L., Ye, X., Li, X., Jia, L., Li, Y., Shue, F., Wang, N., Cheng, Y., Huang, X., Liu, C.-C., Fryer, J. D., Wang, X., Zhang, Y., & Zheng, H. (2020). Activation of FAK/Rac1/Cdc42-GTPase signaling ameliorates impaired microglial migration response to Aβ42 in triggering receptor expressed on myeloid cells 2 loss-of-function murine models. *The FASEB Journal*, *34*(8), 10984–10997. https://doi.org/10.1096/fj.202000550RR
3. Schoppe, O., Pan, C., Coronel, J., Mai, H., **Rong, Z**., Todorov, M. I., Müskes, A., Navarro, F., Li, H., Ertürk, A., & Menze, B. H. (2020). Deep learning-enabled multi-organ segmentation in whole-body mouse scans. *Nature Communications*, *11*(1), 5626. https://doi.org/10.1038/s41467-020-19449-7
4. Zhao, S., Todorov, M. I., Cai, R., -Maskari, R. A., Steinke, H., Kemter, E., Mai, H., **Rong, Z**., Warmer, M., Stanic, K., Schoppe, O., Paetzold, J. C., Gesierich, B., Wong, M. N., Huber, T. B., Duering, M., Bruns, O. T., Menze, B., Lipfert, J., … Ertürk, A. (2020). Cellular and Molecular Probing of Intact Human Organs. *Cell*, *180*(4), 796-812.e19. https://doi.org/10.1016/j.cell.2020.01.030
5. Pan, C., Schoppe, O., Parra-Damas, A., Cai, R., Todorov, M. I., Gondi, G., von Neubeck, B., Böğürcü-Seidel, N., Seidel, S., Sleiman, K., Veltkamp, C., Förstera, B., Mai, H., **Rong, Z**., Trompak, O., Ghasemigharagoz, A., Reimer, M. A., Cuesta, A. M., Coronel, J., … Ertürk, A. (2019). Deep Learning Reveals Cancer Metastasis and Therapeutic Antibody Targeting in the Entire Body. *Cell*, *179*(7), 1661-1676.e19. https://doi.org/10.1016/j.cell.2019.11.013
6. Cheng, B., Li, X., Dai, K., Duan, S., **Rong, Z**., Chen, Y., Lü, L., Liu, Z., Huang, X., Xu, H., Zhang, Y.-W., & Zheng, H. (2021). Triggering Receptor Expressed on Myeloid Cells-2 (TREM2) Interacts With Colony-Stimulating Factor 1 Receptor (CSF1R) but Is Not Necessary for CSF1/CSF1R-Mediated Microglial Survival. *Frontiers in Immunology*, *12*, 633796–633796. PubMed. https://doi.org/10.3389/fimmu.2021.633796
7. Fu, H., Cheng, Y., Luo, H., **Rong, Z**., Li, Y., Lu, P., Ye, X., Huang, W., Qi, Z., Li, X., Cheng, B., Wang, X., Yao, Y., Zhang, Y.-W., Zheng, W., & Zheng, H. (2019). Silencing MicroRNA-

155 Attenuates Kainic Acid-Induced Seizure by Inhibiting Microglia Activation. *Neuroimmunomodulation*, *26*(2), 67–76. https://doi.org/10.1159/000496344

8. Ye, X., **Rong, Z**., Li, Y., Wang, X., Cheng, B., Cheng, Y., Luo, H., Ti, Y., Huang, X., Liu, Z., Zhang, Y., Zheng, W., & Zheng, H. (2018). Protective Role of L-3-n-Butylphthalide in Cognitive Function and Dysthymic Disorders in Mouse With Chronic Epilepsy. *Frontiers in Pharmacology*, *9*. https://www.frontiersin.org/article/10.3389/fphar.2018.00734
9. Sun, L., **Rong, Z**., Li, W., Zheng, H., Xiao, S., & Li, X. (2018). Identification of a Novel Hemizygous SQSTM1 Nonsense Mutation in Atypical Behavioral Variant Frontotemporal Dementia. *Frontiers in Aging Neuroscience*, *10*. https://www.frontiersin.org/article/10.3389/fnagi.2018.00026
10. Zheng, H., Jia, L., Liu, C.-C., **Rong, Z**., Zhong, L., Yang, L., Chen, X.-F., Fryer, J. D., Wang, X., Zhang, Y., Xu, H., & Bu, G. (2017). TREM2 Promotes Microglial Survival by Activating Wnt/β-Catenin Pathway. *The Journal of Neuroscience*, *37*(7), 1772. https://doi.org/10.1523/JNEUROSCI.2459-16.2017
11. Zhan, Y., Zheng, H., Wang, C., **Rong, Z**., Xiao, N., Ma, Q., & Zhang, Y. (2017). A novel presenilin 1 mutation (F388L) identified in a Chinese family with early-onset Alzheimer's disease. *Neurobiology of Aging*, *50*, 168.e1-168.e4. https://doi.org/10.1016/j.neurobiolaging.2016.10.010